SOLAR-HYDROGEN
STAND-ALONE POWER SYSTEM
DESIGN AND SIMULATIONS

A THESIS SUBMITTED TO
THE GRADUATE SCHOOL OF NATURAL AND APPLIED SCIENCES
OF
MIDDLE EAST TECHNICAL UNIVERSITY

BY

ARMAN ULUOĞLU

IN PARTIAL FULFILLMENT OF THE REQUIREMENTS
FOR
THE DEGREE OF MASTER OF SCIENCE
IN
MECHANICAL ENGINEERING

MAY 2010

Approval of the thesis:

SOLAR-HYDROGEN STAND-ALONE POWER SYSTEM DESIGN AND SIMULATIONS

submitted by **ARMAN ULUOĞLU** in partial fulfillment of the requirements for the degree of **Master of Science in Mechanical Engineering, Middle East Technical University** by,

Prof. Dr. Canan Özgen   _____
Dean, Graduate School of **Natural and Applied Sciences**

Prof. Dr. Suha Oral   _____
Head of Department, **Mechanical Engineering Dept., METU**

Asst. Prof. Dr. İlker Tarı   _____
Supervisor, **Mechanical Engineering Dept., METU**

Examining Committee Members:

Assoc. Prof. Dr. Cemil Yamalı   _____
Mechanical Engineering Dept., METU

Asst. Prof. Dr. İlker Tarı   _____
Mechanical Engineering Dept., METU

Assoc. Prof. Dr. Derek K. Baker   _____
Mechanical Engineering Dept., METU

Asst. Prof. Dr. Tuba Okutucu Özyurt   _____
Mechanical Engineering Dept., METU

Assoc. Prof. Dr. Yüksel Kaplan   _____
Mechanical Engineering Dept., Niğde University

Date: **_____**

I hereby declare that all information in this document has been obtained and presented in accordance with academic rules and ethical conduct. I also declare that, as required by these rules and conduct, I have fully cited and referenced all material and results that are not original to this work.

Name, Last name: Arman Uluoğlu

Signature:

ABSTRACT

SOLAR-HYDROGEN STAND-ALONE POWER SYSTEM DESIGN AND SIMULATIONS

Uluoğlu, Arman

M.Sc., Department of Mechanical Engineering

Supervisor: Asst. Prof. Dr. İlker Tarı

May 2010, 107 pages

In this thesis, solar-hydrogen Stand-Alone Power System (SAPS) which is planned to be built for the emergency room of a hospital is designed. The system provides continuous, off-grid electricity during the whole period of a year without any external electrical power supply. The system consists of Photovoltaic (PV) panels, Proton Exchange Membrane (PEM) based electrolyzers, PEM based fuel cells, hydrogen tanks, batteries, a control mechanism and auxiliary equipments such as DC/AC converters, water pump, pipes and hydrogen dryers. The aim of this work is to investigate the optimal system configuration and component sizing which yield to high performance and low cost for different user needs and control strategies. TRNSYS commercial software is used for the overall system design and simulations.

Numerical models of the PV panels, the control mechanism and the PEM electrolyzers are developed by using theoretical and experimental data and the models are integrated into TRNSYS. Overall system models include user-defined components as well as the default software components. The electricity need of

the emergency room without any shortage is supplied directly from the PV panels or by the help of the batteries and the fuel cells when the solar energy is not enough. The pressure level in the hydrogen tanks and the overall system efficiency are selected as the key design parameters. The major component parameters and various control strategies affecting the hydrogen tank pressure and the system efficiency are analyzed and the results are presented.

Keywords: Stand-Alone Power Systems, TRNSYS, Photovoltaic cells, PEM electrolyzers, fuel cells, hydrogen.

ÖZ

GÜNEŞ ENERJİSİ VE HİDROJENLİ ŞEBEKEDEN BAĞIMSIZ ENERJİ SİSTEMİ TASARIMI VE SAYISAL ANALİZİ

Uluoğlu, Arman

Yüksek Lisans, Makina Mühendisliği Bölümü

Tez Yöneticisi: Y. Doç. Dr. İlker Tarı

Mayıs 2010, 107 Sayfa

Bu tezde, bir hastanenin acil servisine kurulması planlanan güneş enerji sistemi tasarlanmıştır. Bu sistemin tek enerji kaynağı güneş enerjisidir. Sistem tüm yıl boyunca şebeke elektriğinden yararlanmadan acil servise kesintisiz elektrik enerjisi sağlar. Güneş enerji sistemi, Fotovoltaik (PV) paneller, PEM bazlı elektrolizörler, PEM yakıt hücreleri, hidrojen tankı, piller, control mekanizması ve DC/AC dönüştürücüler, su pompası, borular ve hidrojen kurutucular gibi yan ekipmanlardan oluşmaktadır. Bu çalışmanın amacı, değişik kullanıcı ihtiyaçlarına ve control stratejilere göre yüksek performansta ve düşük maliyette çalışacak sistem konfigürasyonlarını ve ekipman seçimlerini araştırmaktır. Sistemi tümüyle tasarlamak ve analiz etmek için TRNSYS ticari yazılımı kullanılmıştır. PV panellerinin, kontrol mekanizmasının ve PEM elektrolizörün sayısal modelleri, deneysel ve teorik bilgilerden yararlanılarak oluşturulmuş ve TRNSYS yazılımına eklenmiştir. Tümüyle tasarlanmış system modelleri bu kullanıcı tanımlı elemanlar ve yazılım içerisinde yer alan varsayılan elemanlar kullanılarak oluşturulmuştur. Acil servise ihtiyacı olan enerji doğrudan PV panellerinden ya da güneş enerjisi yeterli olmadığı zamanlar piller ve yakıt hücreleri yardımıyla sürekli ve eksiksiz biçimde

sağlanmaktadır. Hidrojen tankındaki basınç seviyesi ve sistemin toplam verimi anahtar parametreler olarak seçilmiştir. Bu anahtar parametreleri etkileyen ekipman seçimleri ve boyutlandırmaları ile control stratejileri incelenmiş ve sonuçları sunulmuştur.

Anahtar Sözcükler: Şebekeden bağımsız enerji sistemleri, TRNSYS, fotovoltaik piller, PEM elektrolizörler, yakıt pilleri, hidrojen.

To My Family

ACKNOWLEDGEMENTS

TABLE OF CONTENTS

LIST OF TABLES

LIST OF FIGURES

FIGURES

LIST OF SYMBOLS

A_{pem}	PEM surface area
E_g	Band gap energy at 0 K
F	Faraday constant
I	Output current
I_0	Reverse saturation current
I_{0e}	Exchange current
I_{0ref}	Reverse saturation current at Standard Test Conditions
I_D	Diode current
I_{el}	Electrolyzer current
I_L	Light current
I_{PH}	Photo generated current
$I_{sc,ref}$	Short circuit current at reference conditions
I_{SH}	Shunt current
k	Boltzmann's constant
n	Diode ideality factor
N	Normal conditions (0.101325 MPa and 273.15K)
N_{cell}	Total cell number
$\dot{n}h2$	Hydrogen molar production rate
Nm^3	Volume of the gas calculated at normal conditions which are 273K and 1 Atm in m^3
q	Elementary charge
R	Universal gas constant
R_S	Series resistance
R_{SH}	Shunt resistance
T	Absolute cell temperature

T_c	Cell temperature
$T_{cell,ref}$	Cell temperature at reference conditions
U	Cell voltage
U_{eq}	Equilibrium voltage
U_{PV}	Convective heat transfer coefficient
V	Output voltage
Vt	Thermoneutral voltage
w	Wind speed m/s
α	Absorption coefficient of the cell
α_e	Symmetry factor
β	Temperature coefficient of the PV array
γ	Solar irradiance coefficient of the PV array
η	PV panel efficiency
η_F	Faraday efficiency
η_r	Efficiency of the PV array at reference conditions
μ_{Isc}	Temperature coefficient of short circuit
τ	Transmittance of the cell cover
Φ	Solar irradiation (mW/cm^2)

LIST OF ABBREVIATIONS

NOCT	Nominal Operating Cell Temperature
PEM	Proton Exchange Membrane
SAPS	Stand Alone Power System
SOC	Stane of Charge
STC	Standart Test Conditions
TMY	Typical Meteorological Year

CHAPTER 1

INTRODUCTION

1.1 Renewable Energy

As awareness of global warming increases and conventional fuel sources begin to drain, alternative energy sources attract the attention of the community more and more every day. Since the political issues decrease the desirability of nuclear power, a large amount of research and investments focus on renewable energy. Renewable energy is generated from natural resources like sunlight, wind, hydro, geothermal energies or from biodiesel fuels. Energy produced from renewable resources have no major waste products and the resources are naturally replenished. Although the resources are cost-free and environmentally friendly, current high initial costs of equipment, low energy conversion efficiencies and intermittent nature of energy sources decrease economic viability of the renewable energy against the fossil fuels. However, as the renewable technologies step forward, the practical use of renewables is growing. During the last decade, many governments have advanced their support for renewables. According to the Renewable Energy Policy Network [1] research, 15% of global electricity production is provided from large hydropower plants and 3.4% from new renewables (solar, wind, geothermal, biofuels, tidal) in year 2006. In year 2008, the total investment on new renewable energies has been doubled with respect to the year 2006 and the total energy production capacity has been increased by 40%. For the majority of analysts, renewable energy industry is a "guaranteed-growth" sector and even "crisis-proof" because of the worldwide trends and enormous development in the past decade [2].

Solar energy is one of the major sources of renewable energy with the amount of solar radiation reaching the Earth from the Sun. It is a well known fact that the world's one year energy demand can be supplied by the Sun in one hour if it was possible to collect all the solar energy falling on the earth. There are two commonly used ways of benefiting from sunlight; solar energy can be used to produce hot water or air via thermal solar panels or it is possible to convert solar energy into electricity by photovoltaic (PV) cells. Photovoltaic electricity generation has various advantages and disadvantages. Main disadvantages are; high initial cost of the equipment, low efficiency in converting solar energy into electricity and intermittent energy production due to natural reasons such as no sunlight being available during the night and low solar radiation throughout the winter seasons. But, once the PV panels are built, the operation cost of the system is very low and the panels can work up to 20 years without any special maintenance need. Energy produced by the PV panels is cost-free and there is not any waste product. With conventional PV technologies 12 to 18% of solar energy can be converted into electricity however there are new technologies under development where the conversion efficiency reaches 40% [3]. Because of the discontinuous energy production, energy storage or a backup power system is needed for photovoltaic systems. Batteries can be used for daily storage but for seasonal storage batteries are not practical because of the low storage capacity. Storing energy in the form of hydrogen is a possible solution for both daily and seasonal storage.

1.2 Stand Alone Power Systems

A Stand Alone Power System (SAPS) is an off-grid electricity system that can operate without any external power input. Energy input to the system is usually from a renewable source. Stand alone power systems are mostly used in remote locations where transporting electricity is either very difficult or expensive. A typical solar-hydrogen based stand alone power system, which will be investigated in this study, with minimum system elements is shown in Figure 1-1 [4]. Main elements of such systems are the solar energy source, photovoltaic panels, electrolyzer, fuel-cell and the hydrogen tank. Also some auxiliary equipment is needed for the system to work properly. The system is controlled by a universal

controller which decides the operating patterns of the system elements after evaluating the system parameters such as user power demand, available solar energy and hydrogen tank pressure level. Sunlight is used as the energy input to the system, which is converted to electricity by the PV panels. The electricity produced by the PV panels and fuel-cells is direct current and needs to be converted to the alternative current by DC/AC converters before supplying to the user. When the solar generated energy is greater than need of the user and also if the hydrogen tank is not full, the extra energy is given to the electrolyzer to produce hydrogen which is stored in the hydrogen tank for the later usage. The hydrogen stored in the tank is used by the fuel-cell stack to produce electricity when the solar energy is not sufficient for the user, for instance during night hours or winter days when sunlight is not strong enough.
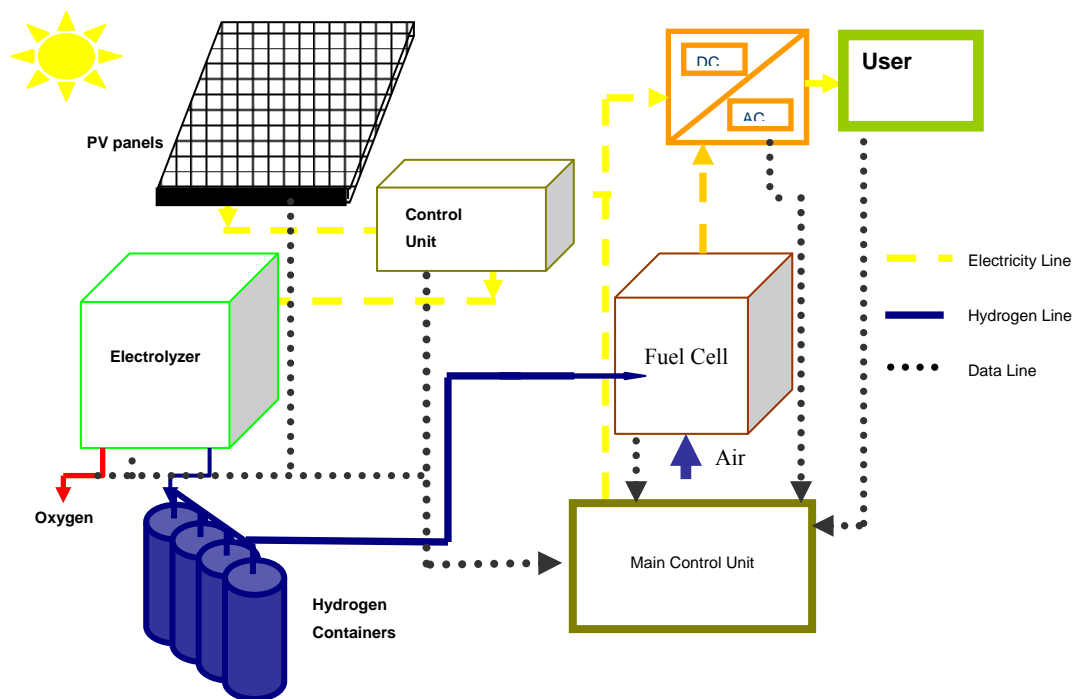
Figure 1-1: Stand Alone Power System that will be investigated in this study
(adapted from [4])

3

To protect the fuel cell from the harmful effects of switching on and off or fluctuating operating power, a battery pack can also be installed to the system. They can be used to help the fuel cell during the peak hours which decreases the fuel cell power and increases the fuel cell efficiency. Also, batteries can supply electricity if the user needs very low amount of energy when it is not safe for fuel cells to operate. Since, the total energy can be stored in batteries is low, they are not suitable for seasonal storage or daily storage where the user power demand is high.

It is important to see the behavior of the system before making the final decision on the singular elements that will be used in the system. To optimize the system size and quality, it is needed to see how the system works under certain circumstances, how the system responds to the variations, how efficient the system is or whether we can supply the demand of the user or not. There are many commercial software's available focused on simulating such systems such as TRNSYS, HOMER and HYBRID2. Also it is possible to simulate these systems by Matlab, FORTRAN, and other programming languages.

1.3 TRNSYS

During this work TRNSYS (The Transient Energy System Simulation Tool) is used for the simulations. It is a dynamic simulation program developed in University of Wisconsin. This tool is one of the most common software for simulations of thermal energy systems in the literature. The software includes many default elements that can be used in a stand-alone power system and also it is a flexible tool that allows any user with a FORTRAN compiler to define their own elements into the software if necessary. Each component in the software is a FORTRAN subroutine with input, output and calculation parameters. Every component can be linked to each other with output/input relations. For instance; a fuel cell component reads its input such as inlet pressures, physical properties, cell current, number of cells, cooling data and membrane properties then runs the subroutine and calculates the output data such as cell voltage, power and temperature, hydrogen consumption or energy efficiency. By linking the hydrogen consumption

output of the fuel cell and hydrogen production output of the electrolyzer to the hydrogen outflow and hydrogen inflow inputs of the hydrogen tank respectively, hydrogen tank subroutine can calculate the hydrogen level in the tank. Upon linking the hydrogen tank output, user power demand and electricity production output of the PV panels to the system controller, the controller can decide how the system should work.

TRNSYS has a wide range of use in HVAC applications, hydronics, building projects and renewable energy systems. Additional component and project libraries can be added to the software. Simulation periods and time step of simulations are very flexible and can vary between a second and several years.

1.4 Literature Survey

Stand-Alone Power Systems based on different renewable energies is a developing topic in the literature. Most of the studies serve as "proof of concept" to using hydrogen as seasonal energy storage for intermittent renewable energy sources. The main focus of studies is proving technical viability of this kind of systems. According to economic point of view, the systems are usually evaluated as not being feasible with the current prices and efficiencies of the equipments used. Investment return is usually found to be over 20 years. Detailed knowledge about renewable energy and system equipment is required to design Stand-Alone Power Systems. Experimental testing or computational techniques can provide the necessary information. There are several works in the literature on the design, operation and simulation processes of renewable energy systems.

1.4.1 Experimental Works

In several studies, performance and viability of renewable energy systems has been experimentally investigated. Hollmuller et al. [5], Miland and Ulleberg [6], Vanhanen et al. [7], Galli and Stefanoni [8], Chaparro et al. [9], Sasitharanuwat et al. [10], Agbossou et al. [11], Shapiro et al. [12] and Kelly et al. [13] have reported experimental results of prototype or actual systems.

Hollmuller et al. [5] studied the performance of a privately owned photovoltaic hydrogen production and storage installation in a single-family house in Switzerland. The system is manually controlled. It consists of an array of roof mounted PV solar panels, a DC–DC converter , an alkaline membrane electrolyzer, a hydrogen purification unit, a compressor, two metal hydride storage tanks and a hydrogen operated minibus. The aim of the study is to investigate commercial and technical viability of using solar energy for seasonal hydrogen storage. It is observed that using automatic control unit, a hydrogen purification unit that does not consume hydrogen and larger hydrogen storage via compressed gas cylinders would increase the system efficiency and performance.

Miland and Ulleberg [6] used a test facility to report the system performance and operational experience of individual components, subsystems and complete renewable power systems. To be able to investigate seasonal performance of the system, PV arrays have been emulated using a programmable power supply unit. Since a real time testing during a whole year is very time consuming, 7 days with different solar energy profiles have been selected to investigate seasonal behavior of the system in a weekly testing. The programmable power supply feeds the emulated PV power to the system consisting of PEM electrolyzer and fuel cell, metal hydride tank, hydrogen purifier, control panels and load. The efficiencies of singular component, subsystems and complete system have been found and ways to improve them have been proposed. The real time operating efficiency of system, excluding PV array efficiency, has been found over 50%.

Vanhanen et al. [7] performed an analysis on small scale seasonal energy storage in the form of hydrogen. Using solid polymer electrolyzers and fuel cells are found to be more efficient than using alkaline electrolyzers and phosphoric acid fuel cells. The hydrogen cycle efficiency is around 40-45% and the system is offered to be viable for small scale stand alone power system which are far away from grid power.

Galli and Stefanoni [8] tested and investigated commercial solar-hydrogen technologies in a demonstrative solar-hydrogen plant built near Rome. Long term reliability of solid polymer fuel cell, alkaline electrolyzer and metal hydride and pressurized storage tank is evaluated. Also the efficiency of storing energy in the form of hydrogen and the performance losses due to intermittent operation is investigated. Weather conditions and the performances of PV panels, electrolyzer, fuel cell and hydrogen tanks are individually monitored.

Chaparro et al. [9] investigated a solar-hydrogen stand alone power system which supplies 3-5 kWh daily energy throughout a year. The electrolyzer works under high pressure to avoid hydrogen compression steps but it is found that absorption-temperature mechanics of metal hydride storage tank is a limiting factor for system performance. 6-7% of the total solar irradiation is found to be supplied to the user at the end of the testing year. Hydrogen cycle is reported to be essential because of the continuous power need, even though the efficiency of this cycle is low.

Sasitharanuwat et al. [10] reported the results of a stand alone power system that has been built with 3 different types of commercial PV panels in an isolated building. They system fails to supply continuous energy to the user since a battery pack was used as the only energy storage. Combining the PV system with a micro-grid is offered to be as a solution. The excess energy from the PV panels during day times would be supplied to the micro-grid and during night times electricity could be drawn from the grid.

Agbossou et al. [11] investigated the performance of a hydrogen stand alone power system. A wind turbine and PV panels are used together as the energy generators. Alkaline electrolyzers, PEM fuel cells, hydrogen storage, batteries, controllers, DC/DC convertors and DC/AC inverters are the other components of the system. The controller defines the flow path of energy in the system. Batteries are used to cover energy demand during peak load powers and load power transients. After 30 days of operation, stand alone power system based on hydrogen as energy storage is found to be safe and reliable.

Shapiro et al. [12] built a prototype stand alone power system system with a PEM fuel cell and electrolyzer, high pressure hydrogen tank and PV panel. The aim is to test stand-alone power system performance, viability of hydrogen as seasonal energy storage and to investigate the experimental electrolyzer and its performance when combined with a PV panel. The performance of electrolyzer as a compressor is found to be promising.

Kelly et al. [13] designed and constructed a system to produce hydrogen for fuel-cell electric vehicles by solar energy. The system consisted of high efficiency PV panels and high pressure electrolyzers. The average efficiency of the system was increased to 8.5% by matching PV panel voltage at maximum power point output and electrolyzer voltage at nominal operating power. The authors claimed that solar-to-hydrogen efficiency of the system is one of the highest values reported in the literature.

1.4.2 Component and System Modeling

Experimental testing on small scaled energy systems is usually expensive and time consuming compared to computational methods. Therefore, the number of computational researches on this topic is greatly higher than experimental studies. Only some of them will be looked over in this section. A typical renewable energy system with hydrogen as energy storage contains electrolyzers, fuel cells, batteries, hydrogen storage tanks, DC/DC convertors, DC/AC inverters and PV panels/Wind Turbines/Micro hydro turbines etc. as mentioned before. Each component should be modeled separately before forming the whole system.

Ulleberg [14], worked on numeric simulation of stand-alone power systems during his Ph.D. studies. The thesis includes the models of each system component separately and verification of the components and the system simulations by using the experimental data of a solar-hydrogen demonstration plant (PHOEBUS) located in Germany. After verifying the models, he examined different control strategies for stand alone power system, to be able to optimize the stand alone power systems. TRNSYS was used for the system simulations, the component models

were integrated into the software. The current commercial version of TRNSYS also includes many of these components.

Ulleberg [15] also investigated the control strategy for a PV system with a hydrogen subsystem using TRNSYS. The investigated system involves an electrolyzer, a pressurized hydrogen gas storage, and a fuel cell. Detailed computer simulation models are developed, tested, and verified against a reference system. The basic control strategy and main logical control variables for a PV-hydrogen system are described. The results from a time series simulation for a typical year are presented.

Dufo-Lopez et al. [16] developed a method for controlling stand-alone hybrid renewable electrical systems with hydrogen storage. The method optimized the control of the hybrid system by minimizing the total cost throughout its lifetime. The optimized hybrid system can be composed of renewable sources, batteries, fuel cell, AC generator and electrolyzer. Also, the control strategy optimizes how the spare energy is used. The important point of this study is; the control strategy determines the most economical way to meet the energy deficit, when the amount of energy demanded by the loads is higher than the one produced by the renewable sources.

Santarelli et al. [17] investigated a stand-alone energy system supplied just with renewable energy sources. This system contains an electrolyzer, a hydrogen tank and a proton exchange membrane fuel cell. The energy systems have been designed in order to supply the electricity needs of a residential user in a mountain environment in Italy during a complete year. In this study, three different renewable sources have been considered : solar irradiance, hydraulic energy and wind speed.

Pedrazzi et al [18] developed a complete mathematical model for a solar hydrogen energy system. Each component and subsystem has been modeled separately by using the information available in the literature. Then the individual models were combined together to form the virtual system. The simulations were conducted on

commercial software MATLAB Simulink. The annual simulations suggested that the system was able to perform as a stand alone power system without any energy need from grid. Thermodynamic, exergy and economic analysis's was planned to be done by using the reference system modeled.

Samaniego et al. [19] models a hydrogen stand alone power system with wind turbine using TRNSYS 15 software. The main aim of the study is to investigate the system performance with respect to 2 different electrolyzer control strategy; electrolyzer working at constant power or varying power. The default component models in the software were used to form the system model. The initial cost of the system is lower with an electrolyzer working at constant power but the system performance is lower and the system returns the investment in 30 years. Although the initial cost of the system is higher with second case, the system returns the investment in 24 years. The investment return is period is found to be excessively long because of the high equipment cost.

Deshmukh and Boehm [20] modeled individuals components for PV array, wind turbine, micro-hydro turbine, electrolyzer, fuel cell and compressed hydrogen, metal hydride and carbon based storages. Electrical and thermal energy consumption of a typical residential house is also modeled. The authors announced the physics of equipments such as PV, fuel cell or hydrogen storages are well understood because of the long investigations and careful attentions on them. But PEM electrolyzer models were not yet to be very accurate as the number of studies on them is very limited on the literature as well.

Nelson et al. [21] developed a computer program using MATLAB to evaluate economics of a hybrid wind/solar hydrogen generation system. The hydrogen generation system is compared with traditional battery storage. The performances of both systems were investigated. The authors offered that battery pack is economically superior to hydrogen as energy storage because of the low efficiency of fuel cell-electrolyzer hydrogen cycle. But they also added that with the improvement in fuel cell and electrolyzer technology they can be competitive in the near future.

Onar et al. [22,23] developed a dynamic model for a solar/wind/hydrogen/ultra-capacitor (UC) energy system using MATLAB Simulink. Wind turbine and PV array were used to generate input energy to the system, while hydrogen cycle contains electrolyzer and fuel cells. UC was set to meet the load demand above maximum power of fuel cell. The components and subsystems are modeled separately. Dynamic responses of the components to load, solar irradiation and wind speed changes are investigated and found to be efficient.

1.5 Brief Outline

In the following chapter, PV panel and electrolyzer are mathematically modeled and the model performances are discussed. In Chapter 3, the effects of different system parameters such as PV panel size and surface slope, electrolyzer size, hydrogen tank capacity, auxiliary equipment, battery pack energy capacity and operation strategies of batteries on the system performance are analyzed. First, different stand alone power system configurations without battery pack are simulated and the results are discussed. Then, detailed analysis on stand alone power systems with battery pack is discussed and energy consumption of auxiliary equipment is briefly discussed. TRNSYS simulation of a small scale actual system is conducted in the last part of Chapter 3. In the last chapter, the results are discussed, some conclusions are drawn and the future work is suggested.

CHAPTER 2

COMPONENT MODELING

Various components of the solar-hydrogen energy system and related modeling approaches are presented in this chapter.

2.1 Photovoltaic Panel

A photovoltaic panel is an assembly of PV cells which are semi-conductor materials generating electricity from electro-magnetic radiation. When the source of radiation is the Sun, the PV cells are called solar cells. Most of the commercial solar panels are produced from silicon based solar cells. According to the quality of the cell, the energy conversion efficiency of the devices from solar power into direct current can be in the range of 5% to 20%. Because of the low energy conversion efficiencies and high cost of the solar panels, practical use of these devices are mostly limited to electricity generation in rural and remote areas, to telecommunication stations and to spacecrafts.

In the following sub-sections, a mathematical model of solar panels will be introduced. The model will be able to predict the output parameters of the PV panel such as power production, cell temperature and efficiency for a given set of meteorological data. In addition, it will be possible to measure the different commercial panel performances in generating electricity by changing the input data provided by producers. In order to use this PV model in the software TRNSYS which is used to model the complete energy system, the code of the model is written in FORTRAN programming language.

2.1.1 Electrical Model

The equivalent electrical circuit of a PV cell is given in Figure 2-1. It is a one diode model which is also known as the 5 parameter circuit. The cell can be modeled by other equivalent circuits as well; such as 7 parameters but the one diode model is the most commonly used circuit in the literature and the solution of the circuit is not as complicated as is the case in other models. The parameters in the circuit are; I_D, I_L, I_{SH}, R_{SH}, R_S, I and V.
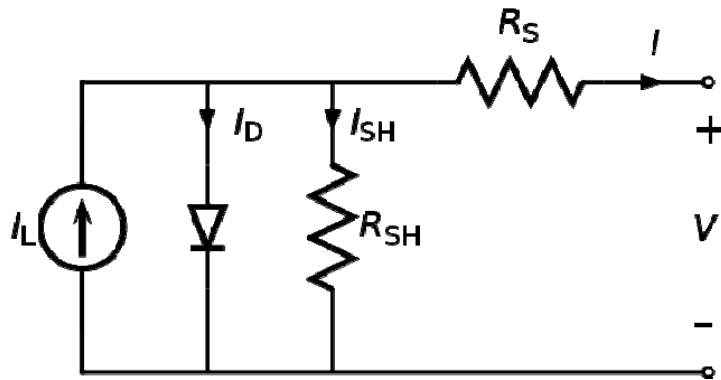
Figure 2-1 Equivalent circuit of a solar cell

From the circuit;

$$I = I_{PH} - I_D - I_{SH} \tag{2.1}$$

I_{PH} (photo-generated current) is also called as I_L (light current) which refers to direct current generated by photovoltaic effect. Whereas I is the output current of the cell.

from Shockley's diode equation;

$$I_D = I_0 \left[\exp(\frac{(V + IR_S)}{nV_t}) - 1 \right] \qquad (2.2)$$

Where;

$$V_t = \frac{kT}{q} \qquad (2.3)$$

By Ohm's Law;

$$I_{SH} = \frac{V + IR_S}{R_{SH}} \qquad (2.4)$$

After substituting equations (2.2), (2.3) and (2.4) into equation (2.1), the equation takes the form of;

$$I = I_{PH} - I_0 \left[\exp(\frac{(V + IR_S)}{AV_t}) - 1 \right] - \frac{V + IR_S}{R_{SH}} \qquad (2.5)$$

Equation (2.5) is the general solar cell characteristic equation which is available in the literature [24].

From the characteristic equation, it is possible to evaluate cell current for a given cell temperature and voltage. However, analytic solution of the equation is not possible and numerical methods will be used to solve the equation. The parameters that need to be defined before solving Equation (2.5) are R_{SH}, R_S, A, I_{PH} and I_0. These parameters are specific to every different commercial PV array and will be calculated from the product data sheet values tested at the Standard Test Conditions (STC) or Reference Point which is 1kW/m^2 solar irradiation and

14

25℃ cell temperature. Knowing these parameters, solar radiation data and the cell temperature will allow us to calculate the electricity generation of the solar cell.

Data sheets of solar arrays supplied by the manufacturers include short circuit current (I_{sc}) and its temperature coefficient (μ_{Isc}), open circuit voltage (V_{oc}) and its temperature coefficient (μ_{Voc}), voltage (V_{mpp}) at maximum power point (MPP), and current (I_{mpp}) at MPP measured at STC. Equation (2.5) is given for a single cell. For a PV array including n_s number of cells connected in series, the characteristic equation takes the form [24];

$$I = I_{PH} - I_0 \left[\exp(\frac{(V + IR_S)}{n_S A V_t}) - 1 \right] - \frac{V + IR_S}{R_{SH}} \tag{2.6}$$

5 equations are needed to find the 5 unknown parameters in Equation (2.6). Manufacturer's data sheet provides cell voltage and current at 3 key points.

At Short Circuit Point the characteristic equation takes the form of,

$$I_{SC} = I_{PH} - I_0 \left[\exp(\frac{I_{SC} R_S}{n_S V_t A}) - 1 \right] - \frac{I_{SC} R_S}{R_{SH}} \tag{2.7}$$

At Open Circuit Point the characteristic equation takes the form of,

$$I_{OC} = I_{PH} - I_0 \left[\exp(\frac{V_{OC}}{n_s A V_t}) - 1 \right] - \frac{V_{OC}}{R_{SC}} = 0 \tag{2.8}$$

At Maximum Power Point the characteristic equation takes the form of,

$$I_{mpp} = I_{PH} - I_0 \left[\exp(\frac{V_{mpp} + I_{mpp} R_S}{n_S A V_t}) - 1 \right] - \frac{V_{mpp} + I_{mpp} R_S}{R_{SH}} \tag{2.9}$$

Derivative of the power with respect to voltage at the maximum power point is equal to zero by the definition of the maximum power point.

$$\frac{dP}{dV} = \frac{d(IV)}{dV} = \frac{d\left\{\left[I_{PH} - I_0\left[\exp(\frac{V_{mpp} + I_{mpp}R_S}{n_s A V_t}) - 1\right] - \frac{V_{mpp} + I_{mpp}R_S}{R_{SH}}\right]V_{mpp}\right\}}{dV} = 0 \quad (2.10)$$

At 3 key points, there are 4 equations written. There should be 1 more equation to extract the 5 unknown parameters. Since the series resistance is relatively small with respect to shunt resistance, I_L can be assumed to be equal to I_{SH} Ulleberg [14].

$$I_L = I_{SC} \quad (2.11)$$

When equation (2.11) is integrated into previous 4 equations, the number of unknown parameters decreases to 4. To solve the 4 non-linear equations with 4 unknowns, modified Newton-Raphson method is used. In this method, by using the derivatives of the equations, non-linear equations are linearized and linear set of equations can be solved with Gauss elimination method.

Reorganizing the equations (2.7), (2.8), (2.9) and (2.10) respectively;

$$f1 = 0 = \left\{I_{PH} - I_0\left[\exp(\frac{I_{SC}R_S}{n_s V_t A}) - 1\right] - \frac{I_{SC}R_S}{R_{SH}}\right\} - I_{SC} \quad (2.12)$$

$$f2 = 0 = I_{PH} - I_0\left[\exp(\frac{V_{OC}}{n_s A V_t}) - 1\right] - \frac{V_{OC}}{R_{SC}} \quad (2.13)$$

$$f3 = 0 = \left\{I_{PH} - I_0\left[\exp(\frac{V_{mpp} + I_{mpp}R_S}{n_s A V_t}) - 1\right] - \frac{V_{mpp} + I_{mpp}R_S}{R_{SH}}\right\} - I_{mpp} \quad (2.14)$$

16

$$f4 = 0 = \frac{d(IV)}{dV} = \frac{d\left\{\left[I_{PH} - I_0\left[\exp(\frac{V_{mpp} + I_{mpp}R_S}{n_S A V_t}) - 1\right] - \frac{V_{mpp} + I_{mpp}R_S}{R_{SH}}\right]V_{mpp}\right\}}{dV} \quad (2.15)$$

Expanding the solution format given for single equation single unknown to multiple variable case yields the following set of equations;

$$\frac{\partial f1_i}{\partial R_S}R_{S_{i+1}} + \frac{\partial f1_i}{\partial R_{sh}}R_{sh_{i+1}} + \frac{\partial f1_i}{\partial I_0}I_{0_{i+1}} + \frac{\partial f1_i}{\partial A}A_{i+1} = -f1_i + R_{S_i}\frac{\partial f1_i}{\partial R_S} + R_{sh_i}\frac{\partial f1_i}{\partial R_{sh}} + I_{0_i}\frac{\partial f1_i}{\partial I_0} + A_i\frac{\partial f1_i}{\partial A}$$

$$\frac{\partial f2_i}{\partial R_S}R_{S_{i+1}} + \frac{\partial f2_i}{\partial R_{sh}}R_{sh_{i+1}} + \frac{\partial f2_i}{\partial I_0}I_{0_{i+1}} + \frac{\partial f2_i}{\partial A}A_{i+1} = -f2_i + R_{S_i}\frac{\partial f2_i}{\partial R_S} + R_{sh_i}\frac{\partial f2_i}{\partial R_{sh}} + I_{0_i}\frac{\partial f2_i}{\partial I_0} + A_i\frac{\partial f2_i}{\partial A}$$

$$\frac{\partial f3_i}{\partial R_S}R_{S_{i+1}} + \frac{\partial f3_i}{\partial R_{sh}}R_{sh_{i+1}} + \frac{\partial f3_i}{\partial I_0}I_{0_{i+1}} + \frac{\partial f3_i}{\partial A}A_{i+1} = -f3_i + R_{S_i}\frac{\partial f3_i}{\partial R_S} + R_{sh_i}\frac{\partial f3_i}{\partial R_{sh}} + I_{0_i}\frac{\partial f3_i}{\partial I_0} + A_i\frac{\partial f3_i}{\partial A}$$

$$\frac{\partial f4_i}{\partial R_S}R_{S_{i+1}} + \frac{\partial f4_i}{\partial R_{sh}}R_{sh_{i+1}} + \frac{\partial f4_i}{\partial I_0}I_{0_{i+1}} + \frac{\partial f4_i}{\partial A}A_{i+1} = -f4_i + R_{S_i}\frac{\partial f4_i}{\partial R_S} + R_{sh_i}\frac{\partial f4_i}{\partial R_{sh}} + I_{0_i}\frac{\partial f4_i}{\partial I_0} + A_i\frac{\partial f4_i}{\partial A}$$

There are 4 linear equations with 4 unknowns,

$$a_1.R_{S_{i+1}} + b_1.R_{sh_{i+1}} + c_1.I_{0_{i+1}} + d_1.A_{i+1} = j$$
$$a_2.R_{S_{i+1}} + b_2.R_{sh_{i+1}} + c_2.I_{0_{i+1}} + d_2.A_{i+1} = k$$
$$a_3.R_{S_{i+1}} + b_3.R_{sh_{i+1}} + c_3.I_{0_{i+1}} + d_3.A_{i+1} = l$$
$$a_4.R_{S_{i+1}} + b_4.R_{sh_{i+1}} + c_4.I_{0_{i+1}} + d_4.A_{i+1} = m$$

This set of linear equations is solved by Gauss elimination method for the unknowns. With forward elimination the 4x4 matrix is reduced into upper-triangle matrix and with backward substitution unknown parameters are calculated. The code starts from the 4 non-linear equations with initial estimation for the unknown parameters and replaces them with calculated ones after the backward

substitution. The iteration is repeated until the desired value of convergence is reached. The convergence of Newton-Raphson method highly depends on the initial guesses of the unknowns and the nature of the functions. With good knowledge of the parameters in the electrical model of a PV cell, the initial guesses should be predicated to increase the effectiveness of the method. There are some cases where this method performs poorly such as; multiple roots or zero slope of a function.

The parameters evaluated after the iterative process are valid for STC; but the cell temperature affects these parameters. There are numerous different models for I_0 and I_{PH} in the literature. One of the commonly used temperature dependency of the parameters is given below by Vachtsevanos and Kalaitzakis [25]. Total solar radiation on the PV surface (Φ) is read by the panel model from the meteorological data for a given location.

$$I_0 = I_{0ref} (\frac{T_{cell}}{T_{cell,ref}})^3 \exp\left[\frac{qE_g}{kA} (\frac{1}{T_{cell,ref}} - \frac{1}{T_{cell}}) \right] \quad (2.16)$$

$$I_{PH} = \left[I_{sc,ref} + \mu_{Isc}(T_{cell} - T_{cell,ref)}) \right] \frac{\phi}{1000} \quad (2.17)$$

The temperature dependency of the parameters R_{SH}, R_S and A are given in Deshmukh and Boehm [20].

$$A = A_{ref} \frac{T_{pv}}{T_{pv_{ref}}} \quad (2.18)$$

$$R_{sh} = R_{sh_{ref}} \frac{\phi_{pv_{ref}}}{\phi_{pv}} \quad (2.19)$$

$$R_S = R_{S_{ref}} \quad (2.20)$$

2.1.2 Thermal Model

The performance of the PV array is significantly affected by the cell temperature. The experiments conducted by Mattei et al. [26] show that the output power of the array decreases from 0.3% up to 0.6% per ^{o}C increase in the cell temperature. Mattei et al. [26] investigate the thermal models of PV cells in the literature, compares their accuracy and offers their own model. One of the common models for calculating cell temperatures given in equation (2.21) by using the Nominal Operating Cell Temperature (NOCT), measured at w=1 m/s wind speed, T_a=20°C ambient temperature and Φ=800W/m^2 solar radiation.

$$T_c = T_a + (NOCT - 20^o C)\frac{\phi}{800} \tag{2.21}$$

The experiments by Mattei et al. show that this model functions adequately under certain circumstances. However, since the effect of wind speed is not included into the model, it does not yield satisfying results under windy environmental conditions.

Another common thermal model, using absorption coefficient (α) and transmittance of the cell cover (τ), is in the form of equation (2.22)

$$\alpha\tau\phi = \eta\phi + U_{PV}(T_c - T_a) \tag{2.22}$$

and the most known cell efficiency equation is given below;

$$\eta = \eta_r \left[1 - \beta(T_c - T_r) + \gamma Log\phi\right] \tag{2.23}$$

Combining equations (2.22) and (2.23)

$$T_c = \frac{U_{PV}T_a + \phi\left[(\alpha\tau) - \eta_r - \beta\eta_r T_r\right]}{U_{PV} - \beta\eta_r\phi} \tag{2.24}$$

Mattei et al. studied the results of many other authors using the same thermal balance equation but using different convective heat transfer coefficients and they offer a heat transfer coefficient given in Equation (2.25).

$$U_{PV} = 24.1 + 2.9w(\text{W}/\text{m}^{2\text{o}}\text{C}) \tag{2.25}$$

A simple TRNSYS software simulation is made to examine and to compare with the default 5-parameter PV array model developed by Beckman et al. [27] in the software.

The result of a four day simulation between March 1 and March 4 is given in the Figure 2-2. All three models have the same parameters and only cell temperatures are compared. From the two offered thermal models, NOCT including model (equation(2.21)) is more consistent with the model by Beckman et al. [27] than the model of Mattei et al. which includes the wind speed on convective heat transfer (equation(2.24)). This is mainly due to the fact that Beckman et al. model is also based on NOCT and does not include any wind speed effect in the thermal model. As it is stated in Mattei et al., equation (2.21) may not yield satisfactory results for roof-integrated PV arrays where wind speed significantly increases the heat transfer from the PV surface.
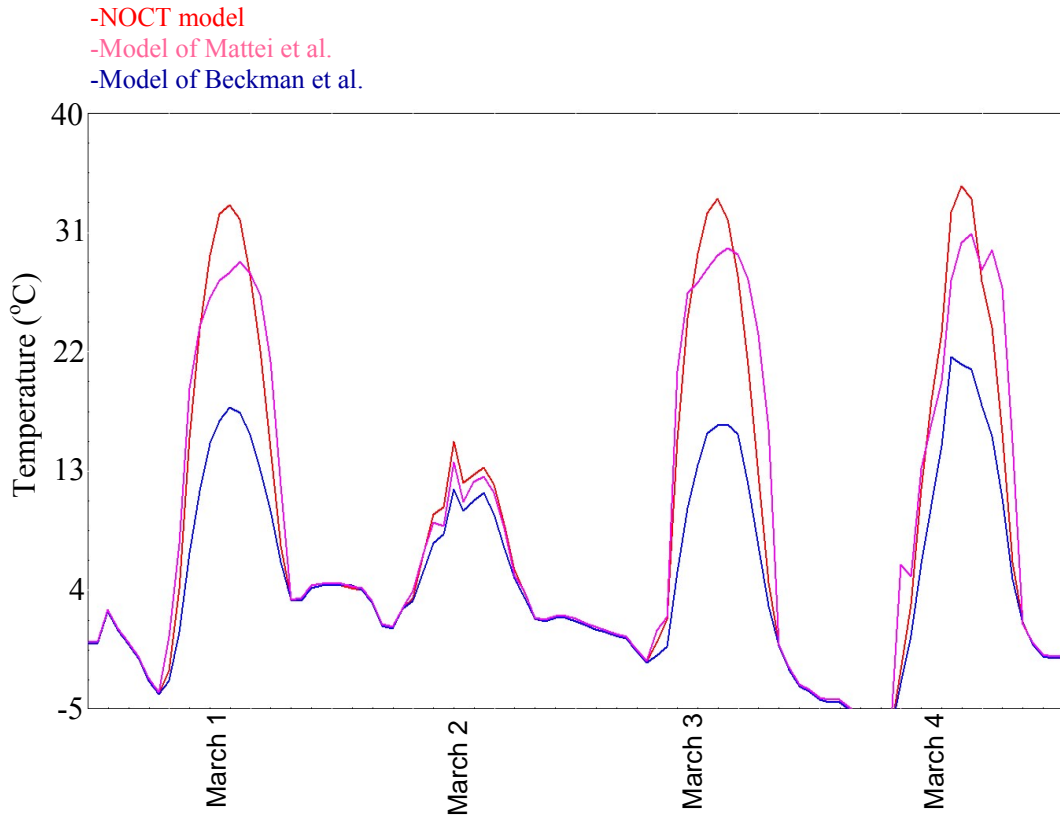
Figure 2-2: Cell temperatures for 3 different thermal models

2.1.3 Maximum Power Point Tracking Model

Maximum power point tracking is an algorithm that finds the optimum output voltage of the PV array that produces maximum available electrical power. It is essential for increasing the cell efficiency. The PV characteristic equation was given in the previous sections (Equation(2.6)) and the unknown parameters were evaluated.

$$I = I_{PH} - I_0 \left[\exp(\frac{(V + IR_S)}{n_S A V_t}) - 1 \right] - \frac{V + IR_S}{R_{SH}}$$

After finding the cell temperature for a given weather condition and modifying the parameters accordingly; dP/dV=0 should be solved to find the optimum voltage that yields to the maximum power.

21

$$\frac{dP}{dV} = \frac{d(IV)}{dV} = I + V\frac{dI}{dV} = 0 \qquad (2.26)$$

Solution algorithm for the MPPT is given in Figure 2-3. For the initial estimation of cell voltage, the cell current is evaluated from the characteristic equation then the derivative of cell power with respect to the voltage is calculated. If the derivative is lesser than zero, the cell voltage is larger than the optimum value and the calculations are repeated after the cell voltage is reduced by the defined step size. If the derivative is larger than zero, the cell voltage is lesser than the optimum value and the calculations are repeated after the cell voltage is increased by a defined step size. The process is repeated until the derivative of cell power with respect to voltage reaches 0.
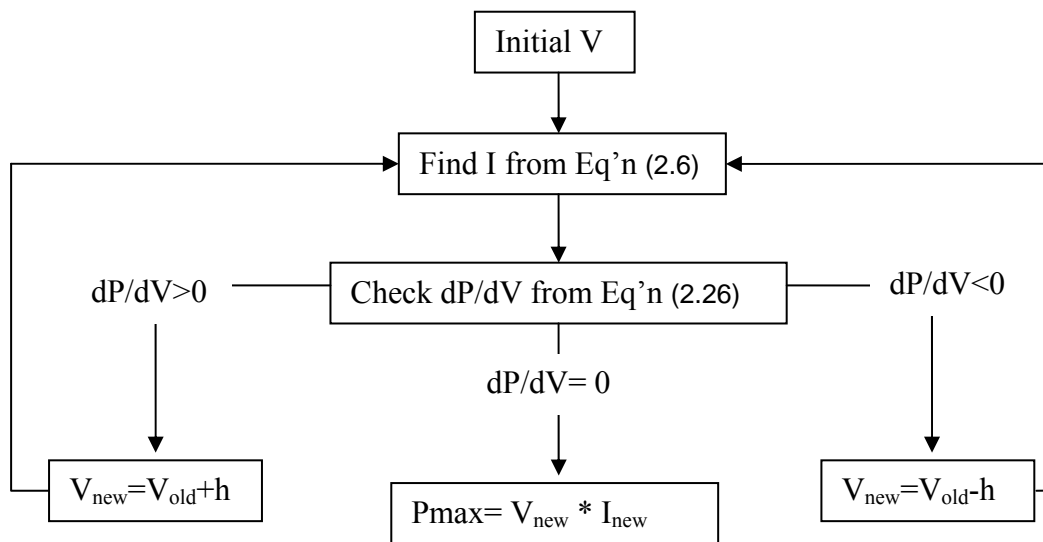
Figure 2-3. Flowchart of Maximum Power Point Tracking

2.1.4 PV Panel Model Results and Discussion

The model performance is compared with the experimental data of Kyocera 130W panels collected in Hidronerji building in Ostim/ANKARA. Manufacturer's data sheet of the panel is given in Appendix A. Fortran codes of the PV panel model are given

in Appendix B. Manufacturer's data sheet parameters, total radiation on the PV surface, the ambient temperature and the wind speed are the input of the model. Then, the model evaluates the output power, the voltage and current, the energy efficiency and the cell temperature.
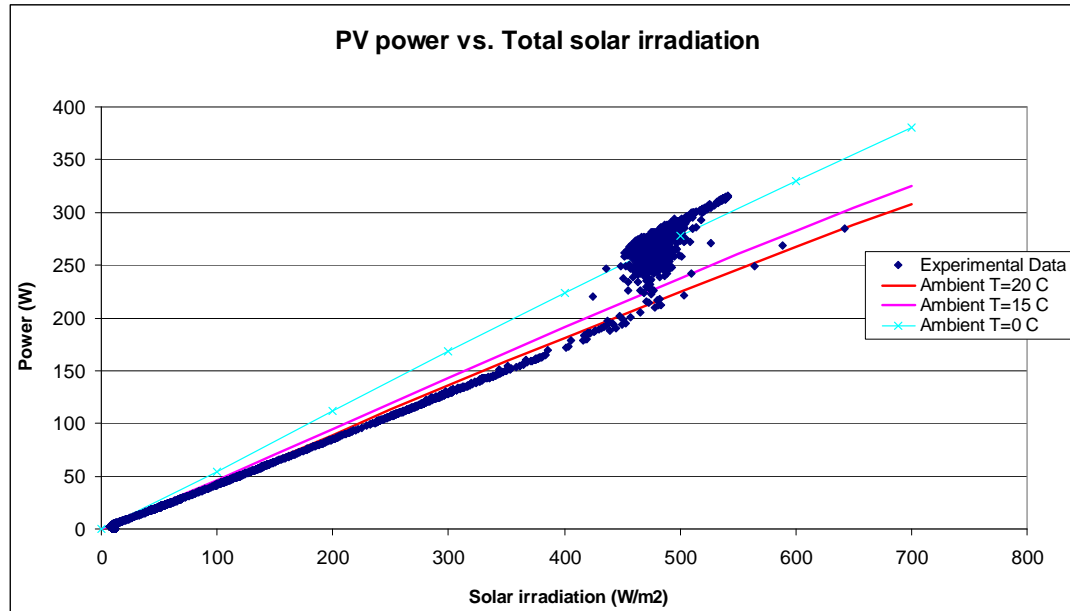
Figure 2-4 Output power vs. solar irradiation for Kyocera 130W

Figure 2-4 shows the comparison between the measured output power and output power of the numerical model with respect to total solar irradiation. There are 4 PV panels in Hidronerji. The connection setup of the PV panels is 2 in series and 2 in parallel. The output current and voltage are both doubled by this configuration. The data collected by Hidronerji does not include the thermal data such as ambient temperature, the wind speed and the cell temperature; therefore the experimental medium cannot be fully projected on the numerical analysis. Three different ambient temperatures are used during the simulation of the mathematical model. Variations in cell temperature and angle between the sun and the PV panels are the possible reasons of the variations in PV power between 450 W and 550 W total solar irradiation. Output voltage and current comparisons of the numerical model

with 15°C ambient temperature and experimental data are given in Figure 2-5 and Figure 2-6 respectively.
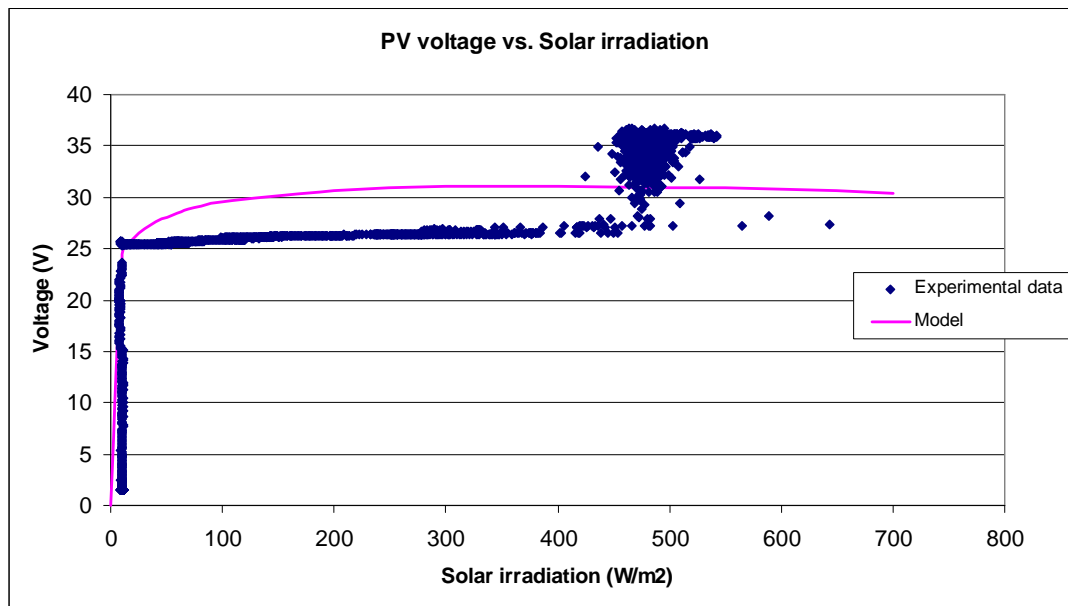
Figure 2-5 PV voltage vs. solar irradiation for Kyocera 130W

The model calculates the voltage at maximum power point greater than its actual value. Therefore the current at maximum power point of the model is calculated less than its actual value. The convergence criteria of the maximum power point algorithm is relatively coarse to decrease the computation time and prevent possible divergences and oscillations of the iterations over very different weather conditions throughout the simulation year. As a result, the accuracy of the voltage at maximum power point is not at desired position. Whereas; the effect of PV voltage on PV output power is relatively small around the maximum power point. At STC, manufacturer's data sheet offers 130W panel power and the numerical model evaluates 129.3W output power.
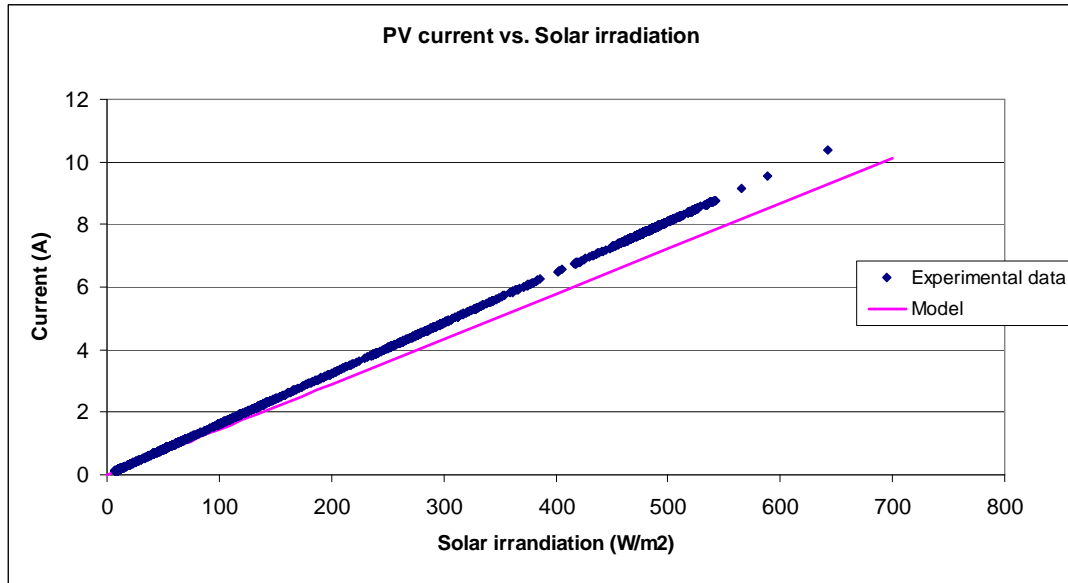
Figure 2-6 PV current vs. solar irradiation for Kyocera 130W

As it can be observed from Figure 2.4, the ambient temperature, therefore the cell temperature of the PV panel, affects the output power of the PV panel. In Figure 2-7, the effect of cell temperature on the output power can be seen. As the cell temperature increases, the output power is decreasing for a constant 1000 W/m^2 radiation. The decrease in output power is around 0.7% per ^{o}C. Figure 2-8 shows the comparison between the current-voltage characteristics of the numerical model and manufacturer's data sheet at 3 different cell temperatures. At 25°C cell temperature, where the parameters of the electrical model is calculated, the characteristics of the model and the characteristic supplied by the data sheet are consistent. On the other hand; as the cell temperature increases, the voltage of the numerical model decreases more rapidly than it is supposed to. The temperature dependencies of the parameters in the electrical model are based on literature, but it should be noted that Newton-Raphson method on systems of non-linear equation is an open method. The accuracy of the method highly depends on the initial estimate of the parameters and the nature of the equations. The parameters in the electrical model have different weights on the model performance. The derivatives of the equations with respect to shut resistance (R_{sh}) are close to zero which causes the performance of Newton-Raphson method drop.

25
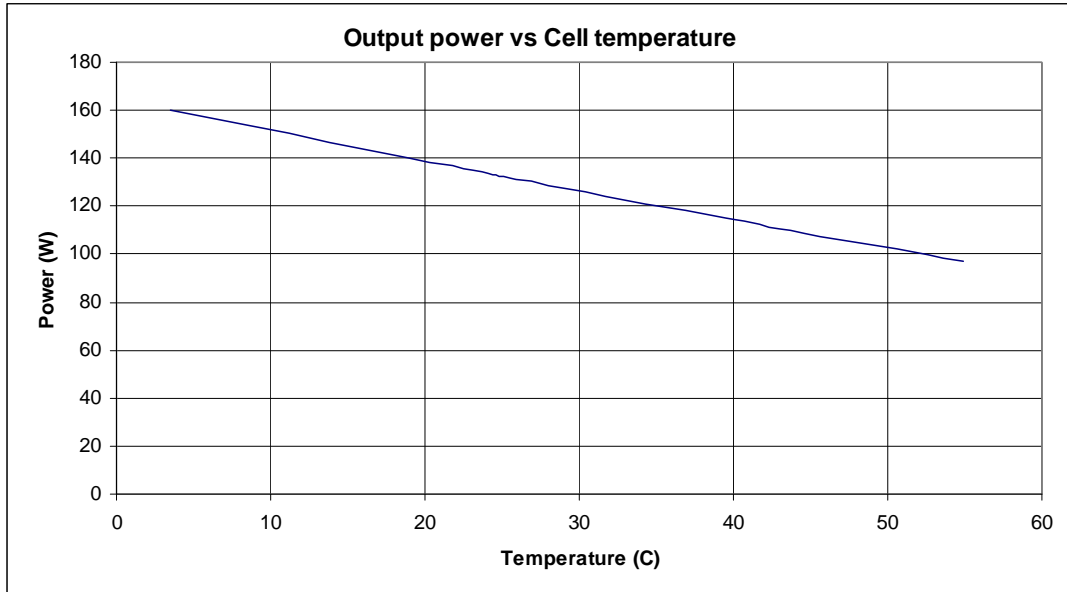
Figure 2-7 Output Power of the PV panel with respect to cell temperature
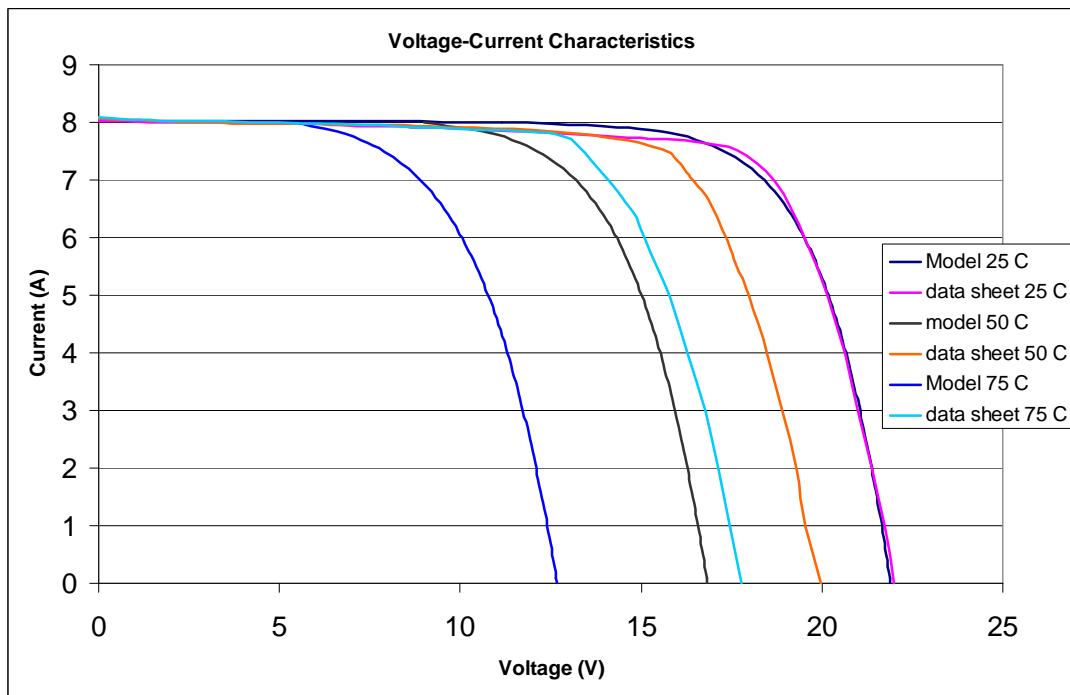
Figure 2-8 Current-voltage characteristics of the Kyocera 130W PV panel with respect to cell temperature

2.2 Proton Exchange Membrane (PEM) Electrolyzer

Separating water molecules into hydrogen and oxygen molecules by external electric current is called electrolysis of water. The total chemical reaction of water electrolysis is given below;

$2H_2O(l) + \text{Electrical energy} \rightarrow 2H_2(g) + O_2(g)$

For decomposition of water into hydrogen and oxygen to occur, a minimum potential difference needs to be applied to the electrodes. At standard conditions the minimum or reversible voltage is equal to $U_{rev}=-1.229V$. The absolute value of the voltage applied to the electrodes cannot be smaller than the absolute value of the reversible voltage. The negative voltage means Gibbs free energy is positive, ΔG includes thermal irreversibility $T\Delta S$, which for a reversible process is equal to heat demand. The reaction cannot occur without adding the necessary energy. The total energy demand (ΔH) is related to thermoneutral voltage which is equal to $U_{tn}=-1.482V$. The electrical energy demand (ΔG) varies with temperature and pressure, whereas the total energy demand (ΔH) remains almost constant [14]. Therefore, while reversible voltage varies with temperature and pressure, thermoneutral voltage remains constant. An electrolyzer cell uses only thermoneutral voltage for electrolysis process, the extra potential difference supplied to the cell generates heat. The energy efficiency of a cell is given below;

$$\eta = \frac{U_{tn}}{U_{cell}}$$

Alkaline solution is a common electrolyte used for water electrolysis and alkaline based electrolyzers cover the majority of the market. However, in this thesis Proton Exchange Membrane electrolyzers are modeled and used. PEM electrolyzers have various advantages over alkaline ones. One of the most important advantages is PEM electrolyzers can operate at high pressures up to 200 bar and this removes the compression stage of hydrogen which needs to be stored in tanks after the electrolysis. Compressing hydrogen inside the electrolyzer is an

isothermal process which is the most efficient way to compress hydrogen. PEM electrolyzers have less parasitic losses and higher efficiency than alkaline electrolyzers which also decreases the cost of hydrogen production.

In addition, highly pure hydrogen can be produced with a long life time by PEM electrolyzers. Since there is no chemical electrolyte such as KOH used, they are ecologically clean. Moreover, PEM electrolyzers have smaller sizes and mass because of the simple and compact design. On the other hand, there are also some disadvantages; high initial cost of equipment like the membrane cost and special alloys for the casings, pure water needs to be supplied, low efficiency at high pressures because of hydrogen permeation and safety issues at low loads in case of hydrogen mixing with oxygen. Since PEM fuel cells and electrolyzers use similar materials and have similar design, they have improving technology parallel to fuel cells.

The schematics of PEM electrolysis is given in Figure 2-9. Water molecules are split into oxygen and hydrogen at the anode by direct voltage which needs to be higher than thermoneutral voltage. Hydrogen atoms pass through the proton exchange membrane and forms hydrogen molecules at the cathode. The proton exchange membrane is a porous medium which only lets hydrogen atoms pass through. The electrodes are also porous and the flow fields are between electrodes and end plates.
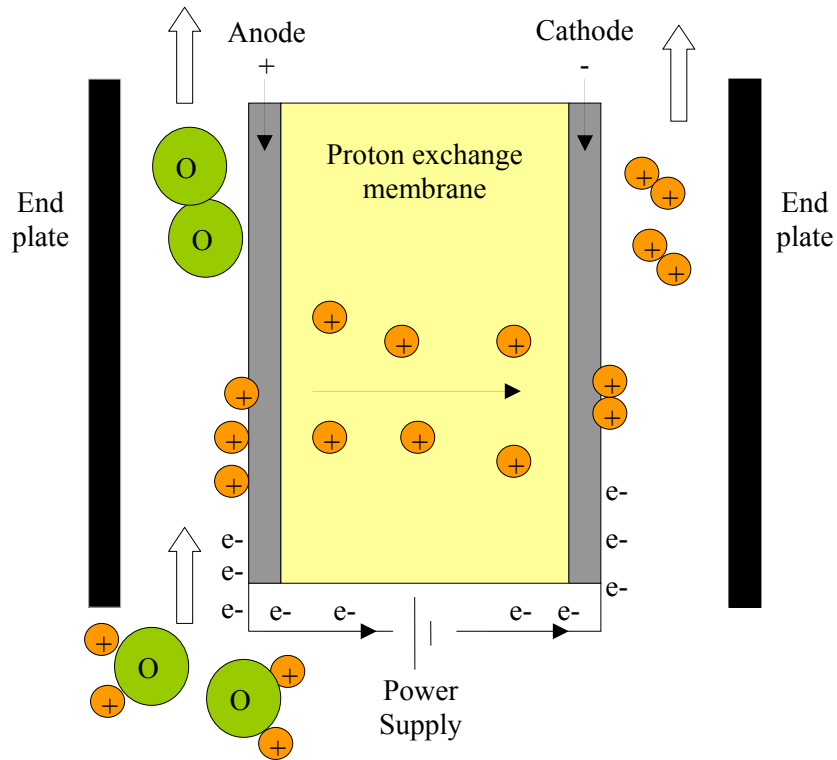
Figure 2-9 Schematics of PEM electrolysis

Mathematical modeling of a PEM electrolyzer is a developing subject in the literature. There are a few models available based on CFD techniques and softwares; but these models cannot be practically used for TRNSYS component modeling. PEM electrolyzer models used for the system simulations in the literature make use of experimental data to build a characteristic equation. Variables of the characteristic equations are the cell voltage, the current and the temperature. According to Faraday's Law of electrolysis, the molar quantity of hydrogen produced by the electrolysis is directly proportional to the quantity of electric charges transferred during the process. If the current across an electrolyzer cell is known, it is possible to evaluate hydrogen and oxygen production. Since the performance of different PEM electrolyzers varies to a large extent, every model in the literature is unique and cannot be used to simulate other electrolyzers.

2.2.1 Electrolyzer Description

In this study, a circular shaped PEM electrolyzer manufactured in Niğde University is modeled. Measured voltage-current isotherm curves of the electrolyzer are given in Figure 2-10. The electrolyzer is rectangular shaped with 10cmx10cm side lengths. There is not any cooling system used except the natural convection with 20°C ambient temperature during the conducted experiments. The ambient temperature is assumed to be constant for the working environment of the model as well.
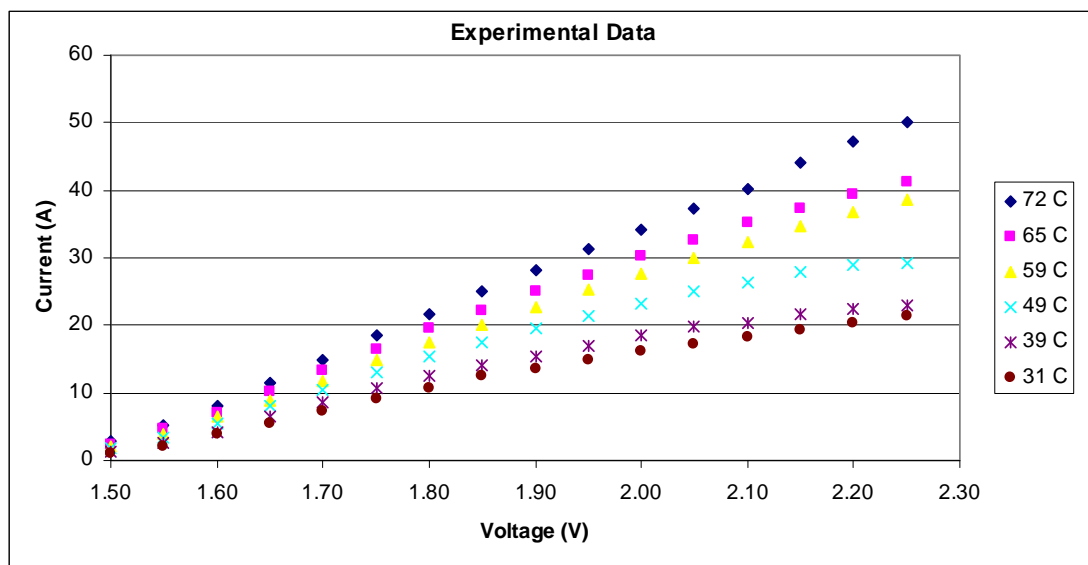
Figure 2-10 Voltage-current-temperature characteristic of PEM electrolyzer

The efficiency of an electrolyzer at low voltage levels is high. However, the characteristic curves show that current drawn by the electrolyzer is very low at low voltage levels which means hydrogen production is low as well. At high voltage levels, the electrolyzer draws high current and produces a large amount of hydrogen. On the other hand, efficiency of the electrolyzer drops very much and the great amount of heat generated creates new problems in heat management. Also high cell temperature damages the equipment and decreases life time. Therefore, the manufacturers recommend operating the electrolyzer at constant 2V potential and cell temperatures around 50°C.

2.2.2 Electrolyzer Modeling

Butler-Volmer equation describes the relation between the electrode current and potential where cathodic and anodic reaction occurs on the same electrode, the equation is given below;

$$I = I_{0e} \left\{ \exp\left[\frac{(1-\alpha_e)n_eF}{RT}(U-U_{eq}) \right] - \exp\left[-\frac{\alpha_e n_eF}{RT}(U-U_{eq}) \right] \right\} \qquad (2.27)$$

where;

F=96 485.34 C.mol^{-1}
R=8.31447 J/mol.K
U_{eq}=1.482 V
n_e=2

The equation above can be applied to water electrolysis. By using the experimental data acquired by Niğde University unknown parameters in Butler-Volmer equation which are I_0, α and U_{eq} can be defined. Non-linear curve fitting software, NLREG [28], is used for this purpose and the results obtained are checked for their effectiveness. The results show that symmetry factor (α_e) can assumed to be constant since the differentials are almost zero with respect to temperature, but the exchange current is highly dependent on the temperature. The parameters are found to be;

$$I_{0e} = -19242.33 + 68.572T \ (A)$$

$$\alpha_e = 0.97092$$

It should be noted that these values are not unique because of the nature of the curve fitting process. The correlation coefficient of this characteristic assumption, which defines the effectiveness of the evaluation, is equal to 93.5%. Voltage-

current isotherm curves evaluated from the electrolyzer model are given in Figure 2-11.

Hydrogen production rate of an electrolyzer is given by Faraday's Law;

$$\dot{n}_{H_2} = \frac{N_{cell} I_{el}}{nF} \eta_F$$

Faraday efficiency (η_F) is the relation between the theoretical electron transfer and actual electron transfer in an electrochemical reaction. There are different formulas offered in the literature for the Faraday efficiency, for most of the cases it is taken as a constant number close to 1. Determining Faraday efficiency from the experimental data is more reliable. Since an essential equipment to produce dry hydrogen is not available in Niğde University, it is not possible to define Faraday efficiency experimentally for the electrolyzer modeled.
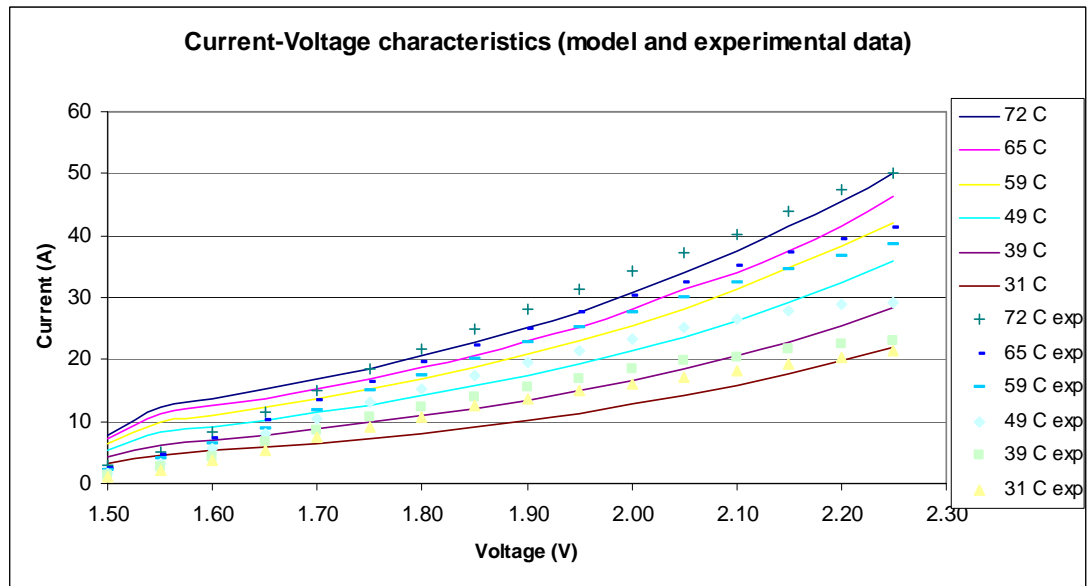
Figure 2-11. Voltage-current-temperature characteristic of PEM electrolyzer

The model requires the parameters of the characteristic equation defined and asks for the cell voltage, the optimum temperature, the maximum temperature, the

number of series connected cells in a stack, total number of parallel connected stacks and power supplied to the electrolyzer. The model first evaluates the maximum power that the electrolyzer operate at from the given inputs number of cells, number of stacks and maximum temperature. If the power supplied is greater than maximum power, the extra power is dumped away. The model tries to operate as close as possible to optimum temperature provided by the user. With respect to supplied electrical power, the number of electrolyzer stacks in operation is optimized to have the cell temperature as close as possible to optimum temperature. By this way, electrolyzer produces a respectable amount of hydrogen with decent efficiency and temperature. 50°C optimum temperature and 2V cell voltage is selected for the simulations as the manufacturers offer. FORTRAN code of the model is given in Appendix C.

CHAPTER 3

SYSTEM SIMULATIONS

System simulations are conducted with TRNSYS. PV panel and PEM electrolyzer models have been implemented in the software. Together with the user-defined and default components, a solar stand alone power system is simulated. Different system scenarios and component sizes are tested for yearly simulations.

3.1 System Description

Emergency room of the hospital is the user. Electric demand of the user is assumed to be 5kW between 6:00 and 24:00 hours and 2kW for the rest of the day. Figure 3-1 shows the load profile. Fluctuations in the load are neglected. The total electric demand of the user is 37.23 MWh in a year. The average efficiency of Kyocera 1300 PV panels is around 12%. If the average efficiency of the fuel cells and the electrolyzers are assumed to be around 40% and 70% respectively, with DC/AC converters having 90% efficiency, the total system is expected to have around 5% energy efficiency. The energy efficiency is defined as the ratio of the final electricity supplied to the user to the total amount of solar energy falling on the PV panels. In the literature; a similar system modeled by Santarelli et al. [17] has 4.7% energy efficiency, a stand alone power system built for a residential house by Hollmuller et al. [5] is announced to have 3.6% efficiency. Kelly et al. [13] uses such a system to produce hydrogen, the system's energy efficiency is claimed to be 8.5% the highest efficiency recorded for similar systems. There are more examples available in the literature. With an initial 5% energy efficiency assumption, there should be a yearly average of 745 MWh solar radiation incident on the PV surfaces.
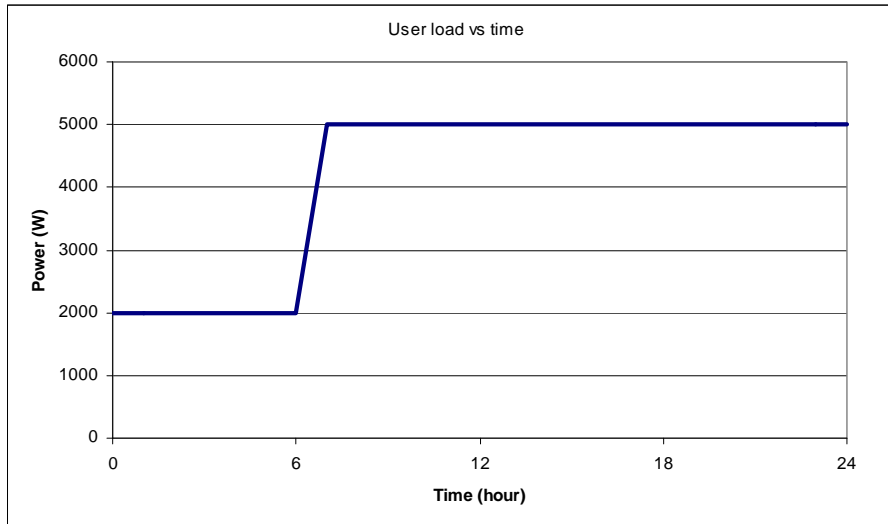
Figure 3-1. Load profile

Typical Meteorological Year (TMY) data is used in the models. A simple average of the yearly data underestimates the amount of variability, so the month that is most representative of the location is selected. For each month, the average radiation over the whole measurement period is determined, together with the average radiation in each month during the measurement period. The data for the month that has the average radiation the closest to the monthly average over the whole measurement period is then chosen as the TMY data for that month. This process is then repeated for each month in the year. The months are added together to give a full year of hourly samples. "TMY 2" is called for the second edition of TMY data. The weather data for "TMY 2" is collected between 1961 and 1990. TMY2 data file exists in default TRNSYS folders provided by Meteonorm [29]. The solar data for Ankara provided by TRNSYS suggests that 440m^2 horizontal area is needed to provide the desired amount of solar radiation. On the other hand, 390m^2 area having 30° surface slope with horizontal axis or 405m^2 area having 50° surface slope with horizontal axis is enough to cover the same amount of solar radiation. Table 3-1 shows the monthly and total energy production of a single PV panel with respect to surface slopes. The maximum total amount of energy is generated by 30° surface slope. Production in summer months is higher than in winter months for 30° surface slope. Since solar irradiation in the summer months

35

is high, PV panels can meet the load power without difficulty during day times and the extra energy is used to produce and store hydrogen for later use. However, in winter months solar irradiation is low and PV panels operate only a few hours a day. The stored hydrogen during summer months is the main electricity supply during the winter months. Table 3-1 shows that as the surface slope increases, the amount of electricity generated is increasing as well in the winter months. This brings the idea of assembling the PV panels with higher surface slope might increase the system performance by increasing electricity produced in winter months. With 50° surface slope PV panels produce more energy in winter while maintaining fair amount of production in summer.

Table 3-1 PV surface slope and monthly energy production (kWh)

Months	PV Surface Slope						
	0	10	20	30	40	50	60
January	1055.0	1307.7	1527.4	1706.4	1839.5	1922.0	1951.1
February	1456.2	1702.2	1903.3	2055.9	2154.7	21965	2179.5
March	2571.3	2853.0	3064.1	3197.2	3247.7	3213.6	3095.9
April	3481.9	3699.0	3821.5	3843.7	3764.7	3590.4	3325.5
May	4515.1	4646.5	4597.0	4464.4	4215.0	3870.3	3437.1
June	5058.5	5105.5	5013.1	4797.2	4455.4	3997.0	3464.4
July	5507.7	5604.9	5552.6	5354.5	5005.1	4513.5	3933.6
August	4910.7	5164.4	5276.5	5241.5	5058.2	4740.6	4305.6
September	3660.9	4052.9	4336.6	4501.9	4542.5	4456.7	4247.3
October	2509.7	2956.9	3327.3	3609.1	3791.6	3868.5	3836.7
November	1479.7	1741.8	2153.1	2406.5	2594.2	2710.2	2750.5
December	889.6	1098.8	1280.1	1427.5	1536.6	1604.4	1628.8
Total	37096.3	39933.6	41852.6	**42605.8**	42205.2	40683.7	38156.0

The simplified TRNSYS model of the system is shown in Figure 3-2. First priority of PV panels is to directly supply electricity to the user. If PV power is greater than

the load, the extra power is supplied into the battery pack or the electrolyzer. First priority of excess energy is charging the battery pack for the systems with battery pack. The battery pack stores and discharges electrical energy with high efficiency. The electrolyzer produces hydrogen and supplies it into the hydrogen tank until the maximum pressure limit in the tank is reached. If PV generates power more than the combination of the user load and electrolyzer need, the extra power is dumped out. When PV power is not enough to supply electricity to the user, the fuel cells and/or the battery pack covers the deficient power depending on the control parameters. The fuel cells use the stored hydrogen and ambient air. DC/AC inverters are used between the fuel cells and the user as well as between the PV panels and the user since both PV panels and fuel cells generate direct current electricity. If there is more hydrogen left in the tanks than the initial hydrogen in the tanks at the end of the year, the initial hydrogen of the next year will be the final hydrogen of the last year. Energy flow chart is given in Figure 3-3 and energy flows are explained in Table 3-2. Energy flows are explained below;
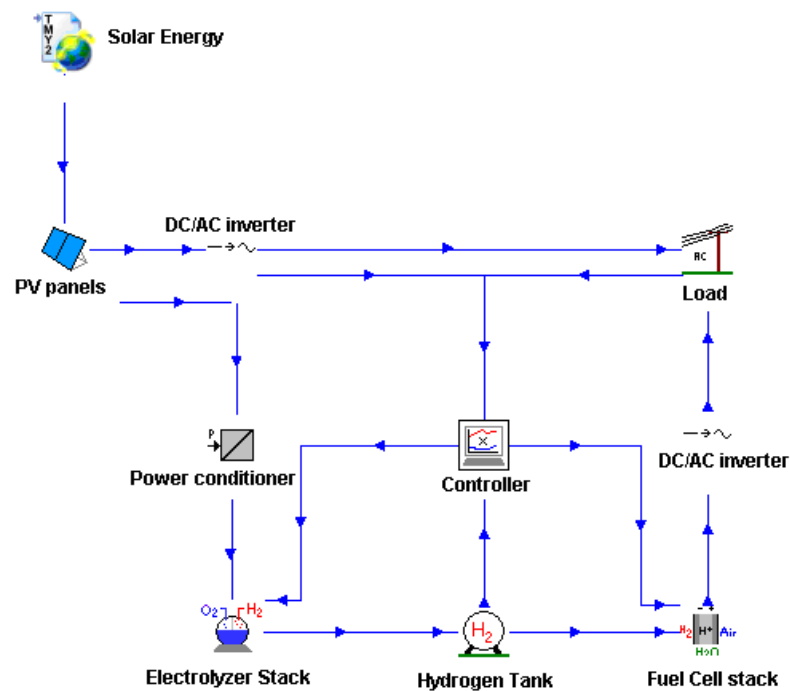
Figure 3-2 TRNSYS schematics of the system
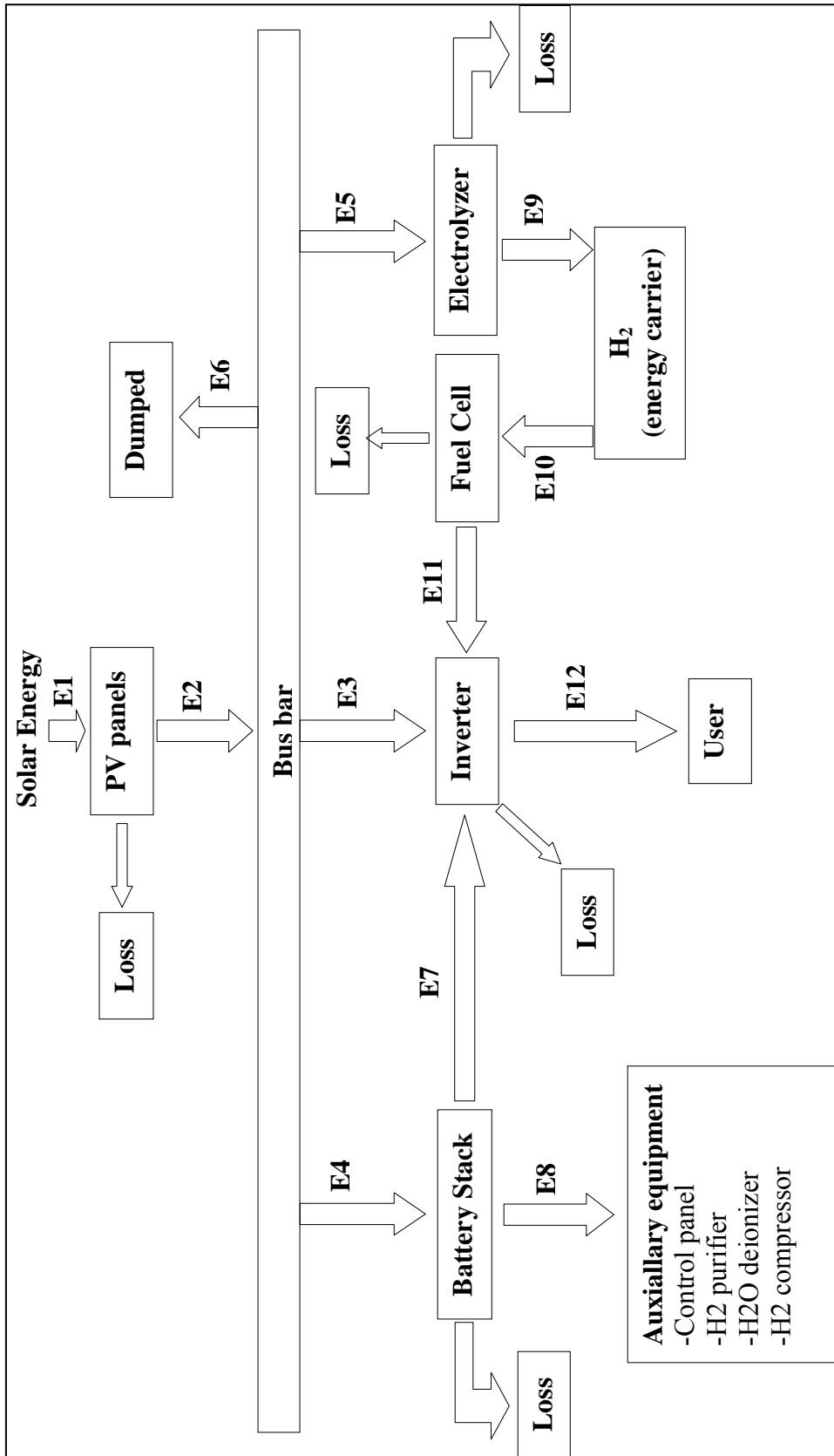
Figure 3-3 Energy Flow chart in the system

Table 3-2 Descriptions of the energy flows in the system

E1	Total solar radiation over the PV surfaces
E2	Energy produced by PV array
E3	Energy supplied from PV array to user inverter
E4	Energy supplied from PV array to battery pack
E5	Energy supplied from PV array to electrolyzer stack
E6	Extra energy dumped from PV array
E7	Energy supplied from battery pack to user inverter
E8	Energy supplied from battery pack to auxiliary equipment
E9	Energy capacity of hydrogen produced by electrolyzer stack based on Lower Heating Value (LHV) of H_2
E10	Energy capacity of hydrogen spent by the fuel cell based on Lower Heating Value (LHV) of H_2
E11	Energy supplied from fuel cell stack to user inverter
E12	Energy given to user from the inverter

3.2 Results and Discussions

3.2.1 Systems without battery storage

In this section, the simulations do not include a battery pack and auxiliary equipment in the systems. All excess energy is spent for generating hydrogen and only the fuel cells supply electricity when PV power is not enough. System simulations are conducted in 2 different PV surface slopes; 30° and 50°. The system parameters are shown in Table 3-3. Electrolyzer stack size is large to benefit from all the extra energy produced by the PV panels, so that as much as possible hydrogen is produced during day times. Each stack has 50 electrolyzer cells in series. Nominal power consumption of the total electrolyzer stack is 25kW with 50^oC cell temperature and maximum power consumption is 33kW with 80^oC cell temperature. Output power of the PV panels, the load and the pressure level in the hydrogen tanks are provided to the controller as inputs.

Table 3-3 System parameters

PV panels	Number of panels: 375
	Total surface area: 355 m^2
PEM Electrolyzer stack	Nominal power consumption: 25kW
	Number of stacks: 10
PEM Fuel Cell stack	Maximum power production: 7kW
	Total number of cells: 85
Hydrogen tanks	Maximum pressure: 95 bar
	Total volume: 35 m^3
	Initial pressure level: %5

Power output of the PV panels is shown in Figure 3-4. Each panel has 0.9467 m^2 area, 30° surface slope with respect to ground and 0° azimuth angle. During the summer days panels operate for long hours and produce high amount of energy. During the winter days when the panels are operating, power output is close to summer days. Whereas the operating times are much shorter and panels produce less energy.
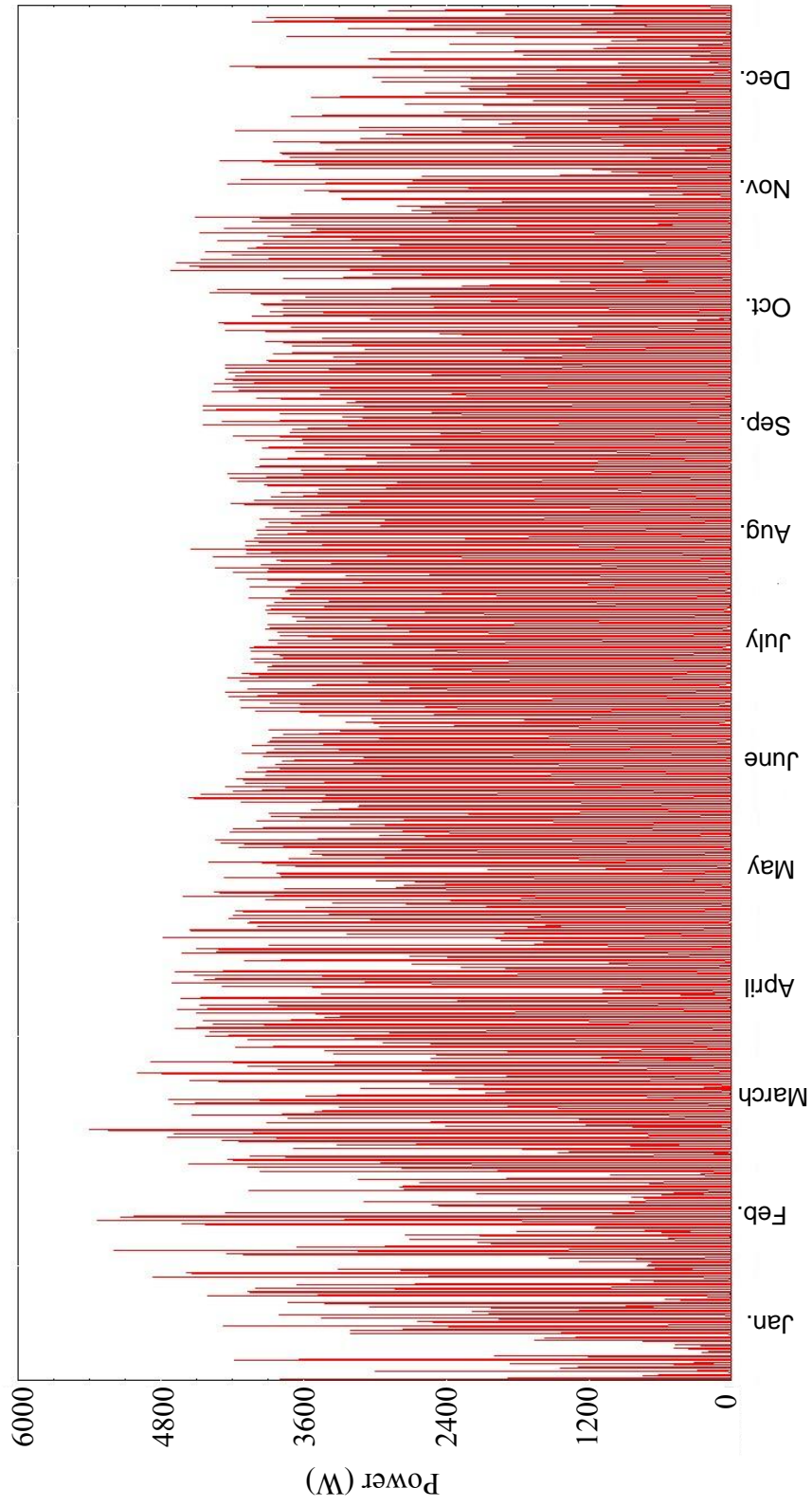
Figure 3-4 Power output of PV panel

41

The power profile of the system components for two sample days is shown in Figure 3-5a and 3-5b. Figure 3-5a shows the power profile for a typical sunny summer day. Until 5:00 there is not any solar power is available, therefore the fuel cell supplies the necessary power to the user. It produces 11% more power than the load because of the inverter losses. After 5:00 the PV panels begin to generate electricity. Until around 6:00 both PV and fuel cell provides electricity to the user, then fuel cell stack turns off and PV panels supply electricity. The extra power produced by the PV panels between 6:00 and 18:00 supplied to the electrolyzer stack. After 18:00 pm fuel cell stack starts up again and produces electricity during the night hours. Pressure level in the hydrogen tank is a worthy indicator of system performance. If the pressure level of the tank at the end of the year is equal to or greater than the initial pressure level, it means the system does not need any external energy supply to maintain. Figure 3-5b shows the power profile for a typical cloudy winter day. The amount of available solar power and the number of sunny hours is much less than a summer day. During the day times, the PV panel output power is usually less than the load power. As a result, the fuel cell stack operates for longer hours and there is enough power to operate electrolyzer stack only for a very short period of time.
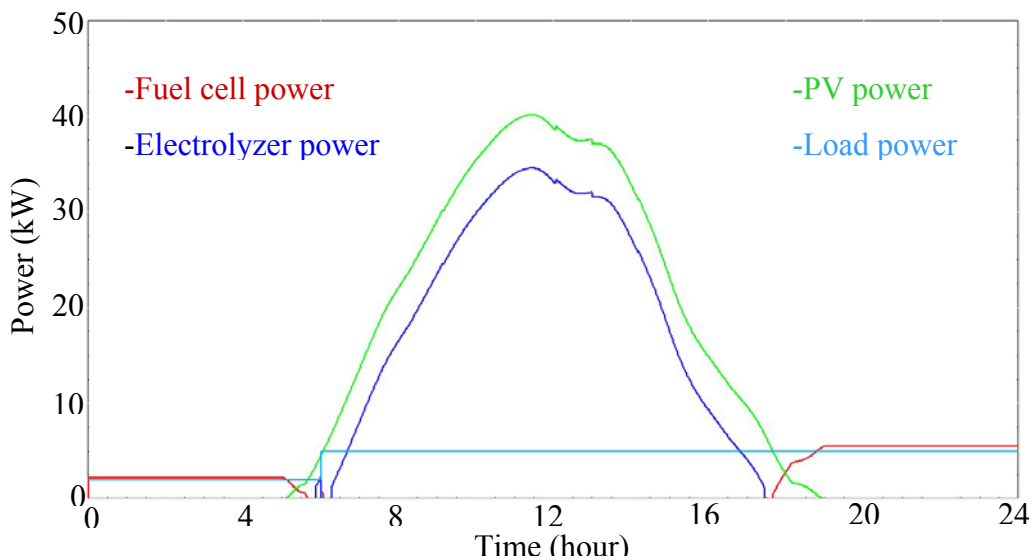
Figure 3-5a Power profile of the components for a summer day
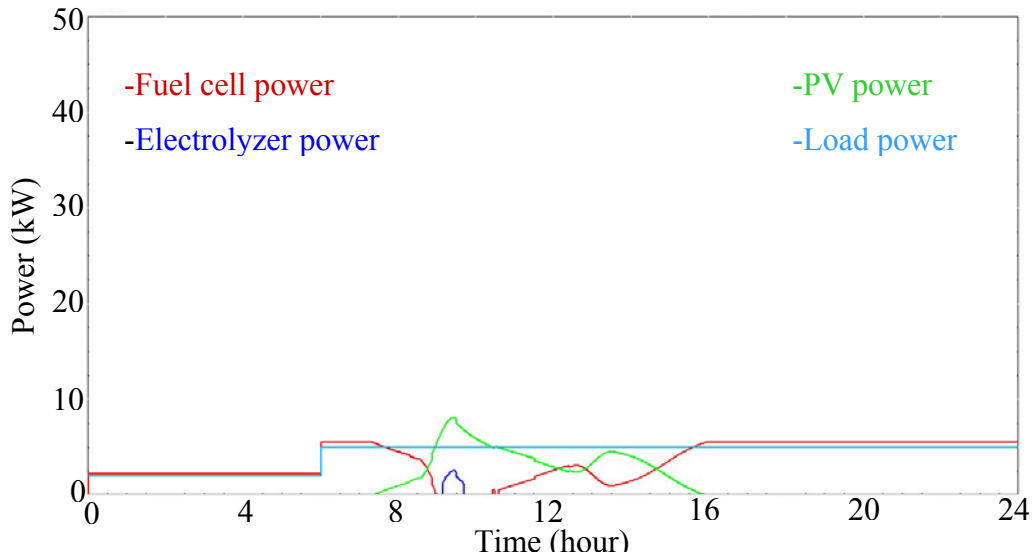
Figure 3-5b Power profile of the components for a winter day

Deck files of the system elements can be found in Appendix D. There are different system simulations for different PV, electrolyzer and hydrogen tank sizes. The simulations start from April 1 and end exactly a year later. Table 3-4 shows the component parameters for the different systems simulated. H_2 balance is the difference between the pressure in the hydrogen tank at the end of the simulation year and at the beginning of the simulation year. Pressure level in the hydrogen tank is a worthy indicator of system performance. If the pressure level of the tank at the end of the year is equal to or greater than the initial pressure level, it means the system does not need any external energy supply to maintain. Annual energy flows between the components for different systems are given in Table 3-5.

Figure 3-6 shows the pressure in hydrogen tank throughout the year for system 1. The initial pressure in the tank is 10 bar and at the end of the simulation year it is 1 bar. Since there is a 9 bar pressure deficit in the tank, the initial pressure is selected as 10 bar to prevent the system failing during winter days.

$$Energy\ efficiency = \frac{Output\ energy + stored\ energy}{Input\ energy}$$

43

The output energy is the energy supplied to the user (defined as E12 in Table 3-2) who needs 37.23 MWh annual energy. Stored energy is the given under the H_2 balance column in Table 3-4 or it can be calculated from the difference between E9 and E10 in Table 3-5. The input energy can be defined in two different ways: for overall efficiency, solar irradiation (E1) is used and for "electricity cycle" efficiency, energy supplied to the cycle by PV panels (E2) is used. The total amount of solar energy irradiating the PV surface (E1) is 682.22 MWh for System 1. The difference between E9 and E10 is -0.9 MWh which means hydrogen deficit inside the hydrogen tank. Energy supplied to the user (E12) is constant 37.23 MWh for all systems since the user load profile is the same for all systems. The overall energy efficiency of the system is then 5.33%.

Table 3-4 Component sizes for different systems

System no	Number of PV panels	PV area (m^2)	PV surface slope	Number of electrolyzer stacks	H_2 Tank size (m^3)	H_2 balance (bar/MWh)
1	375	355.0	30°	10	35	-9.0/0.88
2	375	355.0	30°	15	35	-0.2/0.02
3	385	364.5	30°	15	35	+8.2/0.8
4	385	364.5	30°	15	40	+12.8/1.25
5	385	364.5	50°	15	40	-7.1/0.69
6	400	378.7	50°	15	40	+11.5/1.13
7	400	378.7	30°	15	40	+21.1/2.06
8	400	378.7	$20^o/55^o$	15	40	+31.1/3.04
9	375	355.0	$20^o/55^o$	15	40	+17.1/1.67
10	365	345.5	$20^o/55^o$	15	40	+3.8/0.37

In the system 1, energy produced by the PV panels is equal to 86.04 MWh. The electricity cycle efficiency is then 42.22%. Figure 3-7 shows the electrolyzer power consumption. It can be observed from the figure that the electrolyzer operates at

the maximum allowable power of 33kW and at the maximum allowable temperature of 80°C for long hours. As a result of this, the efficiency of electrolyzer and the electrolyzer life-time drop because of the high cell temperature. Also 1.52 MWh energy is dumped from the electrolyzer stack to avoid further heating in the cells. These losses can be reduced by increasing the number of stacks, but it will increase the initial cost of the system as well.

Table 3-5 Annual energy flows for different systems in MWh (refer to Table 3.2)

Sim. no	E1	E2	E3	E4	E5	E6	E7	E8	E9	E10	E11	E12
1	682.22	86.04	20.85	0	65.19	0	0	0	37.91	38.78	20.52	37.23
2	682.22	86.04	20.85	0	65.19	0	0	0	38.77	38.78	20.52	37.23
3	700.42	88.33	20.90	0	66.39	1.04	0	0	39.49	38.69	20.47	37.23
4	700.42	88.33	20.90	0	67.43	0	0	0	40.10	38.69	20.47	37.23
5	673.07	85.34	20.56	0	64.77	0	0	0	38.52	39.31	20.80	37.23
6	699.29	88.66	20.64	0	68.02	0	0	0	40.44	39.17	20.73	37.23
7	727.71	91.77	20.97	0	68.74	2.06	0	0	40.89	38.56	20.40	37.23
8	752.35	95.05	21.03	0	70.45	3.57	0	0	41.88	38.46	20.33	37.23
9	705.33	89.11	20.92	0	68.19	0	0	0	40.56	38.67	20.45	37.23
10	686.52	86.73	20.87	0	65.86	0	0	0	38.18	38.76	20.50	37.23

46
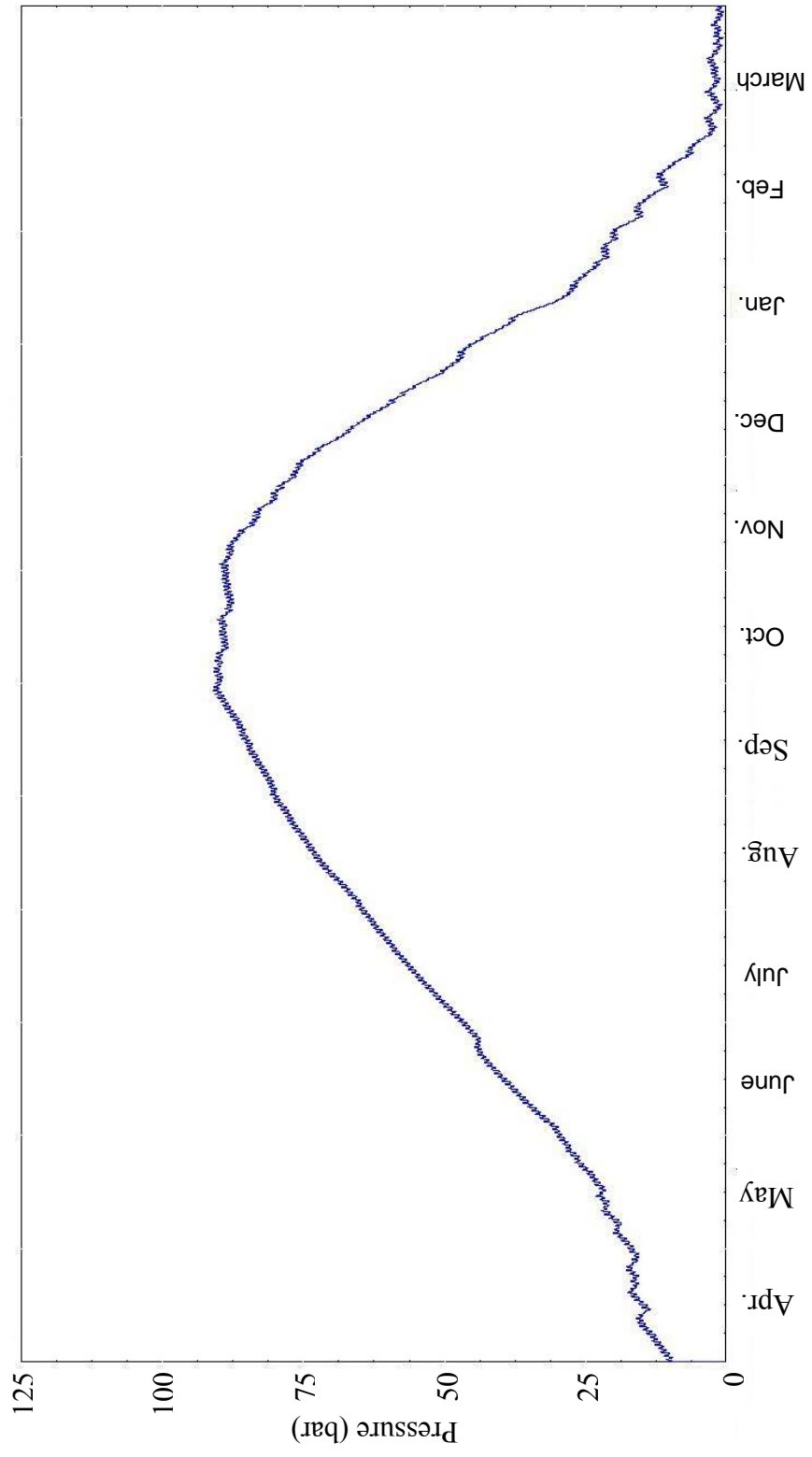
Figure 3-6 Pressure in hydrogen tank for system 1
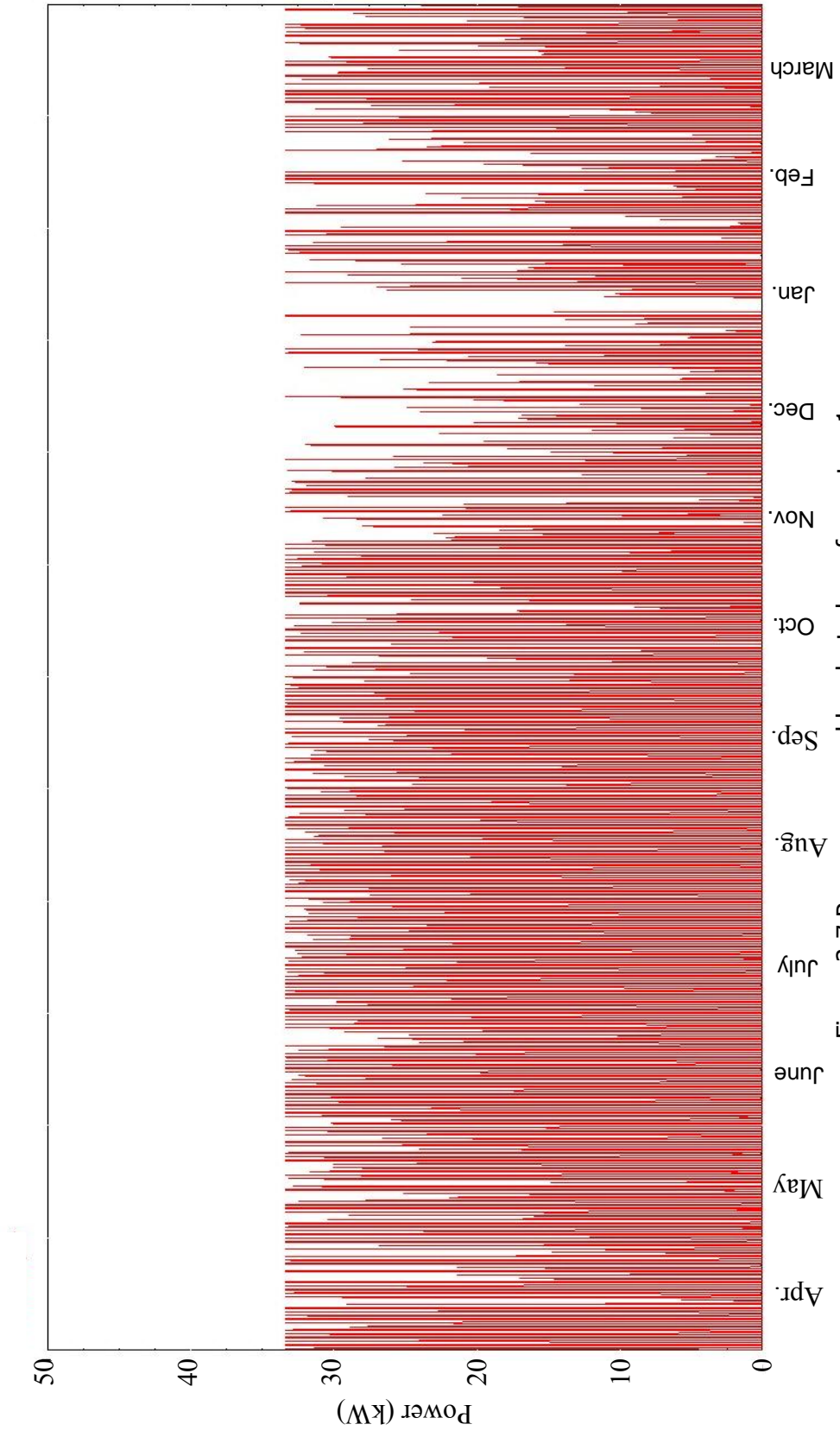
Figure 3-7 Power consumed by electrolyzer for system 1

If 5 more electrolyzer stacks are added to the previous system, the nominal power of the electrolyzer stack increases to 37.5kW and maximum allowable power increases to 50kW. Figure 3-8 shows the pressure level in the hydrogen tank with respect to time. At the end of the simulation year, there is 4.8 bar of hydrogen in the tank. The initial pressure in the hydrogen tank was set back to 5 bar since the hydrogen deficit does not cause any failure during winter days. Energy flow of System number 2 can be examined from Table 3-4. Total hydrogen produced by the electrolyzer stack has 38.77 MWh energy potential based on LHV, whereas hydrogen spent by the fuel cell stack has 38.78 MWh energy potential. Since the weather data used in these simulations are TMY data, it is expected to have different solar irradiation over the years. It is highly possible to have more cloudy days than expected which would make such a closely balanced system fail to provide electricity to the user during winter days. Therefore, it is recommended to have backup hydrogen in the tanks. Figure 3-9 shows the cell temperature of the electrolyzers. It can be observed that the electrolyzer temperature stays around the nominal temperature for the majority of the time, so that the power also stays around the nominal value.
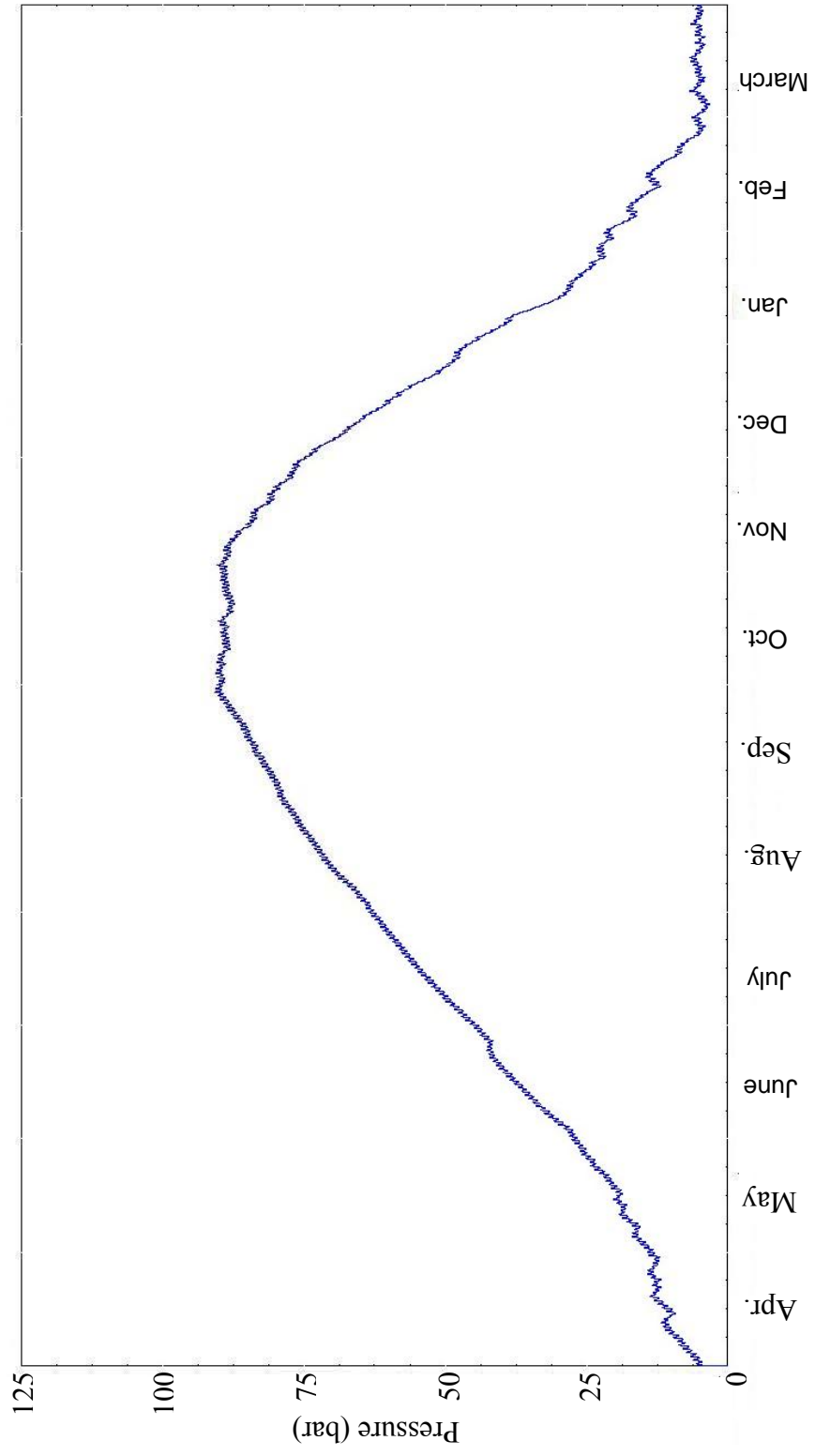
Figure 3-8 Pressure in hydrogen tank for system 2
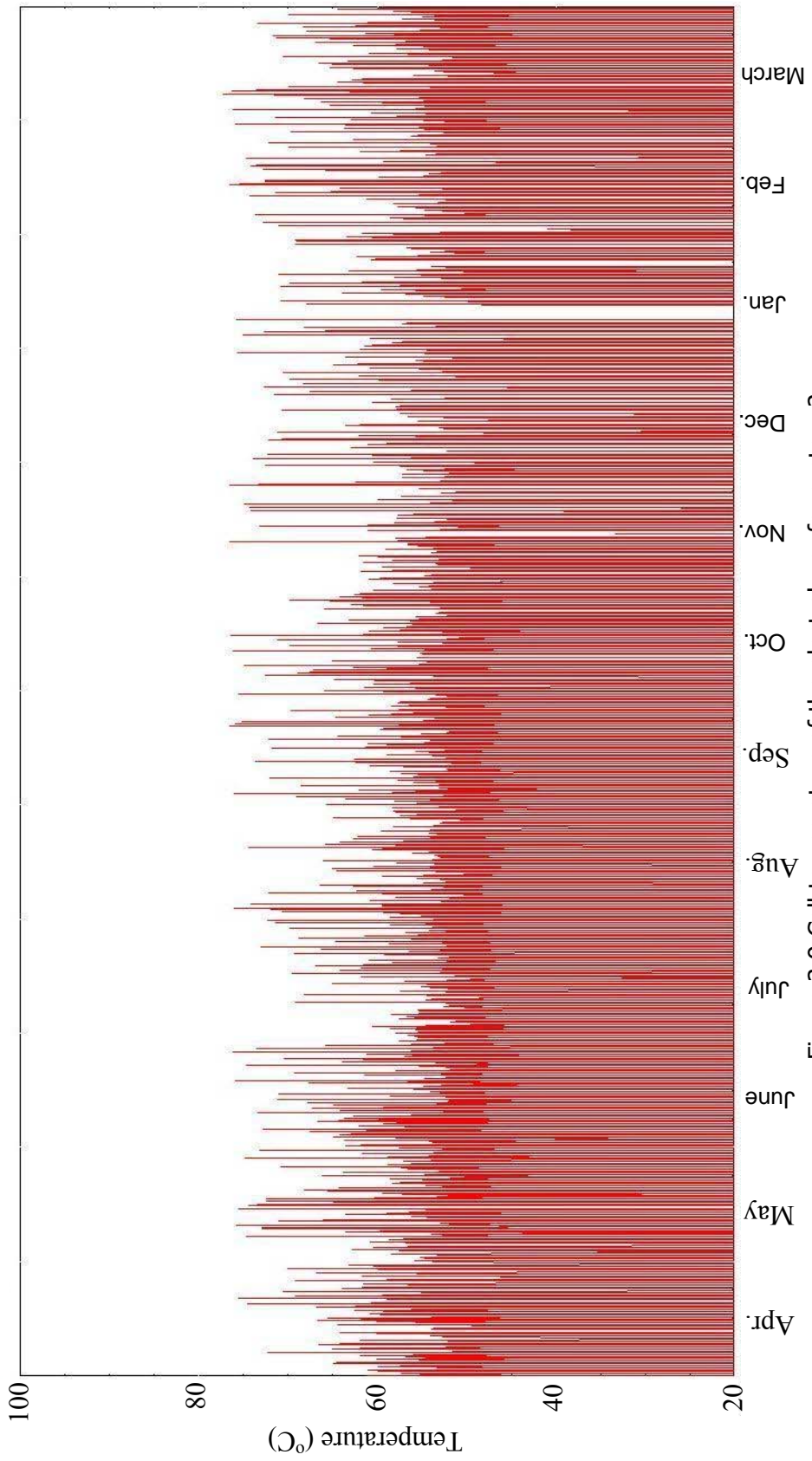
Figure 3-9 Cell temperature of the electrolyzer for system 2

In system 3, the number of PV panels is increased by 10 to a have positive hydrogen balance at the end of the year. Pressure inside the hydrogen tank is given in Figure 3-10 for system 3. During September tank pressure reaches its maximum allowable value of 95 bar and 1.04 MWh energy is dumped by the controller. The overall energy efficiency and electricity cycle efficiency are 5.43% and 43.05% respectively. There is 13.2 bar pressure in the tank at the end of the year which is 8.2 bar more than the initial pressure inside the tank which can be further increased if the tank capacity is larger.

40 m^3 hydrogen tank with 95 bar maximum allowable pressure is used for system 4. There is 17.8 bar pressure inside the hydrogen tank at the end of the simulation year. The amount of hydrogen spent by the fuel cells is the same with system 3 but the electrolyzers produce 206 Nm^3 (Nm^3 is the volume of the gas calculated at normal conditions which are 273K and 1 Atm) more hydrogen than the previous system. The overall energy efficiency and electricity cycle efficiencies are 5.49% and 43.56% respectively. They are slightly higher than the ones in the previous system, since the dumped energy is equal to 0 for this system.

Assembling PV panels with a higher surface slope increases the energy production during winter months. PV panels are assembled to have 50° surface slope for system 5, the other system parameters are the same with the previous system. This system runs out of hydrogen in the middle of February and cannot supply electricity from the fuel cell stack to the user. Therefore, initial pressure inside the hydrogen tank is selected as 20 bar to be able to simulate the whole year. Figure 3-11 shows the pressure inside the hydrogen tank for this system. The pressure inside the hydrogen tank is 12.9 bar at the end of the simulation year which means the system is not able to sustain the user's needs without external energy supply to the system. Total solar irradiation on the PV surfaces is 3.9% less when the PV panels have 50° surface slope with horizontal instead of 30° surface slope. PV panels produce (E2) 85.34 MWh energy in system 5 while it is 88.33 MWh in system 4. 23.3% of the PV energy is directly supplied to the user (E3) in system 4, this ratio is 24.1% in system 5. It is more efficient to supply energy directly to the user instead of using the hydrogen cycle.
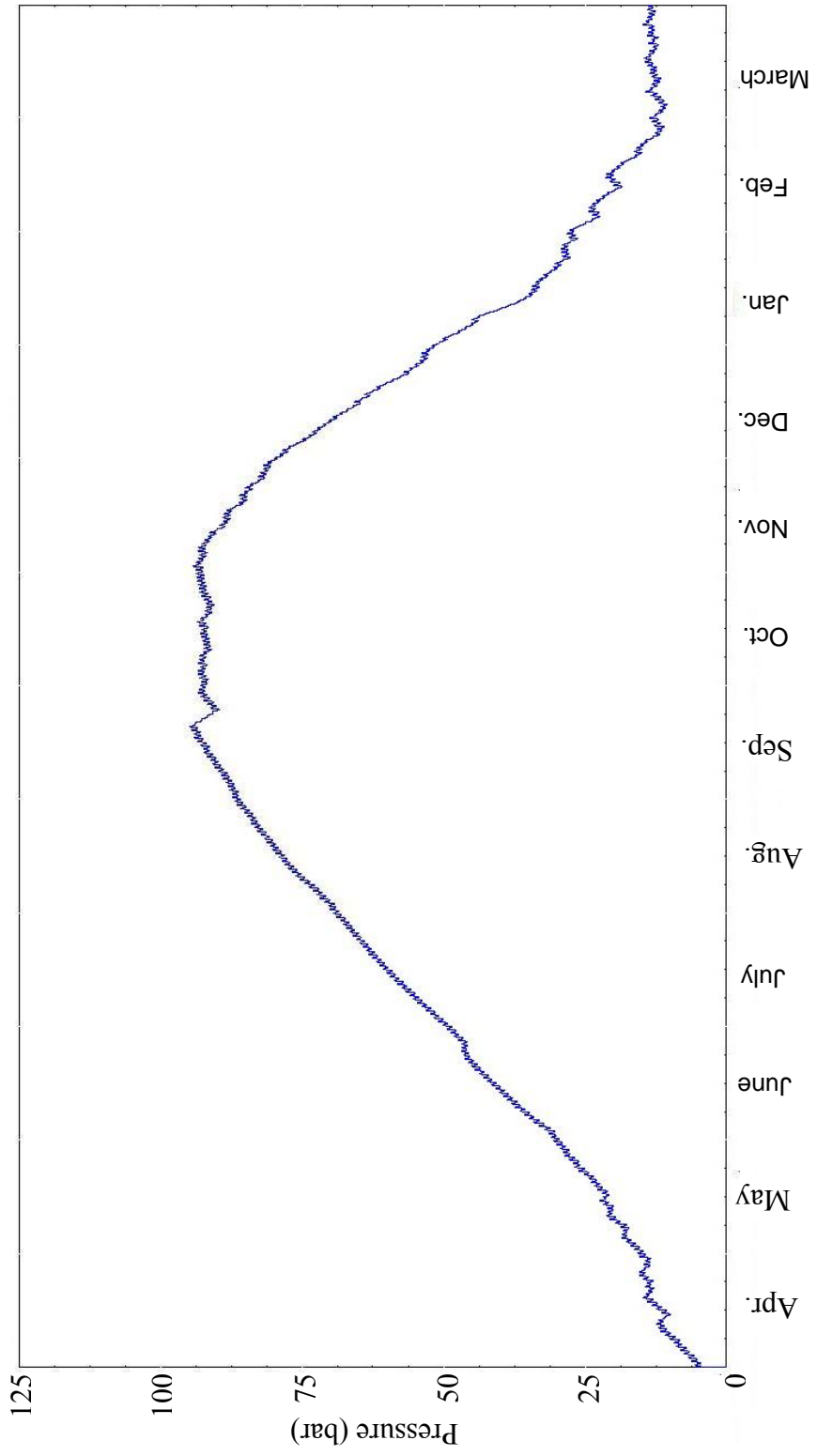
Figure 3-10 Pressure in hydrogen tank for system 3

On the other hand, more hydrogen is spent in system 5 by the fuel cell stack because the total amount of E3 is less than it was in the system 4. In system 4, 12897 Nm^3 hydrogen is spent by the fuel cells while 13368 Nm^3 hydrogen is produced by the electrolyzers. Whereas; in system 5, 13103 Nm^3 hydrogen is spent by the fuel cells while 12841 Nm^3 hydrogen is produced by the electrolyzer stack. With 50° PV surface slope, the system produces less hydrogen and spends more hydrogen. The overall and electricity efficiencies are 5.43% and 42.81% respectively, they are less as well for this system.

In order to have positive hydrogen balance with 50° PV surface slope, the PV area is increased for system 6. 400 PV panels are used in this system. The pressure inside the hydrogen tank is 11.5 bar more than the initial value. Energy produced by 400 PV panels with 50° surface slope is almost the same with the energy produced by 385 PV panels with 30° surface slope. The overall and electricity efficiencies are 5.49% and 43.27%. In system 7, PV surface slope is changed back to 30° while keeping everything else the same as system 6. There is 26.1 bar pressure inside the hydrogen tank at the end of the year. The overall and electric efficiencies are 5.4% and 42.81% which are lower than the previous system. The reason for this is 2.06 MWh energy dumped (E6) by the controller. The maximum allowable tank pressure is reached during September as it can be observed from Figure 3-12.
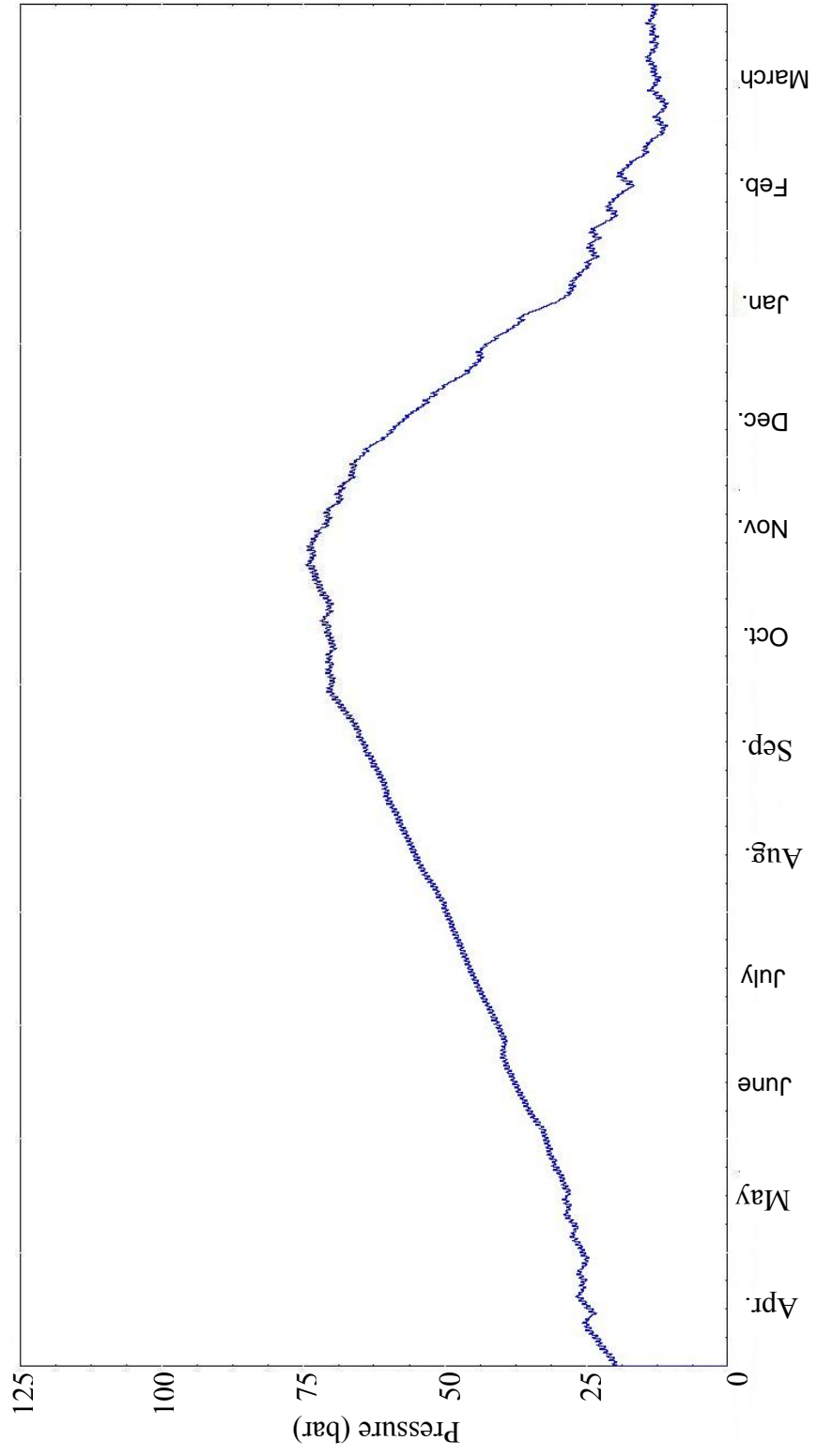
Figure 3-11 Pressure in hydrogen tank for system 5
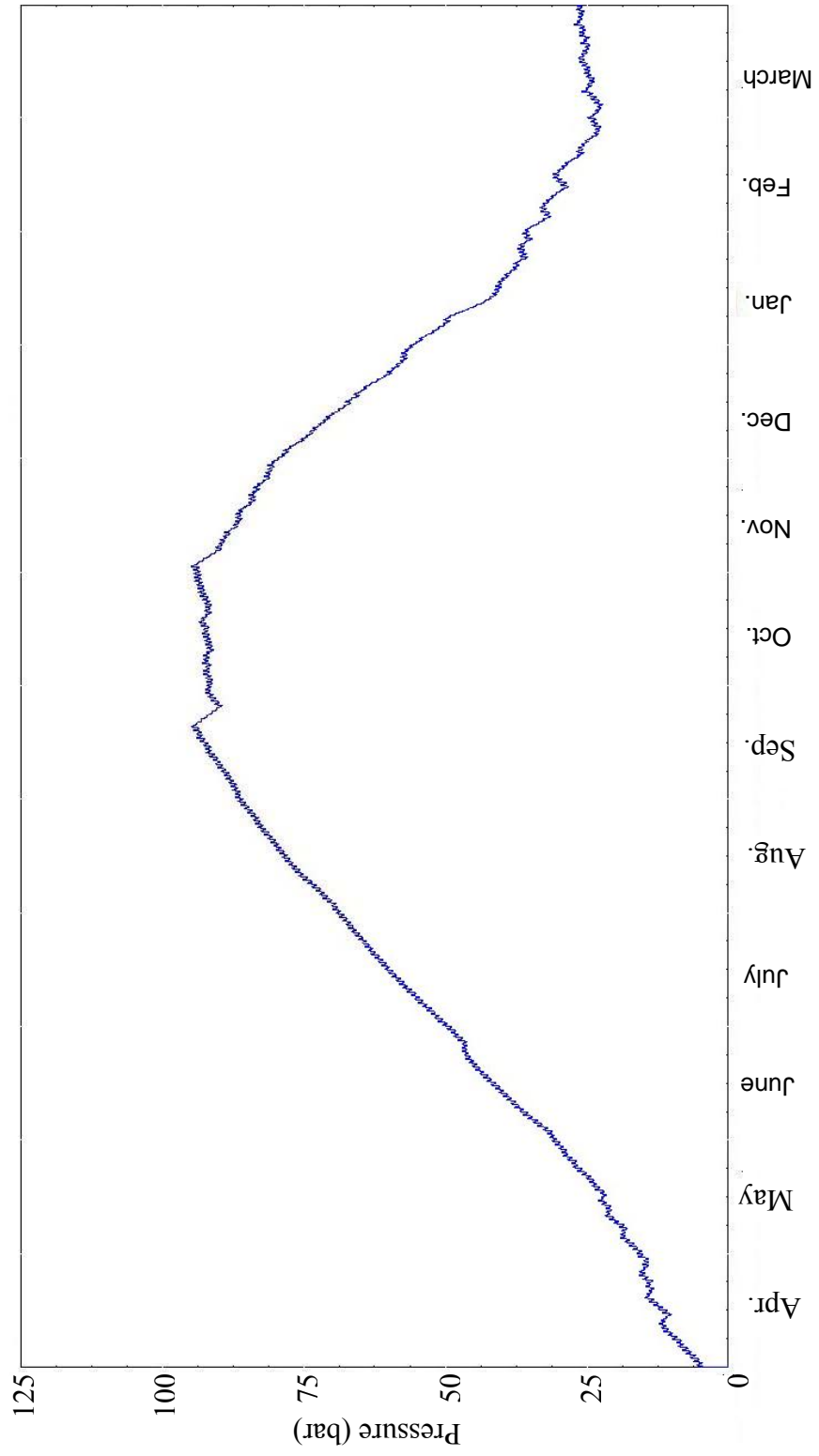
Figure 3-12 Pressure in hydrogen tank for system 7

Even though the systems with 50° PV surface slope produce more energy than the systems with 30° PV surface slope during the critical winter season, these systems are not practical since these systems cannot produce enough energy during the summer season. If the PV panels are constructed in such a way that the surface slope can be adjusted during the year, the performance of the energy system is expected to be increased. Table 3-6 shows the energy production of a single PV panel during the summer and winter seasons with respect to surface slopes. The summer season includes the months from April to September and the winter season includes the months from October to March.

Table 3-6 PV surface slope and seasonal energy production (kWh)

Surface Slope	Winter	Surface Slope	Summer
65	15319	0	27239
60	15505	5	27870
55	**15585**	10	28315
50	15558	15	28571
45	15423	**20**	**28637**
40	15183	25	28519
35	14838	30	28213

The PV panels have the most energy production capacity with 20° surface slope during the summer season and with 55° surface slope during the winter season. New system simulations are performed with variable surface slope of PV panels. Surface slope PV panels is 20° during summer season and 55° during winter season. Volume of the hydrogen tank is 40m³, initial pressure inside the tank is 5 bar and maximum allowable pressure is 95 bar. 15 stacks electrolyzer are used to prevent energy waste during summer season because of high electrolyzer cell temperature.

In system 8, 400 PV panels are used as in the systems 6 and 7. The pressure inside the hydrogen tank at the end of the year is equal to 36.1 bar which is much higher than the previous systems. 3.57 MWh energy is dumped because of the high tank pressure during summer days. The overall and electricity efficiencies are 5.35% and 42.36% which are lower than the previous system because of the high amount of dumped energy. The system is producing more energy than needed. The PV size can be decreased to increase the system efficiency and the initial cost.

In system 9, 375 PV panels are used. There is 22.1 bar pressure inside the hydrogen tank at the end of the year which is 17.1 bar more than the initial pressure. There is no dumped energy and this system is more efficient. The overall and electricity efficiencies are 5.52% and 43.55%. In system 2, the hydrogen balance was -0.2 bar at the end of the year with same system size.

The number of PV panels are decreased by 10 for system 10. Figure 3-13 shows the pressure level inside the hydrogen tank throughout the simulation year. The tank pressure is 8.8 bar at the end of the year and it does not drop below 9 bar during the winter days. The system might fail to supply energy during winter days for a year when the solar irradiation is lower than the expected values.

Initial cost of the system is reducing with using less PV panels but adjustable PV surface slope increases the initial cost as well as complicates the assembly of panels.
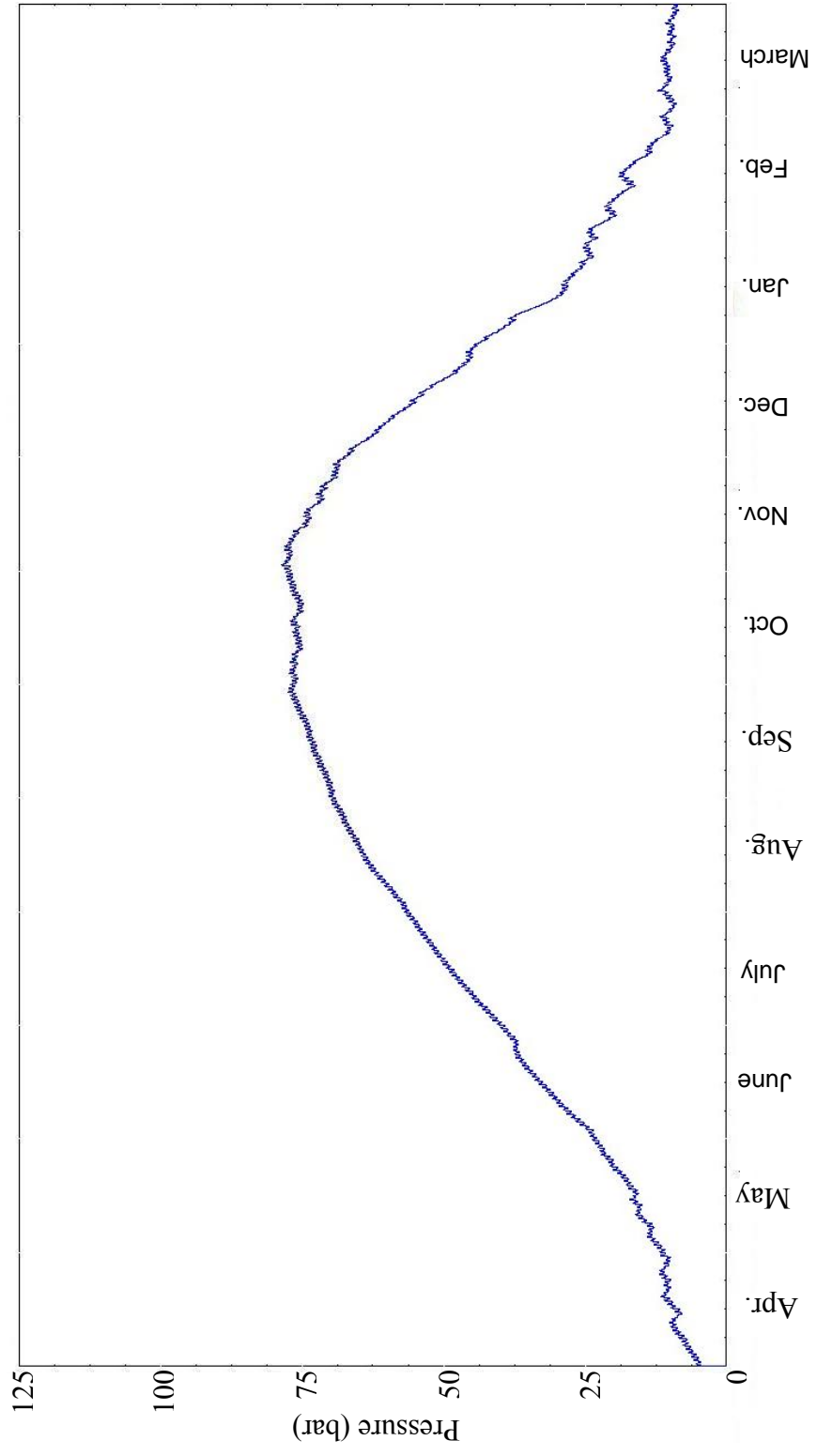
Figure 3-13 Pressure in hydrogen tank for system 10

3.2.2 Systems with battery storage

The electrolyzer manufactured by Niğde Uni. works at 75% energy efficiency at the operating conditions and PEM fuel cell used in the simulations has an average 40% efficiency. Energy efficiency of the electrolyzer is defined as the ratio between thermoneutral cell voltage and cell operating voltage. The electrolyzer cells are designed to work at constant 2V. The total efficiency of the electrolyzer decreases more when Faraday efficiency is taken into account as well which defines the relation between actual and ideal flow rate of product hydrogen. If it is assumed that there is no other loss in the hydrogen cycle and no auxiliary equipment energy consumption, converting electric energy into chemical energy by means of hydrogen and converting the chemical energy back to electric energy has less than 30% efficiency. When the energy consumption of water pumps, hydrogen and water purifiers, controllers and inverters is added to the calculation, the overall hydrogen cycle efficiency drops further more. On the other hand, batteries have high efficiencies and do not require any auxiliary equipment, a usual Lead-acid battery has more than 90% charging efficiency. It is more efficient and economic to use batteries instead of hydrogen cycle for storing energy. However, energy storage capacity of a battery is considerably low with respect to hydrogen storage equipment. Because of this reason, it is not practical to use batteries for seasonal storage, yet they can be used for daily storage.

Operating strategy of the battery stack is to help fuel cell during low insolation hours. The aim is to increase the fuel cell efficiency by decreasing its load and supplying a portion of the required electrical power by the battery stack that has a high energy conversion efficiency. The simplified TRNSYS schematics of the system is shown in Figure 3-14. A maximum desired operating power of the fuel cell is set for the new system with battery stack. When the user needs more power than the fuel cell maximum desired operating power, the battery stack will provide the electricity. By this way, the energy spent on the inefficient hydrogen cycle will be decreased and fuel cell efficiency will be increased since the fuel cells operate more efficient at lower loads. The battery stack has a maximum and a minimum allowable fractional state of charges (SOC_{max} and SOC_{min}) set to 0.8 and 0.4

because of the safety and efficiency reasons. Fractional state of charge is the ratio between the total amount of energy stored in the battery and the total energy capacity of the battery. For usual Lead-acid batteries, charging efficiency drops if SOC is over 0.9 and life time of batteries becomes shorter if they operate at low SOC levels. When battery SOC drops below the minimum allowable value, fuel cell supplies all of the load power. Extra energy provided by the PV array is first supplied to the battery stack if SOC is lower than SOC_{max}. When SOC_{max} is reached or PV power is greater than the maximum allowable charging power (which is selected as 20kW for this battery stack), extra power from the PV array is supplied to the electrolyzer for hydrogen production.

The system parameters for the conducted simulations are given in Table 3-7. Constant PV surface slope of 30° and electrolyzer size of 15 stacks are used considering the results in the previous section. Hydrogen tank size is kept at 35 m^3 since there is the battery pack also helping to the energy storage. Battery start up power is equal to the maximum desired power of the fuel cells. When the power deficit between the user load and the solar energy is less than the battery start up power, only the fuel cells will work. When the power deficit is more than the battery start up power, battery stack will also supply the power with the fuel cells. The energy flow values are given in Table 3-8 for the different systems. E8 is equal to 0 for all systems since no auxiliary equipment is used in systems in this section. The effects of the auxiliary equipment will be examined in the next section.
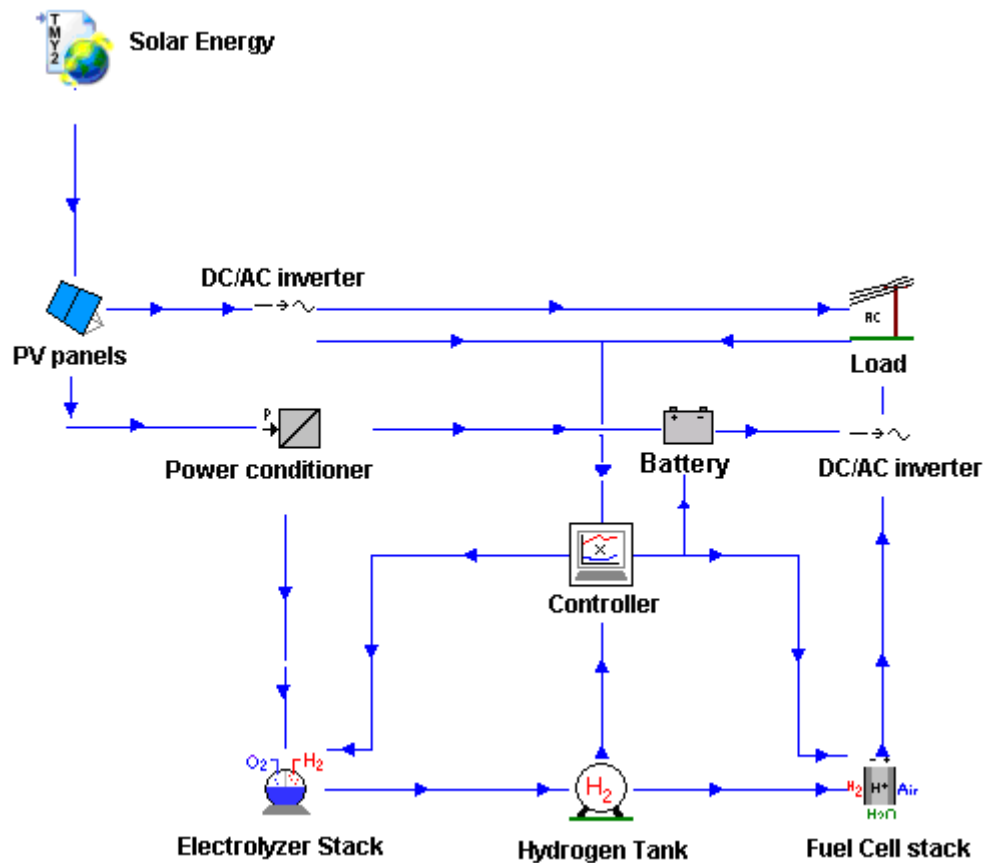
Figure 3-14 TRNSYS schematics of the system with battery pack

Figure 3-15 shows the battery fractional state of charge (SOC) and the pressure level in the hydrogen tank for system 1. The system has 350 PV panels. The battery stack can store up to 30 kWh energy. Initial pressure in the hydrogen tank is 5 bar and initial state of charge of the batteries is 0.5. Battery start-up power is set to 4kW. At the end of the year, there is 14.3 bar hydrogen in the tanks. 400 PV panels were needed to have 14.3 bar pressure in the tanks for the system with the same component parameters but no battery storage (Table 3-4).

Table 3-7 Component parameters for different systems

System no	Number of PV panels	Total PV area (m²)	PV surface slope	Number of electrolyzer stacks	H² Tank size (m³)	Battery capacity(kWh)	Battery start up Power(kW)	H₂ balance (Bar)/MWh
1	350	331.3	30°	15 stacks	35	30	4	+9.3/0.91
2	330	312.4	30°	15 stacks	35	30	4	-20.8/2.03
3	350	331.3	30°	15 stacks	35	30	2	+14.7/1.44
4	350	331.3	30°	15 stacks	35	90	2	+47.6/4.66
5	330	312.4	30°	15 stacks	35	30	2	-4.8/0.47
6	330	312.4	30°	15 stacks	35	90	2	+38.8/3.80
7	350	331.3	30°	15 stacks	35	30	0	+11.4/1.12
8	350	331.3	30°	15 stacks	35	90	0	+50.9/4.98
9	350	331.3	30°	15 stacks	35	180	0	+81.9/8.01
10	330	312.4	30°	15 stacks	35	30	0	-19.6/1.92
11	330	312.4	30°	15 stacks	35	90	0	+41.4/4.05
12	330	312.4	30°	15 stacks	35	180	0	+72.6/7.10
13	250	236.7	30°	15 stacks	35	180	0	+25.3/2.48
14	235	222.5	30°	15 stacks	35	180	0	+4.7/0.46

Table 3-8 Annual energy flows for different systems in MWh (refer to Table 3.2)

Sys. no	E1	E2	E3	E4	E5	E6	E7	E8	E9	E10	E11	E12
1	636.70	80.30	20.69	3.1	56.52	0	2.79	0	33.64	32.75	17.90	37.23
2	600.33	75.71	20.57	3.09	52.07	0	2.78	0	30.98	33.00	18.03	37.23
3	636.70	80.30	20.69	4.78	52.81	2.04	4.30	0	31.43	30.01	16.38	37.23
4	636.7	80.30	20.69	9.51	43.06	7.06	8.55	0	25.63	21.03	12.14	37.23
5	600.33	75.71	20.57	4.76	50.40	0	4.29	0	29.99	30.27	16.52	37.23
6	600.33	75.71	20.57	9.48	42.09	3.59	8.52	0	25.05	21.31	12.29	37.23
7	636.70	80.30	20.69	4.82	53.55	1.25	4.34	0	31.87	30.77	16.35	37.23
8	636.70	80.30	20.69	13.88	33.19	12.55	12.50	0	19.75	14.84	8.18	37.23
9	636.70	80.30	20.69	20.33	20.89	18.41	18.28	0	12.43	4.52	2.41	37.23
10	600.33	75.71	20.57	4.80	48.97	1.38	4.32	0	29.15	31.04	16.49	37.23
11	600.33	75.71	20.57	13.78	32.32	9.05	12.41	0	19.24	15.24	8.40	37.23
12	600.33	75.71	20.57	20.16	20.25	14.75	18.13	0	12.05	5.04	2.68	37.23
13	454.79	57.36	19.90	19.24	17.31	0.93	17.30	0	10.29	7.85	4.19	37.23
14	427.50	53.92	19.73	18.98	15.22	0	17.07	0	9.05	8.60	4.59	37.23

64

In the spring and summer seasons, battery SOC drops to 0.6 throughout the night hours, then it is charged back to 0.8 within a short time after the PV arrays start to work. On the other hand, the battery SOC drops to minimum allowable value several times during the winter season. Figure 3-16 shows the power profile during the 4 days in January while battery SOC is under minimum value. The negative value of the battery power means, the battery stack is discharging; positive value of the battery power means, the battery is charging. While SOC is greater than SOC_{min} during January 7, fuel cell is supplying 4 kW and the battery stack is supplying 1 kW power to user. 1 hour before the PV arrays start to work, SOC drops to minimum allowable value and battery stack stops supplying electricity, fuel cell provides 5 kW power to user meanwhile. For the following 3 days , PV panels cannot produce more power than the user need, therefore the battery stack cannot be charged and the fuel cells supply all of the energy need when there is no solar power available. During this period, the slope of hydrogen pressure curve decreases rapidly. After January 9 solar insolation increases and PV panels are able to charge the battery again, the fuel cell stack operates at the maximum desired operating power. Figure 3-17 shows the fuel cell operating power throughout a year. Because of the high insolation until August, the fuel cells do not operate for long hours. Between August and September, there is a transition period where the fuel cell operating time begins to increase and after September the fuel cell stack is the main energy supplier to the user. The fuel cell stack does not supply more than its maximum desired operating power (4 kW) unless the battery SOC drops under SOC_{min}. In the winter months, the fuel cell stack is forced to operate at maximum power and supply 5 kW electricity to the user for several hours since the battery SOC is under SOC_{min}.
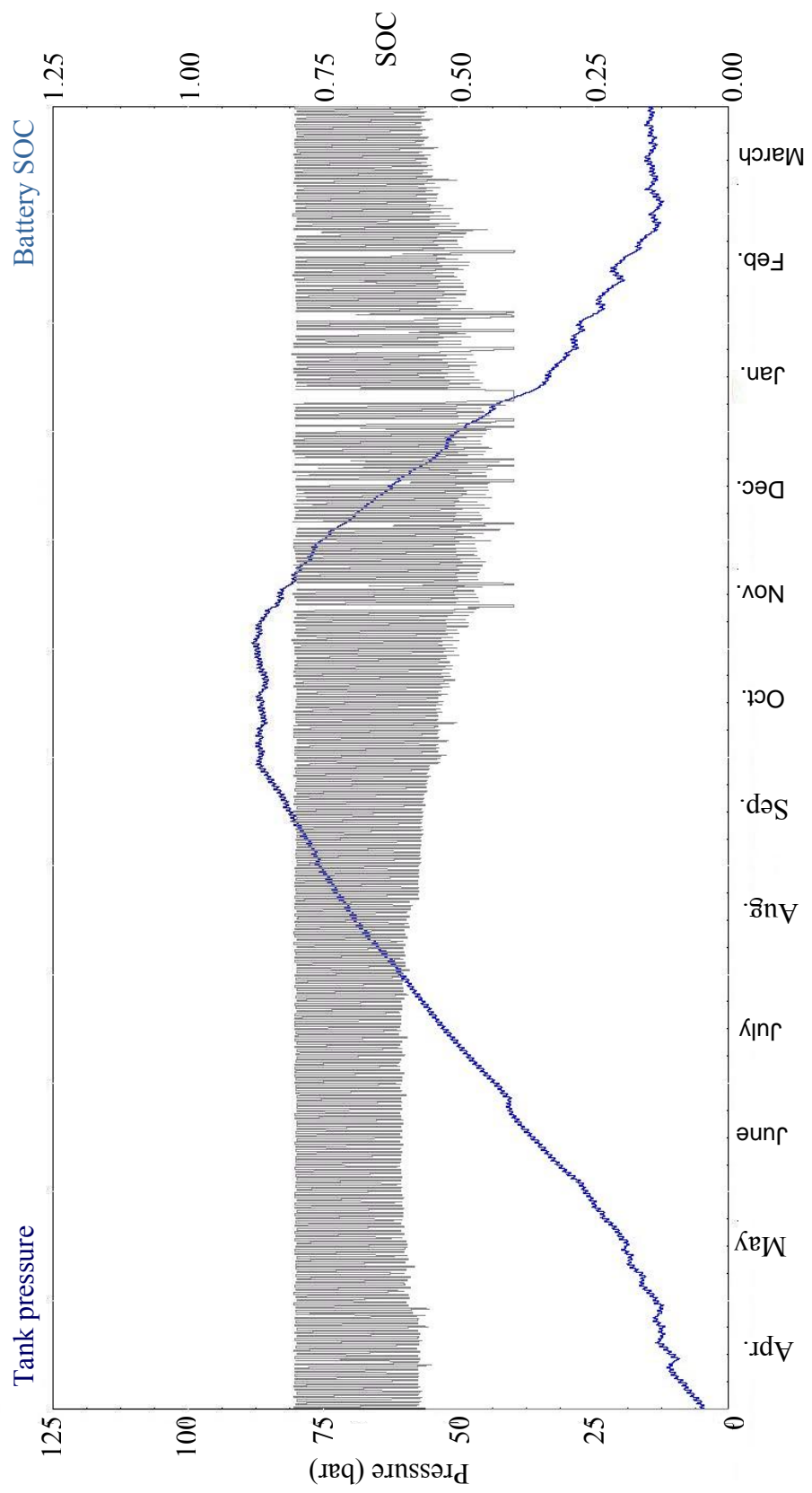
Figure 3-15 Pressure in hydrogen tank and battery SOC for system 1
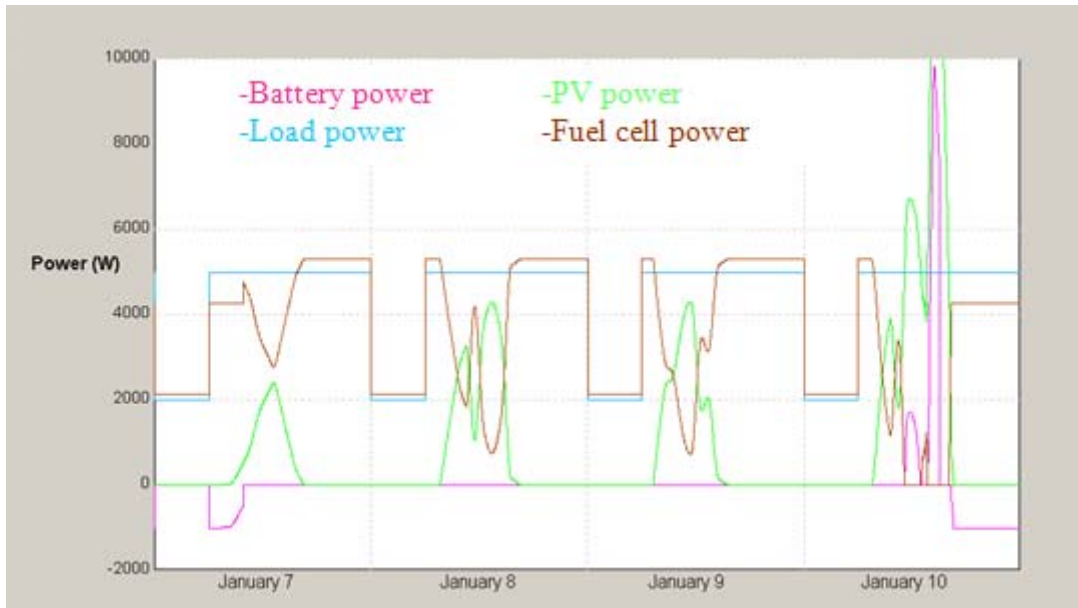
Figure 3-16 Battery, PV, load and fuel cell power profiles

Since there is 14.3 bar hydrogen leftover in the tank at the end of the simulation year of the previous system, it can be observed that the system is generating more energy than needed. To lower the initial cost of the system, 20 PV panels are removed for system 2 for which there is 20.8 bar pressure deficit at the end of the year. It means that the system cannot sustain continuous operation during a whole year.

For system 1; the overall energy of the system is 5.99% and electricity cycle efficiency is 47.5% which are higher than the ones for all systems simulated without battery pack. PV panels produce 80.3 MWh annual energy; 20.69 MWh of this energy is given to the user inverter directly, 3.1 MWh is given to the battery pack, 56.52 MWh is given to electrolyzer stack and no energy is dumped. The energy given to the battery pack is only 5.5% of the energy supplied to the electrolyzer. As a result, the difference between the efficiencies of the systems with and without battery pack is not high. The fuel cell stack supplies 17.9 MWh energy to the user while the battery stack supplies only 2.79 MWh.
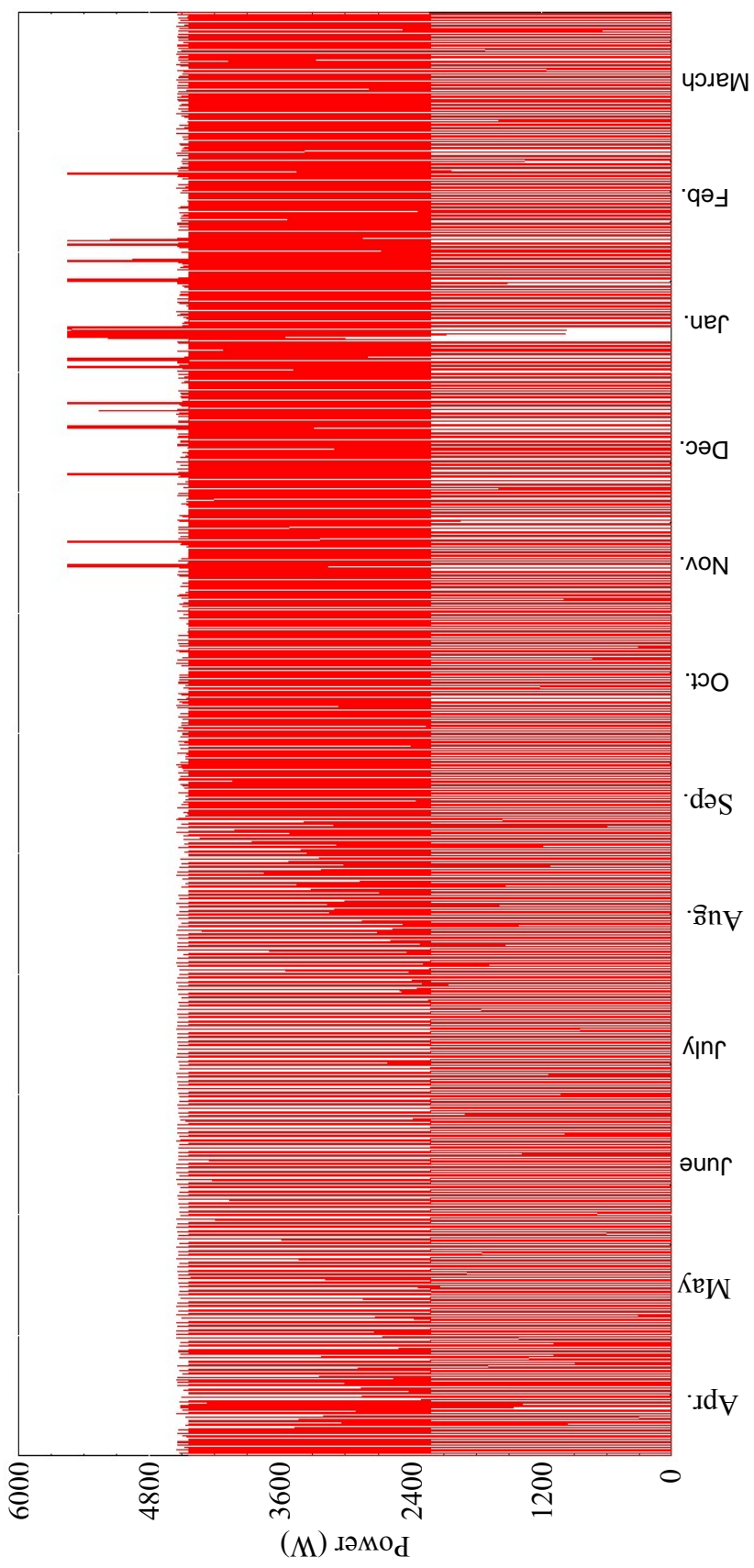
Figure 3-17 Annual fuel cell power for system 1

Increasing the battery pack's role will also increase the system efficiency and to performance further. Battery start-up power can be lowered so that the fuel cells operate less and the batteries will supply more energy. To increase the energy flow through the battery pack, the capacity of the battery stack should also be increased. A typical Lead-acid battery can store 30-40 Wh energy per kilogram of battery weight. A Lead-acid battery stack with 30 kWh energy capacity weights around 750-1000 kg and has around 0.4-0.5 m^3 volume. Life time of these batteries is dependent on how many charge and discharge cycles they do. A typical battery, which is discharging to minimum and charging back to maximum every day, has a life time around 2 years. During the following simulations, the effects of battery pack size and operation strategies on the system performance and size will be analyzed.

In system 3, battery pack energy capacity is 30 kWh and the number of PV panels is 350 as it is the case in system 1. But the battery start-up power is lowered to 2 kW. When solar power is not enough, the fuel cell stack supplies up to 2 kW power to user, the rest of the power need is supplied by the battery pack if the battery state of charge is above minimum allowable value. Figure 3-18 shows the battery fractional state of charge (SOC) and pressure level in the hydrogen tank for system 3. There is 14.7 bar difference between the initial and final pressures in the hydrogen tank. This value is only 5.4 bar improved between system 1 and 3. The energy supplied to the battery stack is 4.78 MWh and the energy supplied from battery to the user is 4.3 MWh while the energy supplied to the electrolyzer is 52.81 MWh and the energy supplied from the fuel cell stack to the user is 16.38 MWh. It can be observed that; the battery SOC fluctuates between its maximum and minimum allowable values. A battery pack with 30 kWh energy capacity fails to store enough energy on a daily basis. Figure 3-19 shows the fuel cell power during the simulation year. The fuel cell stack is working at 5 kW power for long hours while it should not work over 2 kW during high insolation days.
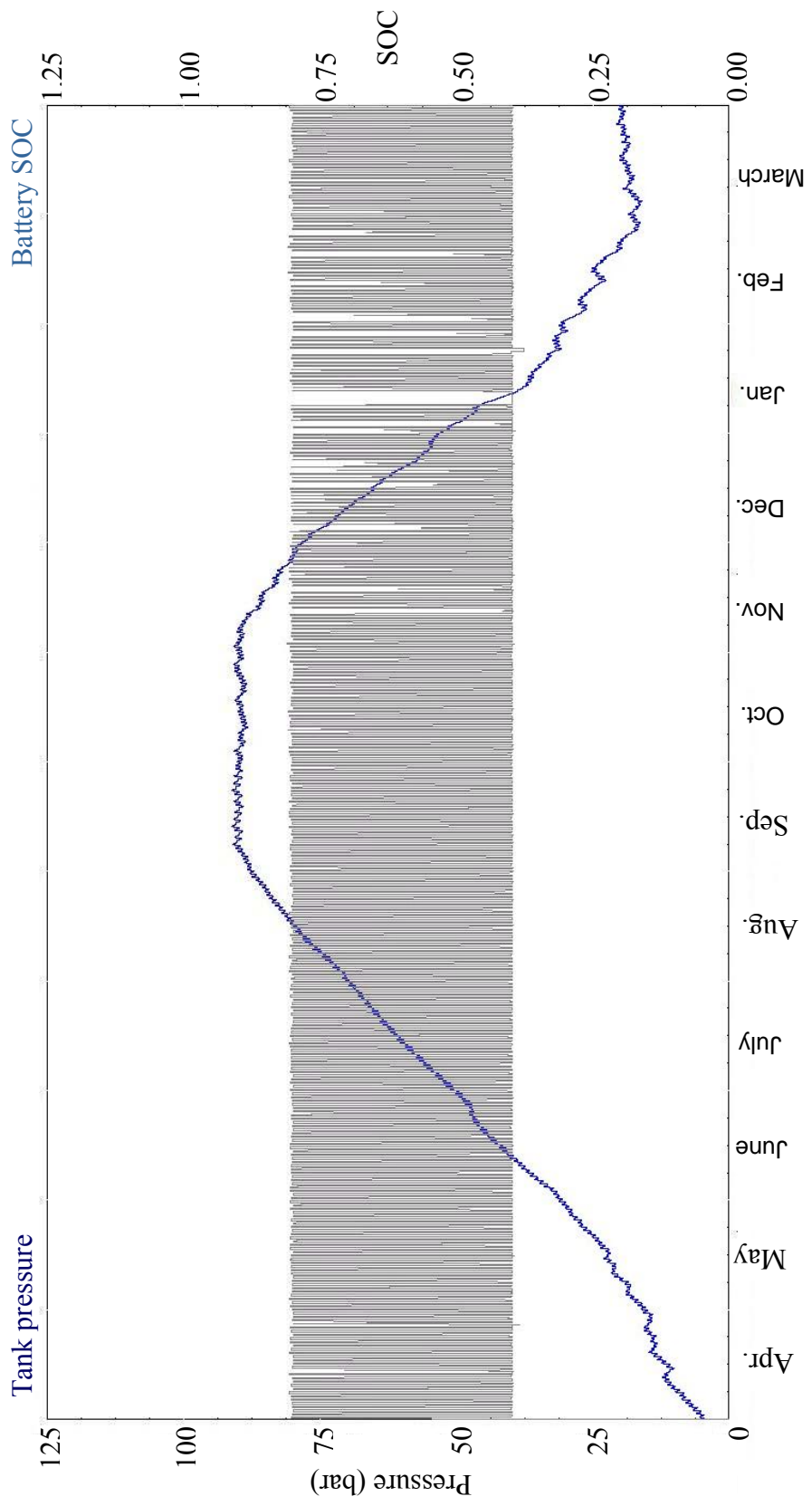
Figure 3-18 Pressure in hydrogen tank and battery SOC for system 3
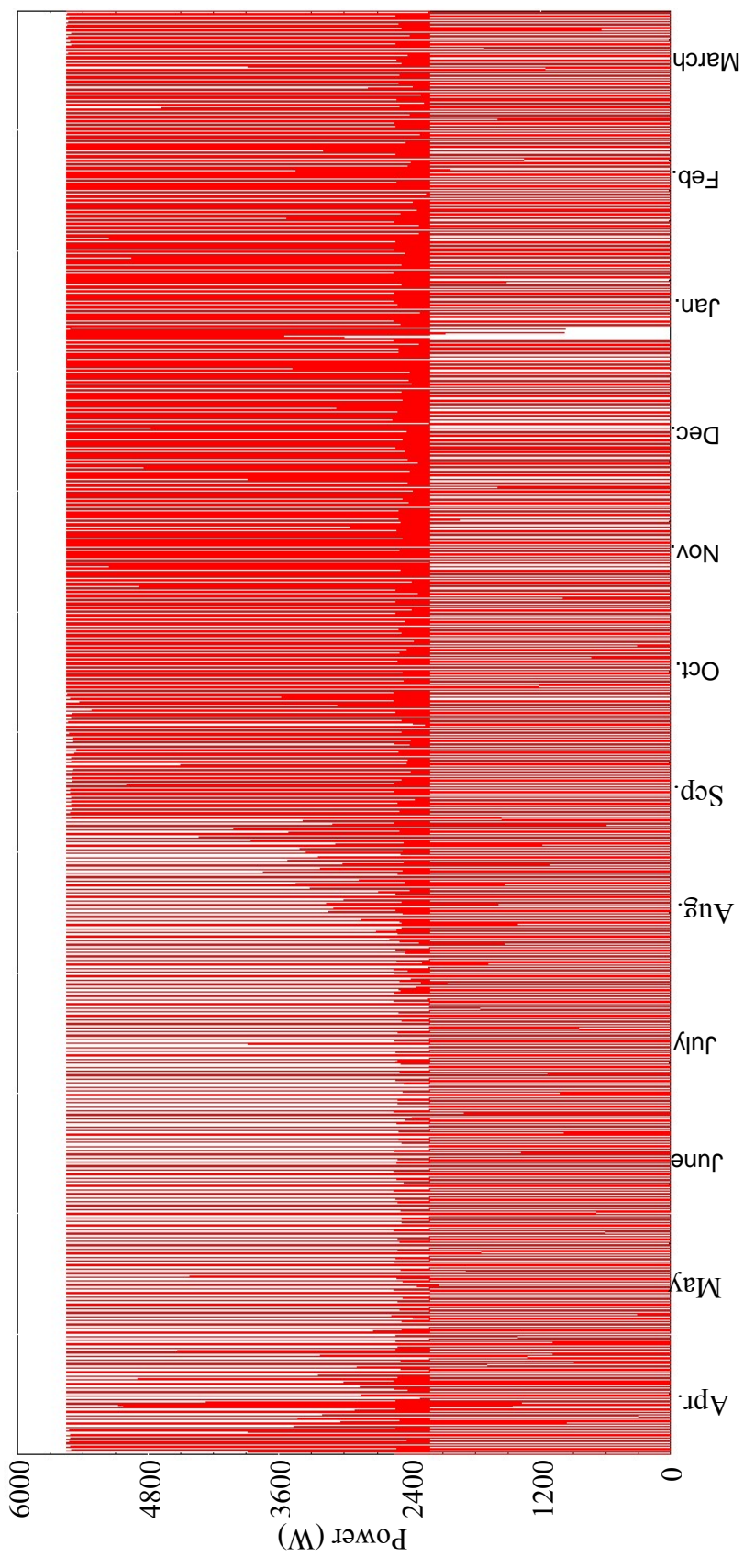
Figure 3-19 Annual fuel cell power for system 3

Increasing the energy capacity of the battery pack may be a solution. But it should be noted that there is a linear relationship between the battery size and the cost. Doubling the battery capacity will also double the initial cost of the battery pack, while the cost difference is very small for hydrogen tanks for the same case.

The battery energy capacity is increased to 90 kWh for system 4. Figure 3-20 shows the battery SOC and the pressure level in the hydrogen tank for system 4. The pressure in the tank is 52.6 bar which is 47.6 bar more than the initial value. The battery SOC does not drop to the minimum until November except once in April and once in September when the solar irradiation is very low because of the cloudy days. During winter days, there are periods where PV panels are not able to charge the battery and the fuel cell stack operates at maximum power during these periods as it can be observed from Figure 3-21. The hydrogen tank is fully filled in early August and stays full until November, meanwhile 7.06 MWh energy produced by PV array is dissipated by the controller. The battery pack supplies 7.06 MWh energy to the user while the fuel cell stack supplies 12.14 MWh energy to the user. The overall and electricity cycle efficiencies are 6,57% and 64.55%. Even though dumped energy is high, the system has better efficiency than the previous systems.

Since the final pressure in the hydrogen tank is high and 7.06 MWh energy is wasted in the previous system, PV array size can be decreased for a lower initial cost. H_2 balance is -4.8 bar for system 5 and +38.8 bar for system 6. The only difference between these systems is the battery pack size. 330 PV panels are used for both systems but system 5 has 30 kWh capacity battery pack where system 6 has 90 kWh capacity battery pack.
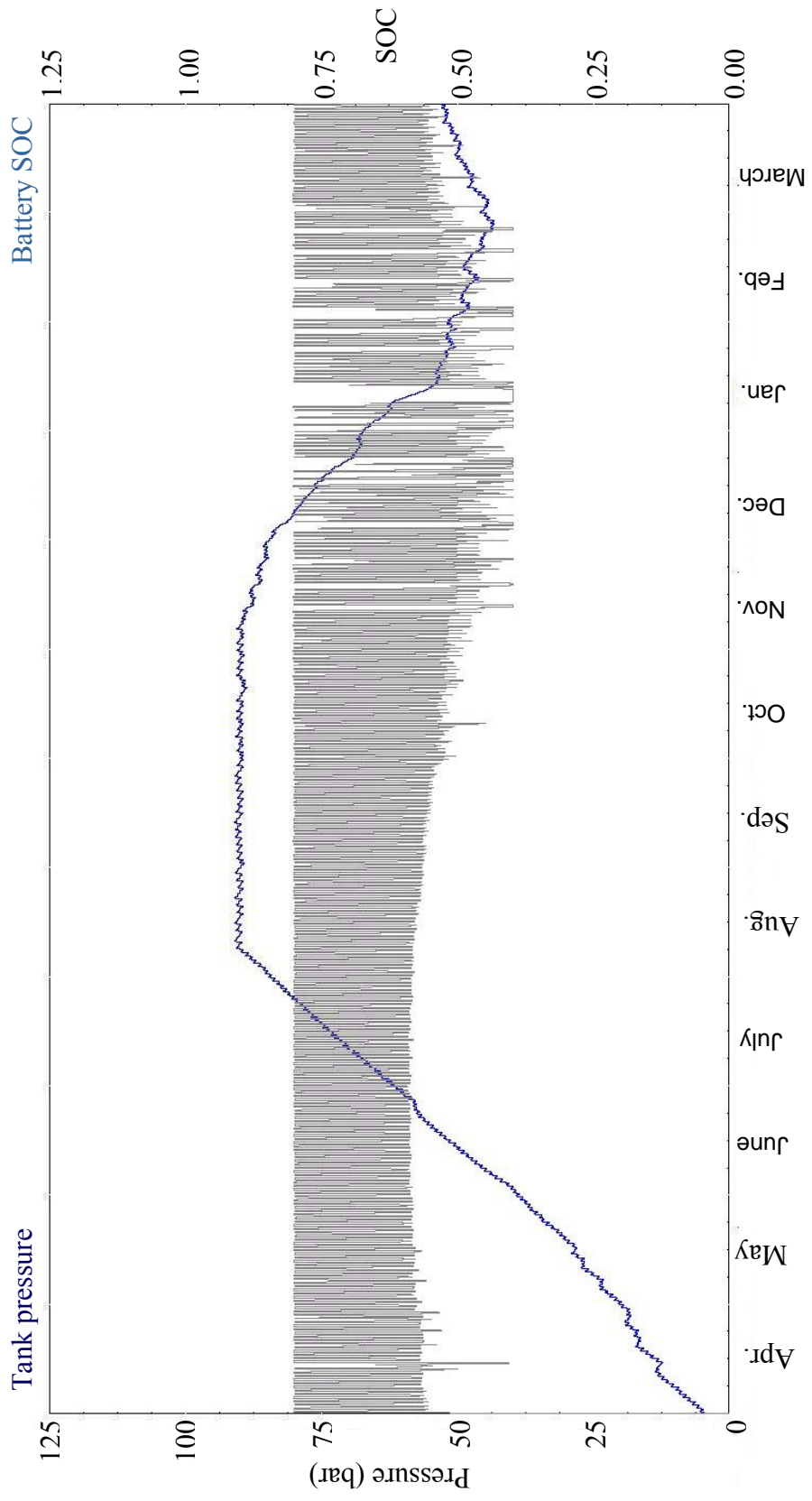
Figure 3-20 Pressure in hydrogen tank and battery SOC for system 4
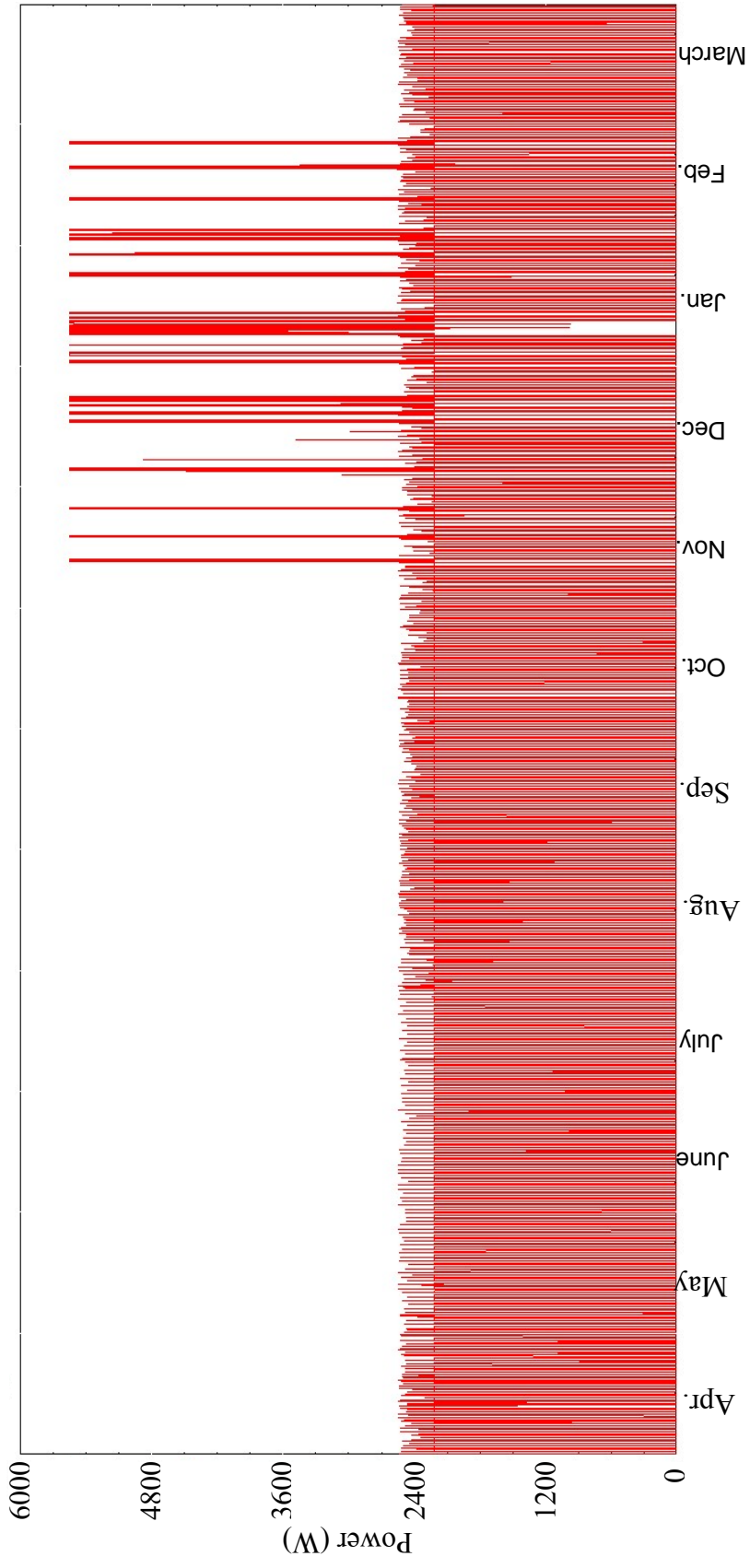
Figure 3-21 Annual fuel cell power for system 4

Another approach to managing solar energy is to use only the batteries for the daily storage and to store hydrogen for the seasonal storage. The load profile of the emergency room is shown in Figure 3-1, the daily energy need of the user is 102 kWh. The battery storage size should be more than this value because of the maximum and minimum allowable state of charges and life time considerations of the batteries. The battery pack always has priority to provide electricity to the user. The fuel cell stack stays as a backup supplier and begins to operate during the times when battery SOC drops under minimum allowable value. 8 different simulations (system 7-14) are conducted for different PV and battery sizes. It can be observed from Table 3-7 and Table 3-8, using battery packs with 90 kWh or 180 kWh energy capacity increases system performance significantly with respect to using battery packs with 30 kWh energy capacity. The amounts of final hydrogen in the tanks are high while systems with 30 kWh energy capacity batteries are not sufficient for such systems. The dumped energies are more than 9 MWh for systems 8, 9, 11, and 12 the systems with 330 or 350 PV panels and using 90 kWh or 180 kWh energy capacity battery packs. To avoid such high losses, the PV panel size can be decreased considerably.

235 PV panels and 180 kWh energy capacity battery pack is used for system 14. The final pressure of the hydrogen tank is 9.7 bar. 53.92 MWh energy is produced by the PV panels. 19.73 MWh of this energy is supplied directly to the user, 18.98 MWh is used to charge the battery pack and 15.22 MWh is supplied to the electrolyzer. The battery pack provides 17.07 MWh energy to the user while the fuel cell only provides 4.59 MWh. The battery pack feeds 3.8 times more energy to the user than the fuel cells so that the effects of inefficient hydrogen cycle are minimized. The overall efficiency is 8.81% and the electricity cycle efficiency is 69.88%.

Operating strategy of batteries mainly depends on the pack size. As the battery size increased, it is possible to decrease the PV size. For Stand-Alone power systems based on solar power, the main initial cost of the system comes from the PV panels. However, it should be noted that the life time of the PV panels are usually more than 20 years whereas lead-acid batteries have 2-5 years life time

usually. Also the cost of storing energy in a battery pack increases linearly unlike to storing energy in the form of hydrogen. It can be observed from the simulations that the increasing battery stack size does not decrease the number of PV panels linearly. A detailed cost optimization can be made by drawing cost curves for different components and finding the intersections.

3.2.3 Auxiliary Equipment

PV panels, electrolyzers, fuel cells and batteries are the main elements of a Stand-alone power system. These components should be supported with other equipment for stable operation. PEM electrolyzers are only able to operate with deionized water, hydrogen should be purified before storing and supplying to the PEM fuel cells, a water pump is needed to provide pressurized water to electrolyzer, the main control panel of the system works with electricity, safety valves are needed for safe operation, direct current produced by the PV array and the fuel cell stack must be converted to alternative current before supplying to the user. DC/AC inverters have already been implemented into the previous systems. The power consumption and effects on system performance of the hydrogen purifier and the compressor, the water deionizer and the control panel will be investigated. The water pump is ignored because of the very low water flow rate and energy consumption.

Figure 3-22 shows the battery fractional state of charge SOC and the pressure level in the hydrogen tank for an annual system simulation. The system has 400 PV panels, 15 stacks of electrolyzers and $35m^3$ hydrogen tank capacity with maximum pressure 95 bar. PV surface slope is constant 30°. Battery stack can store up to 30 kWh energy. The battery stack provides energy for auxiliary equipment. The fuel cell stack charges the battery pack to sustain continuous operation of auxiliary equipment when the battery SOC is lower than SOC_{min}. Initial pressure in the hydrogen tank is 5 bar and the initial state of charge of the batteries is 0.5. Maximum desired operating power of the fuel cell is set to 4kW; the excess power need of the user will be supplied by the battery stack if the state of charge is greater than SOC_{min}. At the end of the year, there is 9 bar hydrogen in

the tanks. The hydrogen tank stays full during summer days and extra energy is dumped by the controller. But during the winter months, the system spends more hydrogen with auxiliary equipment power included.

The modeled electrolyzer in the simulations operates at 20 bar. When the pressure inside the hydrogen tank is above 20 bar, a compressor will pump the hydrogen into the tank. Default hydrogen compressor in TRNSYS library is used in the simulation. The annual energy consumption of the hydrogen compressor is 348 kWh. The control panel and the safety equipment is assumed to operate at 500 W constant power as it was offered for a similar system in the literature [30] and uses 4.34 MWh annual energy.

Silica-gel can be used as hydrogen purifier and a high level of purity can be achieved without using any energy. But the life-time of silica-gels is low for high flow rate hydrogen. They need to be replaced every 6 month. There are electronic purifiers in the market as well. But Silica-gel will be used in the TUBİTAK project.
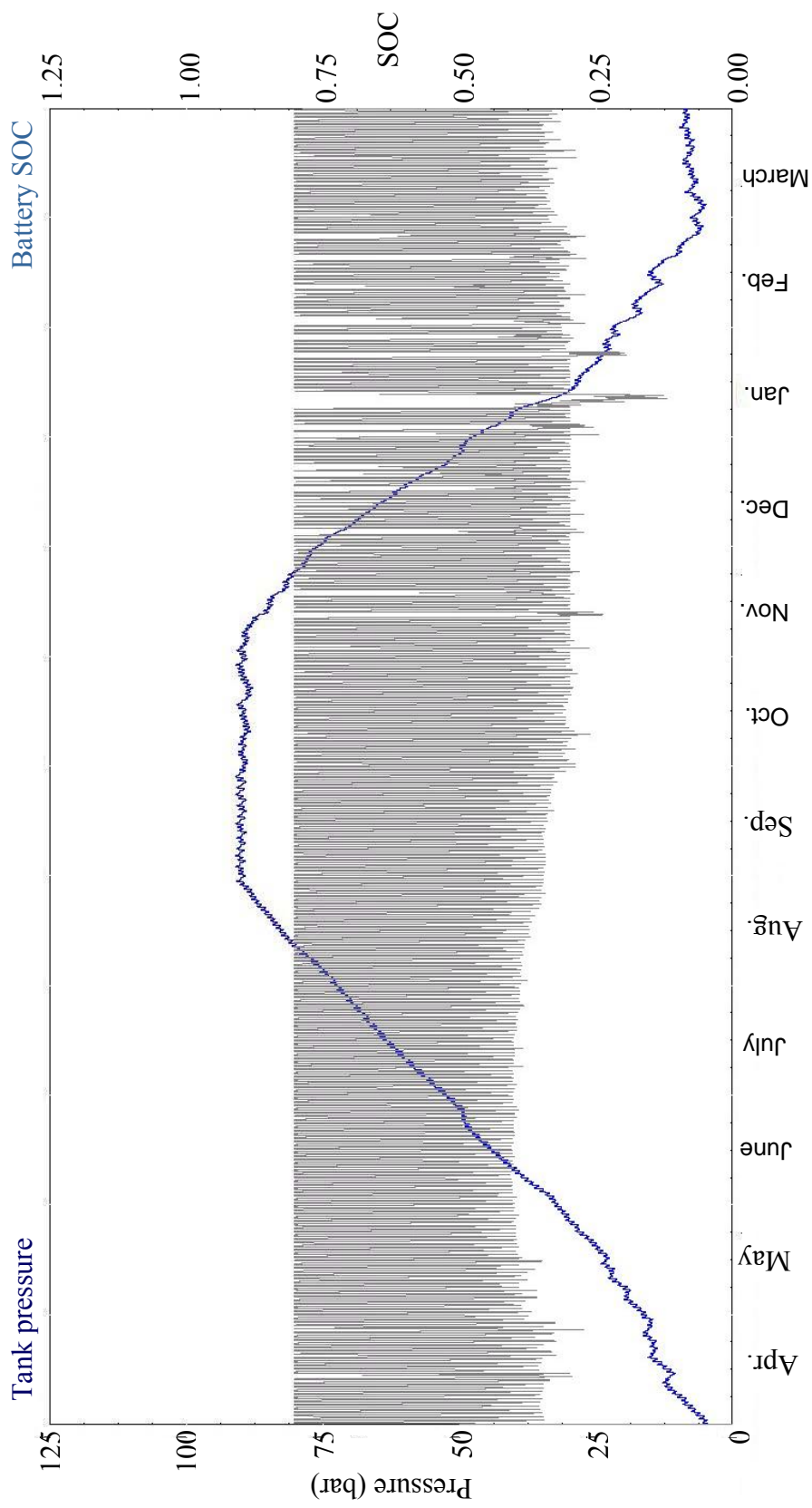
Figure 3-22 Pressure in hydrogen tank and battery SOC

3.3 TRNSYS Simulations of a Prototype System

A prototype system was planned to be built to test the fuel cell, the electrolyzer and the PV panels to determine the operation performance of the system regarding to TUBITAK project. Previously modeled PV panels and electrolyzers would be used with fewer numbers of panels and cells. Main focus of this work was to obtain substantial information on the operation performance of the actual system that is planned to be built as a part of the TUBITAK project. With the information obtained from prototype system, simulation models could be designed as relevant as possible to the real setup. However, the prototype system was not completed in the prescribed time, because of the insufficient testing and measuring equipment and manpower. Therefore, a prototype system from the literature that has been tested before is modeled in TRNSYS. The aim of this work is to find ways to improve the accuracy of the system and component models for a future work comparing the TRNSYS simulations and the experiments.

Miland and Ulleberg [6] constructed a small-scale power system based on solar energy and hydrogen to investigate the properties of using different components and configurations. The authors reported the system performance and operational experience of individual components, subsystems and complete renewable power systems. The model system was a typical stand alone power system with PV panels, an electrolyzer, a fuel cell stack, a battery stack, a hydrogen purifier, control units and a load. The equipment was connected together without using any converter or inverter. Therefore, no power or voltage regulation was available. Since a real time testing during a whole year is very time consuming, 7 days with different solar energy profiles had been selected to investigate seasonal behavior of the system in a weekly testing. Weather data and PV power was emulated with a programmable power supply. Voltage and current data of a computer model PV array for 7 different days was arranged in an order to simulate a relative seasonal weather behavior. A programmable power supply was assigned to supply emulated PV power to the system during 7 days. The electric load was also emulated with a programmable power supply. Power profiles of the selected 7 days and equipment size and parameters provided by [31] are given in Appendix [E]. Experimental

voltage-current characteristics of the PEM electrolyzer and the fuel cell for different cell temperatures are provided in [31]. In this section the selected system is modeled in TRNSYS by using the PEM fuel cell and electrolyzer models as well as battery, control units, hydrogen tank, PV production and load models with respect to experimental data supplied by [31]. Thermal model of the fuel cell and electrolyzer which was developed in [31] by experimental methods is used in the component models. Electrical models of the fuel cell and the electrolyzer were created by using curve-fitting methodology on the experimental data. The FORTRAN subroutines are developed to find the voltage, the current, the power and the hydrogen flow rate output from the electrolyzer and the fuel cell.

Measured battery SOC [31] and simulated battery SOC during 7 days is given in Figure 3-23, while measured H_2 SOC [31] and simulated H_2 SOC by TRNSYS during 7 days is given in Figure 3-24. Measured and simulated battery SOC's shows a good agreement except on   day 4 where there is 10% SOC difference. However, while measured H_2 SOC drops down to 22% during day 3 on the experiment, its minimum value is 25.3% in the simulations. And, the final value of measured and simulated H_2 SOC is 62%, 66.1% respectively. There are two main reasons of this difference. PV power emulated in the experiments is taken with 2 minutes time resolution while the input to TRNSYS weather file is hourly based. Therefore, the fluctuations in the PV power cannot be modeled precisely which affects the whole energy flow between the components in the system. Energy distribution within the small-scale and simulated systems is shown in Table 3-9. Also, energy losses in the wires and the start-up/shut-down losses are not included in the electrolyzer and fuel cell models. Some portion of produced hydrogen is lost due to hydrogen purging in the experiments.
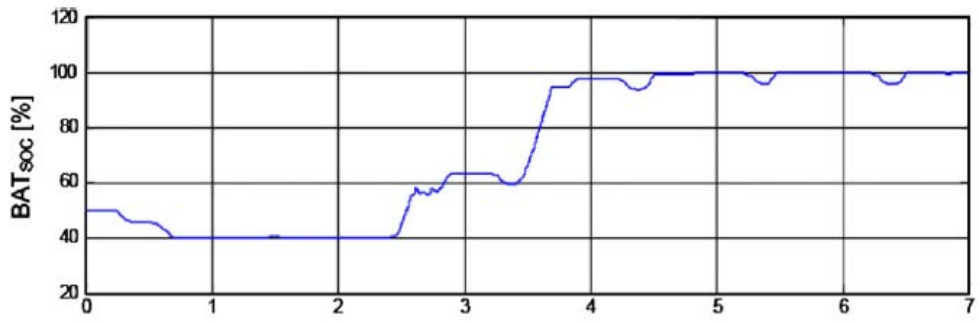
Figure 3-23a Measured battery SOC vs. time (days) (adapted from [31])
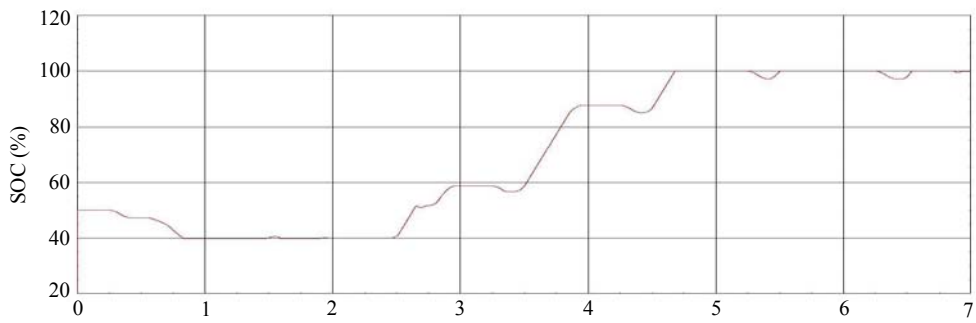
Figure 3-23b Simulated battery SOC vs. time (hours)

Table 3-9 Energy distribution within the system (kWh)

	PV array	Electrolyzer	Fuel cell	Battery(+)	Battery(-)	Load
Measured	39.7	20.2	6.6	11.6	3.5	15.4
Simulated	39.7	19.3	5.2	11.6	3.2	15.8
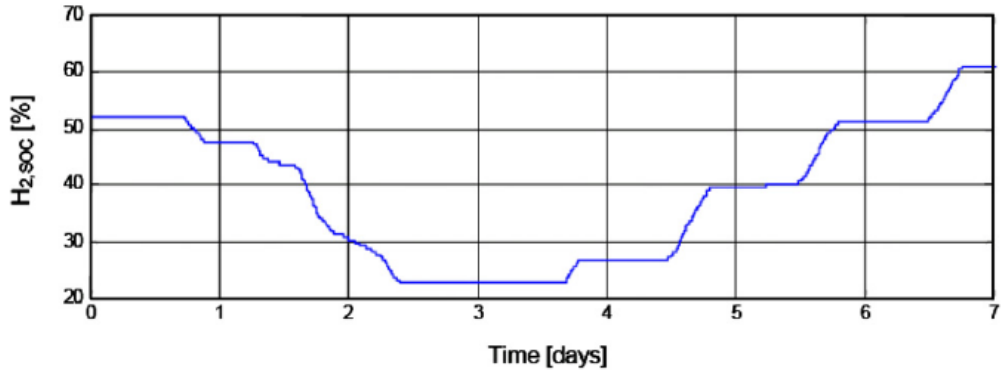
Figure 3-24a Measured hydrogen SOC vs. time (days) (adapted from [31])
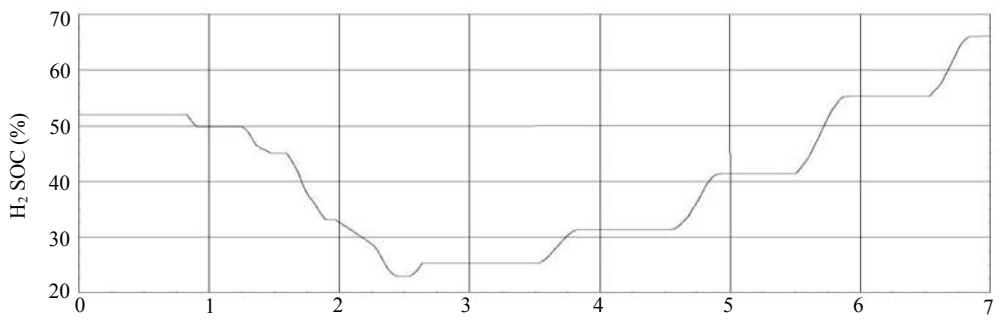
Figure 3-24b Simulated hydrogen SOC vs. time (hours)

CHAPTER 4

CONCLUSIONS

4.1 Results

In this study, stand alone power systems are modeled and system parameters are analyzed using a commercial software. The study is focused on the effects of system components and on the total performance of the system. The photovoltaic panels and the PEM electrolyzers are modeled individually using FORTRAN subroutines. Numerical outputs of these components are compared with the experimental results. The study shows how pressure in the hydrogen tank can be used as a key system performance indicator, provided that no system constraints are violated. The performance of the system can be significantly affected by the small variations made on the system elements.

Hydrogen is the only energy storage for a Stand-Alone Power System without a battery pack. The system is based on electricity-to-hydrogen and hydrogen-to-electricity conversion which is an inefficient way of handling the extra energy. Assembling PV panels with 50° surface slope reduces the amount of this conversion and expected to increase the system performance and thus reduce the size of the equipments used. However, PV panels produce 5% more energy if they are assembled at 30° surface slope, and only 20% of this additional energy is lost during the electricity-hydrogen conversions. Therefore, the system performance is improved by installing the PV panels with 30° surface slope compared to the panels with 50° surface slope. Assembling the PV panels in such a way that the surface slope can be adjusted manually or automatically during the year develops the system performance.

Increasing the number of electrolyzer cells adds additional initial cost to the system but also increases the system efficiency and life time of the whole electrolyzer stack.

Adding a battery pack plays an important role on the system performance and efficiency as well as the size of other components in the system. Increasing the number of batteries used also increases the system efficiency and decreases the other component sizes. On the other hand, the cost of the battery pack increases with a high rate while cost of other equipments decreases with a lesser rate. Energy and power densities of lead-acid batteries are much lower than the hydrogen tanks and the fuel cells. A 100 bar hydrogen tank can store 5 times more energy than a battery pack having the same volume. The trade-offs between the battery pack and the other components in the system should be examined accurately.

Auxiliary equipment brings extra load on the system but they are essential for steady and continuous operation of a stand-alone power system. If grid electricity is not used for auxiliary equipment, a battery pack or a fuel cell stack working continuously should provide energy to these equipment. Since the control panel and similar equipment should work continuously.

4.2 Future Work

Typical Meteorological Year data is used in the system models. Since the weather shows variations throughout the years, it is definite that there will be years with lower solar energy available. The worst case scenarios should be taken into account for the simulations and backup solutions should be considered such as using grid power or extra hydrogen storage.

The load profile used in the simulations is constant for long hours, however the actual load profile of an emergency service has power fluctuations and peak-powers. Fuel cell performance is significantly affected by the load. The performance of the fuel cell and thus the system will change if an actual load

profile is used. Control strategy of the fuel cell should be examined such as the fuel cells can operate under constant power or variable power. Operating the fuel cells under constant power and using batteries for the small fluctuations in the load can perform better than operating the fuel cells under variable power. Also batteries can be used for during peak-hours to reduce the load on the fuel cell since the fuel cell efficiency drops as the load increases. Hydrogen leakage from the connections and storage tank and electrical loses in the wires can be modeled to improve numerical models.

A detailed life-time cost analysis for the modeled systems should be performed to see the actual effects of the parameters. It is necessary to avoid the operating schemes that reduce the life of the electrochemical equipment which are electrolyzers, fuel cells and batteries. Therefore, other system parameters, such as number of start-ups and stops of the fuel cells and electrolyzers, the amount of time when these components are operating under high or low power levels, should also be considered.

REFERENCES

[1] Renewable Energy Policy Network for the 21st Century, "Renewables 2007 Global Status Report", 2007.

[2] Renewable Energy Policy Network for the 21st Century, "Renewables 2009 Global Status Report", 2009.

[3] N. Gupta, G.F. Alapatt, R. Podila, R. Singh, K.F. Poole, "Prospects of nanostructure-based solar cells for manufacturing future generations of photovoltaic modules", International Journal of Photoenergy, vol. 2009, id: 154059, 2009.

[4] TUBITAK Project no: 106G130 Project Proposal, 2006.

[5] P. Hollmuller, J.M. Joubert, B. Lachal, K. Yvon, "Evaluation of a 5kW$_p$ photovoltaic hydrogen production and storage installation for a residential home in Switzerland", International Journal of Hydrogen Energy, vol. 25, pp. 97-109, 2000.

[6] H. Miland, O. Ulleberg, "Testing of a small-scale stand-alone power system based on solar energy and hydrogen", Solar Energy, In Press, Uncorrected Proof, Available online (http://www.sciencedirect.com/science/article/B6V50-4SNPWJF-1/2/4d362d10af5abe0bf1c5a1aaf22c3bea)

[7] J.P. Vanhanen, P.D. Lund, J.S. Tolonen, "Electrolyser-metal hydride-fuel cell system for seasonal energy storage", International Journal of Hydrogen Energy, vol. 23, No 4, pp 267-271, 1998.

[8] S. Galli, M. Stefanoni, "Development of a Solar-hydrogen cycle in Italy", Int. J. Hydrogen Energy, vol 22, pp. 453-458, 1997.

[9] A.M. Chaparro, J. Soler, M.J. Escudero, E.M.L. de Ceballos, U. Wittstadt, L. Daza, "Date results and operational experience with a solar hydrogen system", Journal of Power Sources, vol. 144, pp. 165-169, 2005.

[10] A. Sasitharanuwat, W. Rakwichian, N. Ketjoy, S. Yammen, "Performance evaluation of a 10 kWp PV power system prototype for isolated building in Thailand", Renewable Energy, vol. 32, pp. 1288-1300, 2007.

[11] K. Agbossou, M. Kolhe, J. Hamelin, T.K. Bose, "Performance of a sand-aone rnewable eergy sstem based on eergy storage as hydrogen", IEEE Transactions on Energy Conversion, vol. 19, pp. 633-640, 2004.

[12] D. Shapiro, J. Duffy, M. Kimble, M. Pien, "Solar-powered regenerative PEm electrolyzer/fuel cell system", Solar Energy, vol. 79, pp. 544-550, 2005.

[13] A.N. Kelly, L.T. Gibson, D.B. Ouwerkerk, "A solar-powered, high-efficiency hydrogen fueling system using high pressure electrolysis of water: Design and initial results" International Journal of Hydrogen Energy, vol.33, pp.2747-2764, 2008.

[14] O. Ulleberg, "Stand-alone power systems for the future: Optimal design, operation & control of solar-hydrogen energy systems", Ph.D. dissertation, Norwegian University of Science and Technology Trondheim, Norway, 1998.

[15] O. Ulleberg, "The importance of control strategies in PV-hydrogen systems", Solar Energy, vol. 76, pp. 323-329, 2004.

[16] R. Dufo-Lopez, J.L. Bernal-Agustin, J. Contreras, "Optimization of Control Strategies for Stand-Alone Renewable Energy Systems with Hydrogen Storage", Renewable Energy, vol. 32, pp. 1102-1126, 2007.

[17] M. Santarelli, M. Cali, S. Macagno, "Design and analysis of stand-alone hydrogen systems with different renewable sources", Internal Journal of Hydrogen Energy, vol. 29, pp. 1571-1586, 2004.

[18] S. Pedrazzi, G. Sini, P. Tartarini, "Complete modeling and software implementation of a virtual solar hydrogen hybrid system", Energy Conversion and Management, vol. 51, pp.122-129, 2010.

[19] J. Samaniego, F. Alija, S. Sanz, C. Valmaseda, F. Frechoso, "Economic and technical analysis of a hybrid wind fuel cell energy system", Renewable Energy, vol. 33, pp. 839-845, 2008.

[20] S.S. Deshmukh, R.F. Boehm, "Reviews of modeling details revealed to renewably powered hydrogen systems", Renewable and Sustainable Energy Reviews, vol. 12, pp. 2301-2330, 2007.

[21] D.B. Nelson, M.H. Nehrir, C. Wang, "Unit sizing and cost analysis of stand-alone hybrid wind/PV/fuel cell power generation systems" Renewable Energy, vol. 31, pp. 1641-1656, 2006.

[22] O.C. Onar, M. Uzunoglu, M.S. Alam, "Dynamic modeling, design and simulation of a wind/fuel cell/ultra-capacitor-based hybrid power generation system", Journal of Power Sources, vol. 161, pp. 707-722, 2006.

[23] O.C. Onar, M. Uzunoglu, M.S. Alam, "Modeling, control and simulation of a PV/FC/UC based hybrid power generation system for stand-alone applications", Renewable Energy, vol. 34, pp. 509-520, 2009.

[24] D. Sera, R. Teodorescu, P. Rodriguez, "PV panel model based on datasheet values", Industrial Electronics, 2007. ISIE 2007. IEEE International Symposium, pp. 2392-2396, 2007.

[25] G. Vachtsevanos, K. Kalaitzakis, "A hybrid photovoltaic simulator for utility interactive studies", IEEE Power Engineering Society summer meeting, Mexico City, 1986.

[26] M. Mattei, G. Notton, C. Cristofari, M. Muselli, P. Poggi, "Calculation of a polycrystalline PV module temperature using a simple method of energy balance", Renewable Energy, vol. 31, pp. 553-567, 2005.

[27] W.A. Beckman, W. Desoto, S.A. Klein, "Improvement and validation of a model for photovoltaic array performance" Solar Energy, vol. 80, pp. 78-88, 2006.

[28] Nonlinear Regression and Curve fitting,
http://www.nlreg.com, last accessed at April 2010.

[29] N. Gupta, G.F. Alapatt, R. Podila, R. Singh, K.F. Poole, "Prospects of nanostructure-based solar cells for manufacturing future generations of photovoltaic modules", International Journal of Photoenergy, vol. 2009, id: 154059, 2009.

[30] D.A. Bechrakis, E.J. McKeogh, P.D. Gallagher, "Simulation and operational assessment for a small autonomous wind-hydrogen energy system", Energy Conversion and Management, vol. 47, pp. 46-59, 2006.

[31] H. Miland, "Operational experience and control strategies for a stand-alone power system based on renewable energy and hydrogen", Ph.D. dissertation, Norwegian University of Science and Technology Trondheim, Norway, 2005.

[32] Model KC130TM data sheet, Kyocera Corporation.

APPENDIX A

DATA SHEET OF KYOCERA 130W PV PANEL

Table A-1 Electrical properties

Maximum Power	130 Watts
Tolerance	+10% / -5%
Maximum Power Voltage	17.6 Volts
Maximum Power Current	7.39 Amps
Open Circuit Voltage	21.9 Volts
Short Circuit Current	8.02 Amps
Length	1425 mm
Width	652 mm
Depth	58 mm
Weight	11.9 kg

Table A-2 Thermal properties

|	
Nominal Operating Cell Temperature	47 ^{o}C
Isc Current Temperature Coefficient	(3.18x10-3) A/^{o}C
Voc Voltage Temperature Coefficient	(-8.21x10-2) V/^{o}c
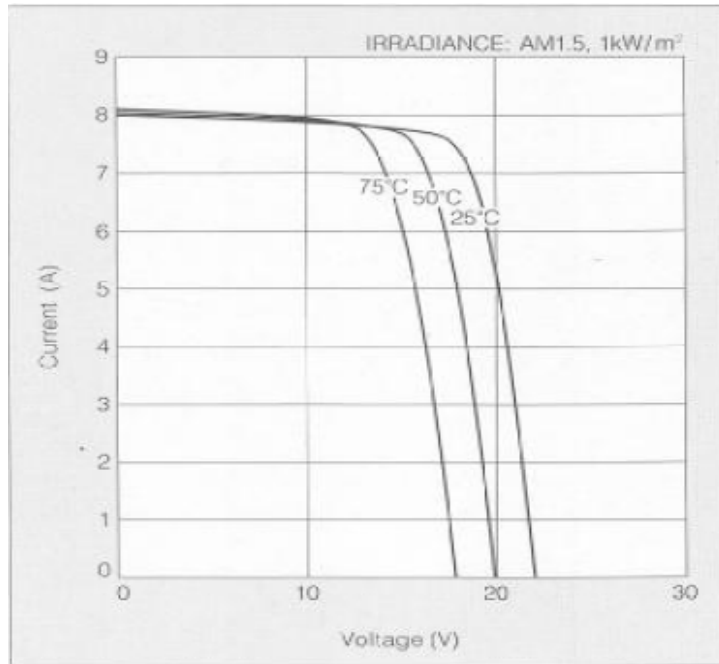
Figure A-1 Current-Voltage characteristic of PV module KC130TM at various cell temperatures (adapted from [32])
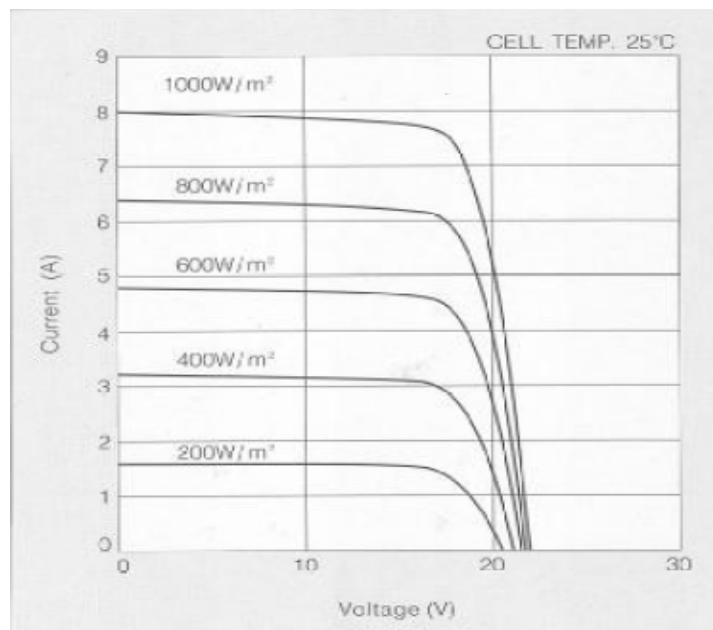

Figure A-2 Current-Voltage characteristic of PV module KC130TM at various irradiance levels (adapted from [32])

APPENDIX B

FORTRAN CODE OF PV PANEL MODEL

```
C       Initial estimations for the PV parameters
        Rs=0.8
        Rsh=100
        A=0.8
        I0=0.00001
        x(1)=Rs
        x(2)=Rsh
        x(3)=A
        x(4)=I0
        N=1
10      N=N+1
        DO 15 i=1,4
              xold(i)=x(i)
15      CONTINUE
        u(1)=Iph-Isc-(x(4)*(exp((Isc*x(1))/(ns*Vt*x(3)))-1))-((Isc*x(1))/
        .x(2))
        u(2)=Iph-Impp-(x(4)*(exp((Vmpp+Impp*x(1))/(ns*x(3)*Vt))-1))-
        .((Vmpp+Impp*x(1))/x(2))
        u(3)=Iph-x(4)*(exp((Vmpp+Impp*x(1))/(x(3)*Vt*ns))-1)-((Vmpp+Impp*
        .x(1))/x(2))-Vmpp*((1/x(2))+((x(4)*exp((Vmpp+Impp*x(1))/(x(3)*Vt*
        .ns)))/(x(3)*Vt*ns)))
        u(4)=Iph-(x(4)*(exp(Voc/(ns*Vt*x(3)))-1))-(Voc/x(2))
C       partial derivatives of FIsc wrt. Rs, Rsh, A and I0 respectively
        FIscdRs=-(Isc/Rsh)-((I0*Isc*exp((Isc*Rs)/(A*Vt*ns)))/(A*Vt*ns))
        coef(1,1)=FIscdRs
        FIscdRsh=(Isc*Rs)/(Rsh*Rsh)
        coef(1,2)=FIscdRsh
        FIscdA=(I0*Isc*Rs*exp((Isc*Rs)/(A*Vt*ns)))/(A*A*Vt*ns)
        coef(1,3)=FIscdA
        FIscdI0=1-exp((Isc*Rs)/(ns*Vt*A))
        coef(1,4)=FIscdI0
C       partial derivatives of FMpp wrt. Rs, Rsh, A and  I0 respectively
        FMppdRs=-(Impp/Rsh)-((I0*Impp*exp((Vmpp+Impp*Rs)/(A*Vt*ns)))/
        .(A*Vt*ns))
        coef(2,1)=FMppdRs
        FMppdRsh=(Vmpp+Impp*Rs)/(Rsh*Rsh)
```

```fortran
      coef(2,2)=FMppdRsh
      FmppdA=(I0*exp((Vmpp+Impp*Rs)/(A*Vt*ns))*(Vmpp+Impp*Rs))/
     .(A*A*Vt*ns)
      coef(2,3)=FMppdA
      FMppdI0=1-exp((Vmpp+Impp*Rs)/(ns*A*Vt))
      coef(2,4)=FMppdI0
C     partial derivatives of FdPdV wrt. Rs, Rsh, A and I0 respectively
      FdPdVdRs=-(Impp/Rsh)-((I0*Impp*exp((Vmpp+Impp*Rs)/(A*Vt*ns))))/
     .(A*Vt*ns))-((I0*Impp*Vmpp*exp((Vmpp+Impp*Rs)/(A*Vt*ns))))/
     .(A*A*Vt*Vt*ns*ns))
      coef(3,1)=FdPdVdRs
      FdPdVdRsh=(2*Vmpp+Impp*Rs)/(Rsh*Rsh)
      coef(3,2)=FdPdVdRsh
      FdPdVdA=Vmpp*(((I0*exp((Vmpp+Impp*Rs)/(A*Vt*ns)))/(A*A*Vt*ns))+
     .((I0*exp((Vmpp+Impp*Rs)/(A*Vt*ns))*(Vmpp+Impp*Rs))/
     .(A**3*Vt**2*ns**2)))+(I0*exp((Vmpp+Impp*Rs)/(A*Vt*ns))*
     .(Vmpp+Impp*Rs))/(A**2*Vt*ns)
      coef(3,3)=FdPdVdA
      FdPdVdI0=0
      coef(3,4)=FdPdVdI0
C     partial derivatives of FVoc wrt. Rs, Rsh, A and I0 respectively
      FVocdRs=0
      coef(4,1)=FVocdRs
      FVocdRsh=0
      coef(4,2)=FVocdRsh
      FVocdA=(I0*Voc*exp(Voc/(A*Vt*ns)))/(A*A*Vt*ns)
      coef(4,3)=FVocdA
      FVocdI0=1-exp(Voc/(ns*Vt*A))
      coef(4,4)=FVocdI0
      DO 20 i=1,4
      b(i)=-u(i)+x(1)*coef(i,1)+x(2)*coef(i,2)+x(3)*coef(i,3)+x(4)*
     .coef(i,4)
20    CONTINUE
C     Forward elemination
      DO 40 k=1,3
      DO 40 i=k+1,4
           factor=coef(i,k)/coef(k,k)
      DO 30 j=k+1,4
           coef(i,j)=coef(i,j)-factor*coef(k,j)
30    CONTINUE
           b(i)=b(i)-factor*b(k)
40    CONTINUE
C     Backward Subsitituon
      x(4)=b(4)/coef(4,4)
      DO 60 i=3,1,-1
           sum=0
      DO 50 j=i+1,4
           sum=sum+coef(i,j)*x(j)
```

```
50      CONTINUE
                x(i)=(b(i)-sum)/coef(i,i)
60      CONTINUE
C       percent error between old and new estimations
        DO 65 i=1,4
                pererr(i)=((x(i)-xold(i))/x(i))*100
65      CONTINUE
        IF(ABS(pererr(1)).LT.0.1 .AND. ABS(pererr(2)).LT.0.1 .AND.
       .ABS(pererr(3)).LT.0.1 .AND. ABS(pererr(4)).LT.0.5) GO TO 70
        IF(N .LT. 1000) GO TO 10
70      CONTINUE
        Rs=x(1)
        Rsh=x(2)
        A=x(3)
        I0=x(4)
C       THERMAL MODEL
C       converting temperature to K and irradiation to W/m^2
        Ta=Ta+273
        GT=GT/3.6
        Tcell=((24.1+2.9*Vwind)*Ta+GT*(alfatao-effr-beta*effr*
       .Tr))/(24.1+2.9*Vwind-beta*effr*GT)
C       TEMPERATURE DEPENDANCY OF PARAMETERS
        At=A*(Tcell/Tr)
        Ipht=(Isc+mIsc*(Tcell-Tr))*(GT/1000)
        Rst=Rs
        IF (GT.EQ.0) GO TO 75
        Rsht=Rsh*(GTr/GT)
75      Rsht=Rsh
C       q=1.6E-19, k=1.38E-23; to prevent losing significant digits > Vkq=k/q=8.625E-5
C       Vt=Vkq*T
        Vkq=0.00008625
        I0t=(I0*(Tcell/Tr)**3)*exp((Eg/(At*Vkq))*((1/Tr)-
       .(1/Tcell)))
C       Operating Point of PV
        IF(GT.EQ.0) THEN
        OUT(2)=0
        OUT(3)=0
        OUT(4)=0
        OUT(5)=0
        GO TO 115
        ELSE
        GO TO 80
        ENDIF
80      CONTINUE
        Vpv=Vmpp*0.95
98      Iup=40
        Ilow=0
100     Imid=(Iup+Ilow)/2
```

```
      IF(abs(Iup-Ilow).LT.0.002) THEN
      GO TO 105
      ENDIF

      IPVmid=Ipht-Imid-I0t*(exp((Vpv+Imid*Rst)/
     .(ns*At*Vkq*Tcell))-1)-((Vpv+Imid*Rst)/Rsht)
      IPVup=Ipht-Iup-I0t*(exp((Vpv+Iup*Rst)/
     .(ns*At*Vkq*Tcell))-1)-((Vpv+Iup*Rst)/Rsht)
      ProductIPV=IPVmid*IPVup
      IF(ProductIPV>0) Iup=Imid
      IF(ProductIPV<0) Ilow=Imid
      GO TO 100
C     Maximum Power Point Tracking
105   Ipv=Imid
      dPdV=Ipht-I0t*(exp((Vpv+Ipv*Rst)/(At*Vkq*Tcell*ns))-1)
     .-((Vpv+Ipv*Rst)/Rsht)-Vpv*((1/Rsht)+((I0t*
     .exp((Vpv+Ipv*Rst)/(At*Vkq*Tcell*ns)))/(At*Vkq*Tcell*ns)))
      IF (abs(dPdV).LT.0.02) GO TO 110
      IF (dPdV.GT.0) Vpv=Vpv+0.005
      IF (dPdV.LT.0) Vpv=Vpv-0.005
      GO TO 98
110   CONTINUE
      Ppv=Ipv*Vpv
C           Tc
              OUT(1)=Tcell-273
C           V
              OUT(2)=Vpv
C           I
              OUT(3)=Ipv
C           P
              OUT(4)=Ppv
C           Efficiency
              OUT(5)=Ppv/Gt
115   CONTINUE
```

APPENDIX C

FORTRAN CODE OF PEM ELECTROLYZER MODEL

```
C      Calculating maximum power that can electrolyzer work at
       Tmax=Tmax+273
       Pmin=25*ns
       Tambient=20
10     Iup=200
       Ilow=0
15     Imid=(Iup+Ilow)/2
       IF(abs(Iup-Ilow).LT.0.000001) THEN
       GO TO 20
       ENDIF
       Ielemid=(A*(Ioa*Tmax+Iob)*(exp(((1-alfa)*n*F*(Vcell-Veq))/
      .             (R*Tmax))-exp(((-alfa)*n*F*(Vcell-Veq))/(R*Tmax))))-Imid


       Ieleup=(A*(Ioa*Tmax+Iob)*(exp(((1-alfa)*n*F*(Vcell-Veq))/
      .             (R*Tmax))-exp(((-alfa)*n*F*(Vcell-Veq))/(R*Tmax))))-Iup
       ProductIele=Ielemid*Ieleup
       IF(ProductIele>0) Iup=Imid
       IF(ProductIele<0) Ilow=Imid
       GO TO 15
20     CONTINUE
       Imax=Imid
       Pmaxcell=Imax*Vcell
       Pmaxele=Pmaxcell*ns*npmax
       Pwasted=Pmaxele-Pele
       IF(Pwasted>0) Pwasted=0
       IF(Pele>Pmaxele) Pele=Pmaxele
       IF(Pele.LT.Pmin) THEN
                   Pele=0
                   Ic=0
                   Tcell=Tambient
                   Efficiency=0
                   Vh2actual=0
                   npar=0
                   GO TO 60
       ELSE
       CONTINUE
```

```
       END IF
C      Calculating the optimum number of parallel electrolyzer stacks that would make
the electrolyzer work as close as possible to reference cell temperature
25     Iup=200
       Ilow=0
30     Imid=(Iup+Ilow)/2
       IF(abs(Iup-Ilow).LT.0.000001) THEN
       GO TO 35
       ENDIF
       Ielemid=(A*(Ioa*Tcref+Iob)*(exp(((1-alfa)*n*F*(Vcell-Veq))/
      .      (R*Tcref))-exp(((-alfa)*n*F*(Vcell-Veq))/(R*Tcref))))-Imid


       Ieleup=(A*(Ioa*Tcref+Iob)*(exp(((1-alfa)*n*F*(Vcell-Veq))/
      .           (R*Tcref))-exp(((-alfa)*n*F*(Vcell-Veq))/(R*Tcref))))-Iup
       ProductIele2=Ielemid*Ieleup
       IF(ProductIele2>0) Iup=Imid
       IF(ProductIele2<0) Ilow=Imid
       GO TO 30
35     CONTINUE
       Ic=Imid
       nstack=Pele/((Ic*Vcell)*ns)
       npar=NINT(nstack)
       IF(npar.GT.npmax) npar=npmax
       Pc=Pele/(ns*npar)
       Ic=Pc/Vcell


C      Calculating cell temperature for given stack number
40     Tup=1000
       Tlow=200
45     Tmid=(Tup+Tlow)/2
       IF(abs(Tup-Tlow).LT.0.000001) THEN
       GO TO 50
       ENDIF
       Telemid=(A*(Ioa*Tmid+Iob)*(exp(((1-alfa)*n*F*(Vcell-Veq))/
      .           (R*Tmid))-exp(((-alfa)*n*F*(Vcell-Veq))/(R*Tmid))))-Ic


       Teleup=(A*(Ioa*Tup+Iob)*(exp(((1-alfa)*n*F*(Vcell-Veq))/
      .           (R*Tup))-exp(((-alfa)*n*F*(Vcell-Veq))/(R*Tup))))-Ic
       ProductTele=Telemid*Teleup
       IF(ProductTele>0) Tup=Tmid
       IF(ProductTele<0) Tlow=Tmid
       GO TO 45
50     CONTINUE
       Tcell=Tmid-273
       Tstan=0
       Nh2ideal=ns*npar*(Ic/(2*F))
       Vh2ideal=(Nh2ideal*R*(Tstan+273)*3600)/100000
       Vh2actual=Vh2ideal*Feff
```

```fortran
      Efficiency=Vtn/Vcell
60    CONTINUE
C           Pused
            OUT(1)=Pele
C           Iele
            OUT(2)=Ic*npar
C           Tc
            OUT(3)=Tcell
C           Efficiency
            OUT(4)=Efficiency
C           Vh2
            OUT(5)=Vh2actual
C           np
            OUT(6)=npar
C           Vo2
            OUT(7)=Vh2actual/2
C----------------------------------------------------------------------------------
-----------------------------------
C    EVERYTHING IS DONE - RETURN FROM THIS SUBROUTINE AND MOVE ON
      RETURN 1
      END
```

APPENDIX D

INPUT FILES OF THE SYSTEM ELEMENTS

```
* Model "Type109-TMY2" (Type 109) TMY 2 weather data
*
UNIT 3 TYPE 109    Type109-TMY2
*$UNIT_NAME Type109-TMY2
*$MODEL .\Weather Data Reading and Processing\Standard Format\TMY2\Type109-TMY2.tmf
*$POSITION 148 72
*$LAYER Main #
PARAMETERS 4
2           ! 1 Data Reader Mode
34          ! 2 Logical unit
4           ! 3 Sky model for diffuse radiation
1           ! 4 Tracking mode
INPUTS 3
0,0         ! [unconnected] Ground reflectance
0,0         ! [unconnected] Slope of surface
0,0         ! [unconnected] Azimuth of surface
*** INITIAL INPUT VALUES
0.2 30 0.0
*** External files
ASSIGN "C:\Program Files\Trnsys16\Weather\Meteonorm\Europe\TR-Ankara-171300.tm2" 34
*|? Weather data file |1000
*-----------------------------------------------------------------------------

* Model "Type14h" (Type 14)
*

UNIT 7 TYPE 14    Type14h
*$UNIT_NAME Type14h Load Profile
*$MODEL .\Utility\Forcing Functions\General\Type14h.tmf
*$POSITION 247 245
*$LAYER Main #
PARAMETERS 10
0           ! 1 Initial value of time
2000        ! 2 Initial value of function
6           ! 3 Time at point-1
2000        ! 4 Value at point -1
```

```
6            ! 5 Time at point-2
5000         ! 6 Value at point -2
24           ! 7 Time at point-3
5000         ! 8 Value at point -3
24           ! 9 Time at point-4
0            ! 10 Value at point -4
*-----------------------------------------------------------------------------


* Model "Type230" (Type 230) PV array
*

UNIT 5 TYPE 230    Type230
*$UNIT_NAME Type230
*$MODEL .\My components\Type230.tmf
*$POSITION 254 164
*$LAYER Main #
PARAMETERS 14
21.9         ! 1 Voc
8.02         ! 2 Isc
72           ! 3 Ns
0.0259           ! 4 Vt
7.36         ! 5 Impp
17.6         ! 6 Vmpp
0.00318          ! 7 mIsc
-0.0821          ! 8 mVoc
298          ! 9 Tr
1000         ! 10 GTr
1.16         ! 11 Eg
0.81         ! 12 alfatao
0.16         ! 13 effr
0.0044           ! 14 Beta
INPUTS 3
3,18         ! Type109-TMY2:total radiation on tilted surface ->GT
3,1          ! Type109-TMY2:Ambient temperature ->Ta
3,3          ! Type109-TMY2:wind velocity ->Vwind
*** INITIAL INPUT VALUES
3600 0 0
*-----------------------------------------------------------------------------


* Model "Type232" (Type 232) Controller
*

UNIT 2 TYPE 232    Type232
*$UNIT_NAME Type232
*$MODEL .\My components\Type232.tmf
*$POSITION 432 292
*$LAYER Main #
```

```
PARAMETERS 11
0             ! 1 PfcMin
5200          ! 2 PfcMax
4000          ! 3 PfcNom
0             ! 4 PeleMin
40000         ! 5 PeleMax
0.9           ! 6 SOCmax
0.2           ! 7 SOCmin
0.2           ! 8 SOCfclimit
0.95          ! 9 PLEVup
0.9           ! 10 PLEVlow
0.90          ! 11 InverterEff
INPUTS 4
Pout          ! Equa:Pout ->Ppv
7,1           ! Type14h:Average value of function ->Pload
0,0           ! [unconnected] SOC
12,3          ! Type164a:PLEV ->PLEV
*** INITIAL INPUT VALUES
0 10000 0.95 0.9
*-------------------------------------------------------------------------------


* Model "Type48a" (Type 48) Inverter
*

UNIT 10 TYPE 48    Type48a
*$UNIT_NAME Type48a
*$MODEL .\Electrical\Regulators and Inverters\System w_o battery storage\Type48a.tmf
*$POSITION 390 566
*$LAYER Main #
PARAMETERS 2
0             ! 1 Mode
0.95          ! 2 Efficiency
INPUTS 2
8,1           ! Type170f:P_FC ->Input power
7,1           ! Type14h:Average value of function ->Load power
*-------------------------------------------------------------------------------


* Model "Type170f" (Type 170) Fuel Cell
*

UNIT 8 TYPE 170    Type170f
*$UNIT_NAME Type170f
*$MODEL .\Hydrogen Systems\Fuel Cells\PEMFC\Air-H2\TMODE=2\RTCTMODE=3\Type170f.tmf
*$POSITION 390 449
*$LAYER Main #
*$# OXMODE=1.        Air on the cathode side.
*$# TMODE=2.          TSTACK is calculated
```

101

```
*$# RTCTMODE=3.    User supplied R_t & C_t values
PARAMETERS 12
1             ! 1 OXMODE
2             ! 2 TMODE
85            ! 3 NCELLS
1             ! 4 NSTACKS
260           ! 5 A_PEM
0.0118            ! 6 T_PEM
0.0           ! 7 GAMMA
0.7           ! 8 UC_MIN
700           ! 9 IC_MAX
3             ! 10 RTCTMODE
0.06179           ! 11 Rt
32197         ! 12 Ct
INPUTS 11
2,5           ! Type232:FCswitch ->SWITCH
11,2          ! Type175a-2:Iout ->IFC
0,0           ! [unconnected] TSTACKin
0,0           ! [unconnected] p_H2_in
0,0           ! [unconnected] p_O2_in
0,0           ! [unconnected] S_H2
0,0           ! [unconnected] S_O2
0,0           ! [unconnected] Tamb
0,0           ! [unconnected] TCWin
0,0           ! [unconnected] DELTATCW
0,0           ! [unconnected] Xevap
*** INITIAL INPUT VALUES
1 160 70 3 3 1.15 2.5 20 30 20 0.25
*----------------------------------------------------------------------------

* Model "Type175a-2" (Type 175)
*

UNIT 11 TYPE 175   Type175a-2 Power Conditioner
*$UNIT_NAME Type175a-2
*$MODEL .\Electrical\Power Conditioning\Power INPUT is known\Type175a.tmf
*$POSITION 339 366
*$LAYER Main #
*$# MODE=1.   Input power (power source) is known.
PARAMETERS 7
1             ! 1 Mode
10000         ! 2 Pn
0             ! 3 P0Pn
2.06          ! 4 Us
50            ! 5 RiPn
1             ! 6 MP
0             ! 7 Paux
INPUTS 3
```

```
8,2          ! Type170f:Ustack ->Uin
8,2          ! Type170f:Ustack ->Uout_set
2,1          ! Type232:Pfc ->P
*** INITIAL INPUT VALUES
22E3 135 0
*-------------------------------------------------------------------------------


* Model "Type231" (Type 231) Electrolyzer
*

UNIT 13 TYPE 231   Type231
*$UNIT_NAME Type231
*$MODEL .\My components\Type231.tmf
*$POSITION 701 196
*$LAYER Main #
PARAMETERS 14
0.0025           ! 1 A
50           ! 2 ns
15           ! 3 npmax
1.482        ! 4 Veq
0.97092          ! 5 alfa
68.572           ! 6 Ioa
-19242.33        ! 7 Iob
2            ! 8 n
96485.34         ! 9 F
8.314472         ! 10 R
323          ! 11 Tcref
80           ! 12 Tmax
0.95         ! 13 Feff
20           ! 14 Pressure
INPUTS 2
0,0          ! [unconnected] Vcell
2,2          ! Type232:Pele ->Pele
*** INITIAL INPUT VALUES
2 0
*-------------------------------------------------------------------------------


* Model "Type164a" (Type 164) Hydrogen tank
*

UNIT 12 TYPE 164   Type164a
*$UNIT_NAME Type164a
*$MODEL .\Hydrogen Systems\Compressed Gas Storage\Hydrogen\Ideal Gas\Type164a.tmf
*$POSITION 659 449
*$LAYER Main #
*$# PMODE=1.  Ideal Gas.
PARAMETERS 4
1            ! 1 PMODE
```

```
100          ! 2 PMAX
35           ! 3 VOL
2.016        ! 4 MOLAR
INPUTS 4
13,5         ! Type231:Vh2 ->VDOT_IN
8,6          ! Type170f:V_H2 ->VDOT_OUT
0,0          ! [unconnected] TGAS
0,0          ! [unconnected] PLEV_INI
*** INITIAL INPUT VALUES
0 0 20 0.05
*------------------------------------------------------------------------------

END
```

APPENDIX E

COMPONENTS PARAMETERS AND EXPERIMENTAL MODELS

Table E-1 Technical data of the PEM electrolyzer system (adapted from [31])

Peak power	1750 Watts
Nominal voltage	48 V
Maximum operating current	35 A
Number of cells	26
Operating pressure	15 bar
Operating temperature	75 $^{\circ}$C
Hydrogen productivity	390 Nl/h H_2
Active area per cell	57 cm^2

Table E-2 Specification for the PEM fuel cell system (adapted from [31])

|	
Rated power	500 W
Peak power	630 W at 15 A
Power density	0.1 W/cm^2 at 500 W
Operating voltage	46 V at 12 A
Open circuit voltage	65 V
Active electrode area per cell	64
Typical efficiency	42%
Operating pressure	0.34 bar
Operating temperature	0-40 $^{\circ}$C
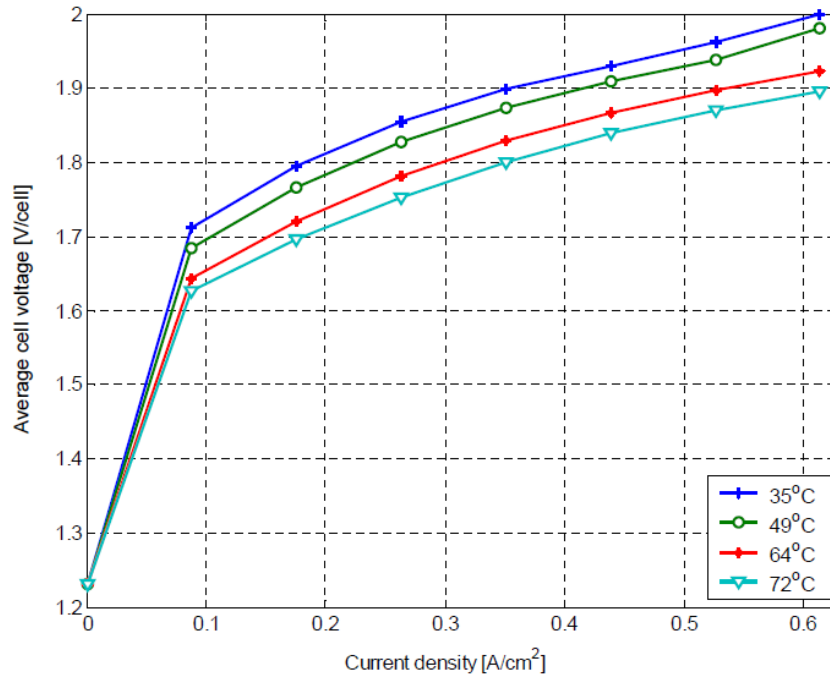
Figure E-1 Measured current-voltage characteristic at four different electrolyzer stack-temperatures (adapted from [31])
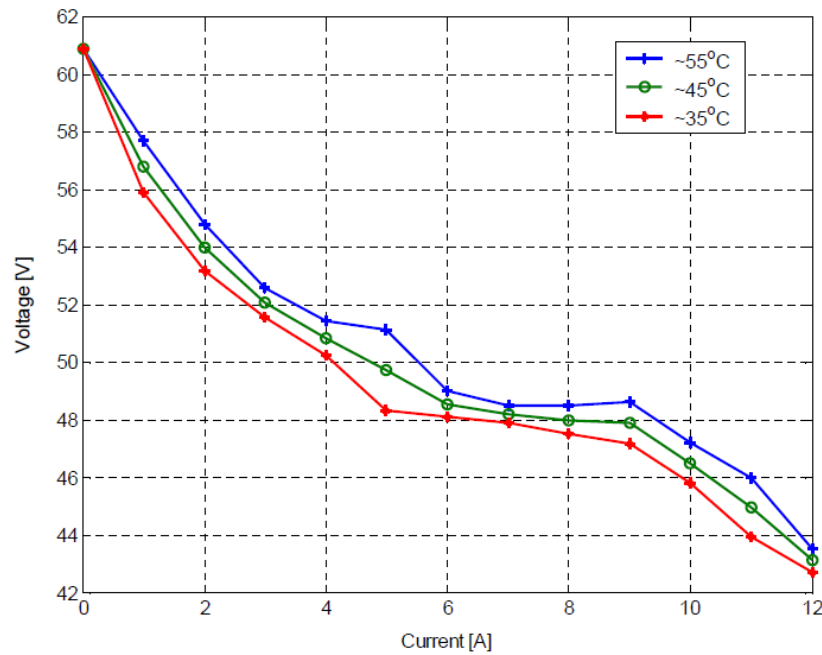

Figure E-2 Measured current-voltage curves at three different fuel cell stack-temperatures (adapted from [31])
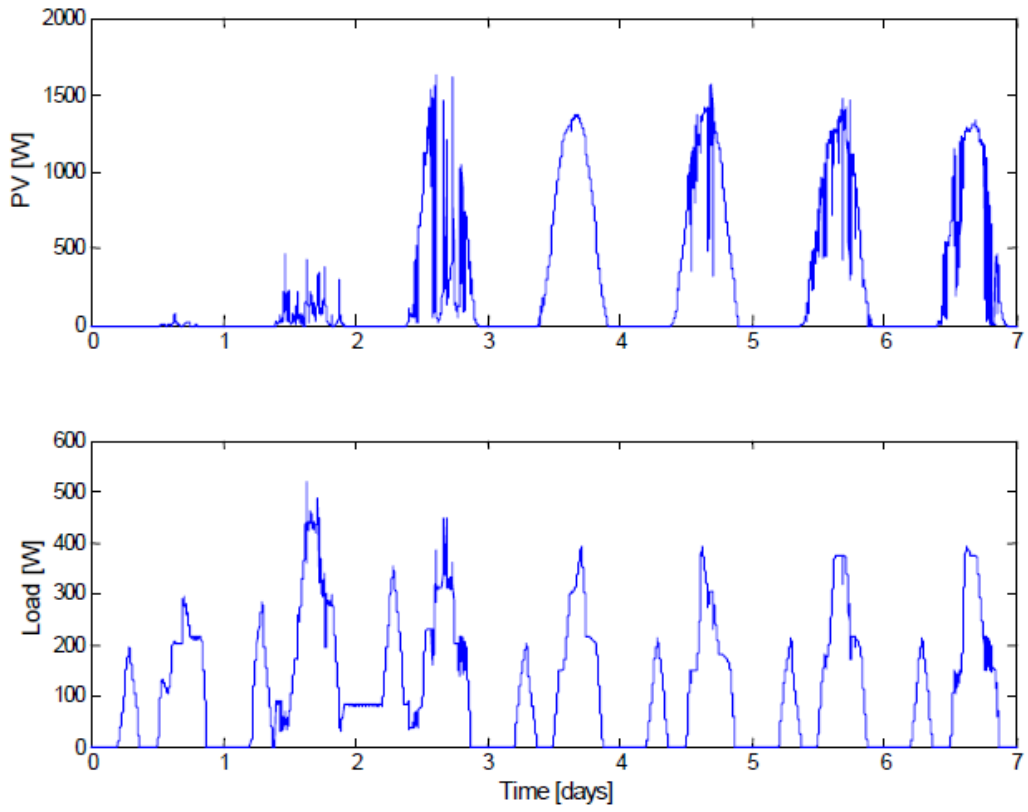
Figure E-3 PV power (above) and load (below) profiles emulated by the programmable power supply used in the experiments(adapted from [31])